# Surface velocity and ice thickness of the Müller ice cap, Axel Heiberg Island

### Ann-Sofie Priergaard Zinck

November 30, 2020

Supervisor:
Associate Professor Aslak Grinsted

**Abstract**

Müller ice cap is situated on Axel Heiberg Island in Arctic Canada. It is characterised by a mountanious region separating the ice cap in the east from the outlet glaciers in the west. Research has taken place on the outlet glaciers of the ice cap since 1959, but only limited research has been conducted on the main ice cap, and no full depth ice cores have ever been drilled. The interesting location of the ice cap facing the Arctic Ocean, the chance of finding ice dating back to the Innuitian Ice Sheet, and the fact that no full depth ice cores have been drilled, makes it an obvious place to do so. In order to achieve a long and undisturbed chronology of the ice core, one needs to find a location for the drilling site, where there is a great ice thickness, low surface velocity and little melt. In this project the aim is to make surface velocity maps of the ice cap and estimate the ice thickness to be able to come up with suggestions of possible drill site areas.

Surface velocities are calculated using feature tracking of optical satellite images from the Landsat satellites in the period of 2004-2019. A median velocity map of all Landsat 8 velocity maps is used as validation in modelling the ice thickness and in the investigation of possible drill site areas.

To estimate the ice thickness various methods are used and are being compared to the ice thickness measured by Operation IceBridge. The first method is an iterative inverse method where the ice sheet model PISM works as a forward model. The model is found to work rather well on the ice cap, with a root mean squared error (RMS) of 138.9 m, but overestimates the ice thickness on the outlet glaciers. The second model uses a simple inversion of the shallow ice approximation. It overestimates the ice thickness in areas with low surface slope, but has a RMS of 131.4 m on the ice cap. The third and and fourth models uses Monte Carlo sampling methods of the shallow ice approximation without and with sliding, respectively. The latter uses an initial ice thickness guess, and the modelled ice thickness was proofed not to differ from that initial guess at all. The RMSs on the ice cap of the two models were found to be 132.1 m and 129.9 m, respectively. Finally, the fifth model uses the PISM setup but with an initial geometry defined by the SIA inversion. The RMS on the ice cap is found to be 135.4 m.

Based on the median Landsat 8 surface velocity map, the modelled ice thicknesses and the surface elevation from the Arctic Digital Elevation Model, a map of suggested drill site areas is made. The site which fulfilled the criteria the most is located at 526629 m easting and 8866463 m northing in UTM zone 15N. In this site the surface velocity is 1.2 m yr$^{-1}$, the surface elevation is 1804 m and the modelled ice thicknesses varies from 535-579 m. The melt in this area is estimated to be less than 20 melt days per year based on the backscatter from Sentinel-1.

# Acknowledgements

First of all I would like to thank Associate Professor Aslak Grinsted, for being an excellent supervisor throughout my thesis. I also want to thank everyone at Physics of Ice, Climate and Earth, for a great environment, interesting talks and excellent facilities for me as a student. I am grateful for the fruitful discussions and presentations in the ice flow modelling group arranged by Associate Professor Christine Schøtt Hvidberg.

Furthermore, I would like to thank Professor Dorthe Dahl-Jensen for inviting me to give a talk on my thesis for partners in Denmark and Canada. This talk lead to data sharing of velocity maps with Assistant Professor Wesley Van Wychen at the University of Waterloo, which I am very grateful for.

In my PISM modelling I received great help from Iben Koldtoft, which I am very thankful for. It made the steep learning curve of PISM much smoother for me.

I am grateful for computing resources and technical assistance provided by the Danish Center for Climate Computing, a facility built with support of the Danish e-Infrastructure Corporation, Danish Hydrocarbon Research and Technology Centre, VILLUM Foundation, and the Niels Bohr Institute. Here I would like to send a special thanks to Research Coordinator Roman Nuterman.

Finally, I would like to thank my two friends Falk Oraschewski and Jakob Lass for all of the hours of proof reading that they have invested in my thesis.

# Contents

# 1 Introduction

## 1.1 Historical data from the Müller ice cap

The Müller ice cap is situated in Arctic Canada on Axel Heiberg Island highlighted in Figure 1.1. It is characterised by a mountainous region separating the ice cap in the east from the outlet glaciers in the west as seen in Figure 1.2. The ice cap is named after the Swiss glaciologist Fritz Müller [Adams, 2000] who was the scientific leader of the yearly expeditions to Axel Heiberg Island for many years [Müller, 1962]. Prior to Fritz Müller's death the ice cap was named Akaioa ice cap [Adams, 2000].

The yearly expeditions started in 1959 where stakes were put into White Glacier (marked in the red square in Figure 1.2) to study the mass balance. Since then White Glacier has been studied thoroughly [Cogley and Adams, 2000, Cogley et al., 1996, 2011, Hambrey and Müller, 1978, Müller, 1962, Thomson et al., 2016] and especially the mass balance is well studied with almost yearly measurements [Cogley et al., 1996, Müller, 1962, Thomson et al., 2016].

Initially, very limited research was conducted on the ice cap. In the early years of the annual expeditions to White Glacier the Müller ice cap was studied briefly. On the ice cap it was found that during the summer of 1961 lakes were formed and drained within 24 hours. Thus,
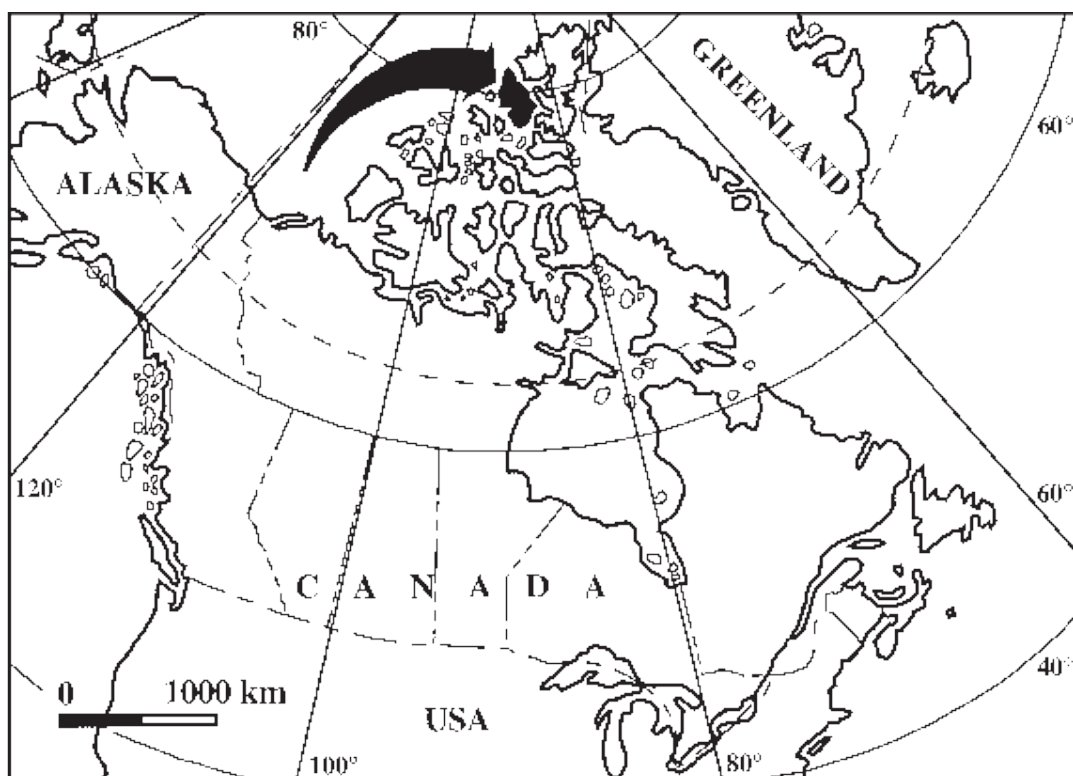


*Figure 1.1: Map showing the location of Axel Heiberg Island [Jagels et al., 2001].*

9
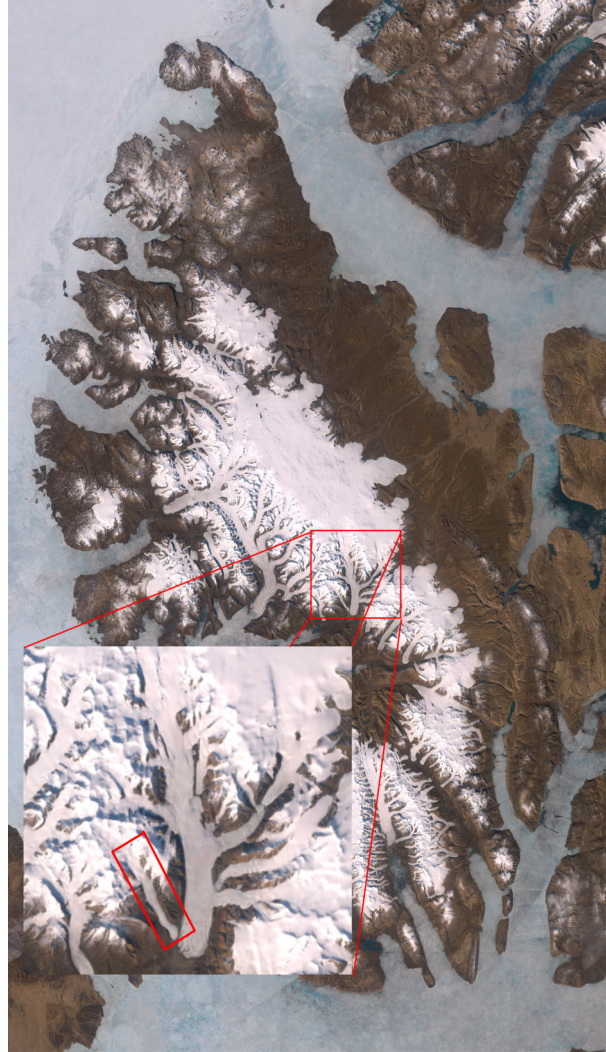
*Figure 1.2: Satellite image of Axel Heiberg Island, the Müller ice cap and White Glacier marked in the red square.*

the entire ice cap was experiencing wet snow in the summer. It was suggested that the very top might remain cold in very cold summers [Müller, 1962]. Because of the limited research conducted on the ice cap, Koerner [1979] did a traverse on the ice cap in 1974 and gathered ice cores studying the accumulation rates from the period 1962-1974. The accumulation rate was found to be around 160-220 kg m$^{-2}$ yr$^{-1}$. From the ice cores, $\delta^{18}O$ was also measured, and it was found that the northwestern part of the ice cap is isotopically warmer than the southeastern part. The northwestern part of the island faces the Arctic Ocean, indicating that the Arctic Ocean works as moisture source in the northwestern part of the ice cap, causing the higher amount of $\delta^{18}O$.

In the later years the ice cap has also been studied using remote sensing data. Winter surface velocity maps, using speckle tracking of radargrams, have yearly been made since 2012 [Van Wychen et al., 2014, 2016]. Furthermore, Thomson et al. [2011] studied the aerial cov-

erage of all ice masses on Axel Heiberg Island in the period of 1959-2001, and found that the area of the Müller ice cap has increased by 1% excluding the outlet glaciers, respectively by 14% including them. Some of this advance can be described by the fact that some of the outlet glaciers are surge type glaciers, but it is also suggested that the ice cover gain can be explained by more ice being transported from higher elevations by increasing ice velocities. Hence, it should be noted that the aerial increase does not necessarily mean volumetric increase.

## 1.2   Scientific perspective

The location of the Müller ice cap is of special interest as it is facing a part of the Arctic Ocean where no full depth ice core has been drilled. Furthermore, there is a chance of finding ice dating back to the Innuitian ice sheet, which was the ice sheet in between the Laurentide and Greenland ice sheet during the last glaciation [England et al., 2006]. This makes the Müller ice cap an interesting place to drill a full depth ice core.

Researchers from the University of Manitoba, Canada, and University of Copenhagen, Denmark, have therefore decided to drill such a full depth ice core on the Müller ice cap. What remains is to determine the optimal location to perform the ice core drilling. This position depends on many parameters, e.g. ice thickness, ice velocity, bedrock topography, surface melt and summer temperatures, and thereby elevation. These effects have to be taken into account to ensure that the highest number of years can be captured and that the ice stratification is such that annual layer counting is possible. The aim of this thesis is thus to create surface velocity maps and estimate the ice thickness of the Müller ice cap. The velocity maps and ice thickness will then be used to narrow down on suggested areas where ground based radargrams are to be conducted forming the base for the final drill location decision.

In this thesis I will first go through the basic theory related to ice flow necessary to follow the subsequent chapters. This will be followed by a chapter on the surface velocities, and three chapters on different methods of estimating the ice thickness. I will then combine these aspects of the thesis into a discussion of advantages and disadvantages of the models. Finally, the thesis is ended by my estimates of the best possible drill areas followed by a short conclusion.

# 2 Theoretical background

This chapter provides a brief overview of the theory behind ice flow necessary to follow the subsequent chapters of this thesis. All theory is based on Cuffey and Paterson [2010] and Greve [2018] and it is further assumed that the reader is familiar with tensors.

## 2.1 Stress, strain and conservation laws

When dealing with the modelling of ice flow, it is of great importance to be able to describe the different forces acting on the ice and how the ice itself reacts to these. This relation is explained by using two quantities; the stress and the strain.

### 2.1.1 Stress

Stress is a measure of how much the ice is being pushed or pulled by external forces and is defined as force per area. The stress tensor, $\boldsymbol{\sigma}$, describes the stress applied on all sides of an infinitesimal cube of ice inside the ice column (see Figure 2.1) and is given by

$$\boldsymbol{\sigma} = \begin{pmatrix} \sigma_{xx} & \sigma_{xy} & \sigma_{xz} \\ \sigma_{yx} & \sigma_{yy} & \sigma_{yz} \\ \sigma_{zx} & \sigma_{zy} & \sigma_{zz} \end{pmatrix} \tag{2.1}$$

where the diagonal elements are the normal stresses and the off-diagonal elements are the shear stresses. It is assumed that the ice is not rotating around itself but instead flows smoothly. This
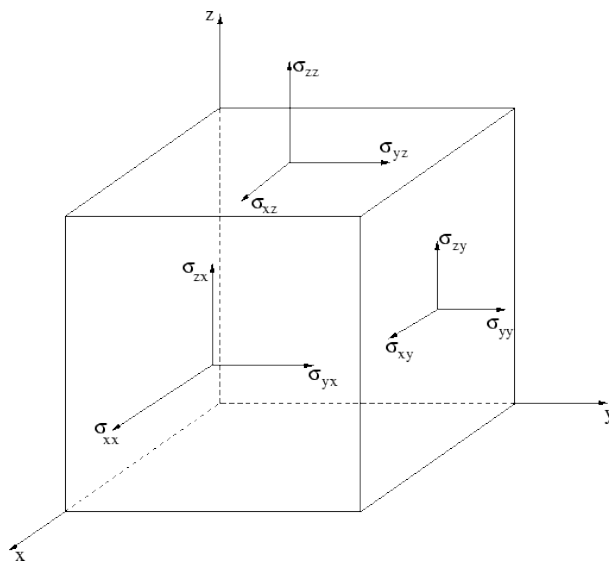


*Figure 2.1: Components of the stress tensor.*

requires the stress tensor to be symmetric ($\sigma_{ij} = \sigma_{ji}$) since angular momentum would not be conserved if $\sigma_{ij} \neq \sigma_{ji}$ and the cube would start to rotate.

Pressure, $p$, is a type of stress and if the ice is only under influence of isotropical pressure, the stress tensor reduces to

$$\boldsymbol{\sigma} = -p\mathbf{I}, \tag{2.2}$$

where $\mathbf{I}$ is the identity matrix. This means that the pressure can be defined as

$$p = -\frac{1}{3}\text{tr}(\boldsymbol{\sigma}) = -\frac{1}{3}(\sigma_{xx} + \sigma_{yy} + \sigma_{zz}). \tag{2.3}$$

For simplification ice is often considered to be an incompressible material, which means that the pressure does not contribute to any deformation of it. Then, instead of dealing directly with the stress tensor, one works with the deviatoric stress, $\boldsymbol{\tau}$, given by

$$\boldsymbol{\tau} = \boldsymbol{\sigma} - \text{tr}(\boldsymbol{\sigma})\mathbf{I}. \tag{2.4}$$

It should be noted that the shear stresses of the stress and deviatoric stress tensors are identical.

## 2.1.2 Strain

Strain, $\boldsymbol{\epsilon}$, describes the deformation of the ice, and like stress it can be divided into normal and shear strain. Consider an ice parcel of length $L$, where some normal stress (pulling) is applied at the end of the parcel in the x-direction. Then the length of the parcel is increased by $\Delta L$, and the strain is defined by

$$\epsilon_{xx} = \frac{\Delta L}{L}. \tag{2.5}$$

When studying ice, the deformation in itself is not an interesting quantity, but rather the change of deformation with time, given as strain rates. Consider the same case as above and let us assume that the deformation happens over a time interval $\Delta t$. Then the strain rate, $\dot{\epsilon}_{xx}$, is defined by

$$\dot{\epsilon}_{xx} = \frac{\epsilon_{xx}}{\Delta t} = \frac{\Delta L}{L\Delta t}. \tag{2.6}$$

When $\Delta t \to 0$, $\dot{\epsilon}_{xx} = \frac{1}{L}\frac{dL}{dt}$ and thus it can be shown that the full strain rate tensor, $\dot{\boldsymbol{\epsilon}}$, reads

$$\dot{\boldsymbol{\epsilon}} = \begin{pmatrix} \frac{\partial v_x}{\partial x} & \frac{1}{2}\left(\frac{\partial v_x}{\partial y} + \frac{\partial v_y}{\partial x}\right) & \frac{1}{2}\left(\frac{\partial v_x}{\partial z} + \frac{\partial v_z}{\partial x}\right) \\ \frac{1}{2}\left(\frac{\partial v_x}{\partial y} + \frac{\partial v_y}{\partial x}\right) & \frac{\partial v_y}{\partial y} & \frac{1}{2}\left(\frac{\partial v_y}{\partial z} + \frac{\partial v_z}{\partial y}\right) \\ \frac{1}{2}\left(\frac{\partial v_x}{\partial z} + \frac{\partial v_z}{\partial x}\right) & \frac{1}{2}\left(\frac{\partial v_y}{\partial z} + \frac{\partial v_z}{\partial y}\right) & \frac{\partial v_z}{\partial z} \end{pmatrix}, \tag{2.7}$$

where $(v_x, v_y, v_z)$ are the velocity components of the ice in the $(x, y, z)$ directions of the velocity field $\mathbf{v}$. Like the stress tensor it can be seen that the strain rate tensor is symmetric.

### 2.1.3 Conservation laws

The fundamental equations to describe how density, velocity and temperature evolve over time can be derived by considering the conservation of mass, energy and momentum. In the following the corresponding conservation laws are given. However, their derivations exceed the scope of this thesis, but can be found in Greve [2018].

The conservation of mass is given by

$$\frac{\partial \rho}{\partial t} + \nabla \cdot (\rho \mathbf{v}) = 0, \tag{2.8}$$

where $\rho$ is the density and $\nabla \cdot$ is the usual sum of the spatial derivatives. In the case where ice is considered an incompressible material eq. (2.8) can be reduced to

$$\nabla \cdot \mathbf{v} = 0. \tag{2.9}$$

The momentum balance reads

$$\rho \frac{\mathrm{d}\mathbf{v}}{\mathrm{d}t} = \nabla \cdot \boldsymbol{\sigma} + \mathbf{f}, \tag{2.10}$$

where $\mathbf{f}$ are direct volume forces such as gravity. Finally the energy balance is described by

$$\rho \frac{\mathrm{d}u}{\mathrm{d}t} = -\nabla \cdot \mathbf{q} + \mathrm{tr}(\boldsymbol{\sigma} \cdot \dot{\boldsymbol{\epsilon}}) + \rho r, \tag{2.11}$$

where $u$ is the specific internal energy, $\mathbf{q}$ is the heat flux and $r$ is the specific radiation power.

## 2.2 Ice flow

### 2.2.1 Glen's flow law

The relation between stress and strain was first described by Glen [1955] and is therefore called Glen's flow law, which writes

$$\dot{\epsilon} = A\tau^n, \tag{2.12}$$

where $A$ is called the creep parameter or rate factor and $n$ is the creep exponent. Glen's flow law was empirically derived in laboratory experiments and is therefore not derived from first principles. The rate factor is temperature dependent and is usually expressed by an Arrhenius law as seen in Figure 2.2. A wide range of studies have tried to find the proper value of the creep exponent, where most agree that it takes a value of approximately 3, but can range from 1 to 4 [Cuffey and Paterson, 2010].

### 2.2.2 Driving stress and basal shear stress

Glaciers and ice sheets flow due to gravity pulling down the ice. This downward force, called the driving stress, $\tau_d$, causes horizontal flow due to the slope of the bedrock and pressure gradients
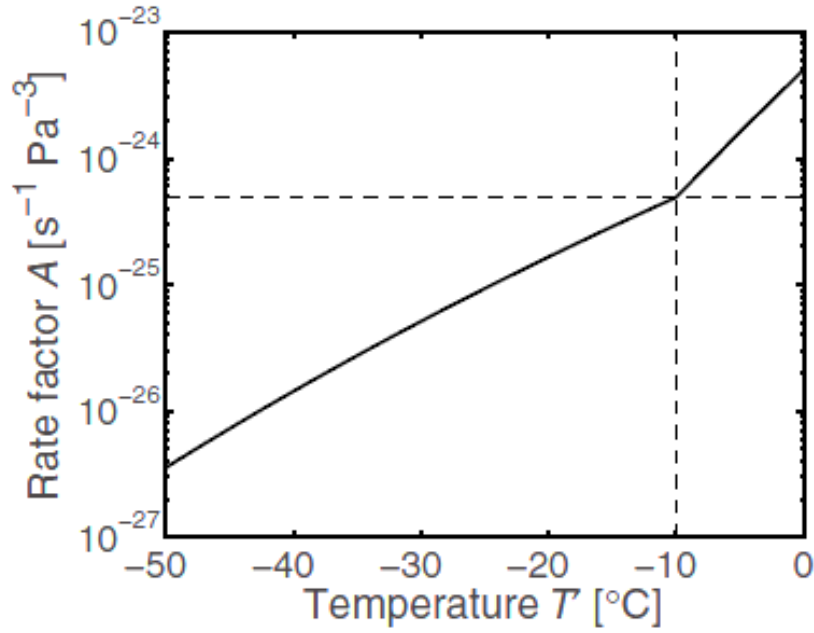
*Figure 2.2: The rate factor as a function of the temperature relative to the pressure melting point, $T'$ [Greve, 2018].*

in the ice. In the case of an ice mass resting on a close to flat bed the driving stress can be well-described by

$$\tau_d = \rho g H \alpha, \tag{2.13}$$

where $g$ is gravity, $H$ is the ice thickness and $\alpha$ is the surface slope. To balance the driving stress there are a number of resistive stresses of which the basal shear stress (or basal drag), $\tau_b$, is considered the most important, and in the simplified cases that will be used in this thesis the driving stress is assumed to be balanced by the basal shear stress such that

$$\tau_b = \tau_d. \tag{2.14}$$

## 2.2.3 Parallel flow

Solving the full system of equations behind glacier flow is very complicated, which is why simpler models are often used. One such model is parallel flow where it is assumed that the glacier deforms by simple bed parallel shear. The problem is reduced to a 2D problem with no flow in the y-direction and thus the deviatoric stress tensor can be reduced to

$$\tau = \begin{pmatrix} 0 & 0 & \tau_{xz} \\ 0 & 0 & 0 \\ \tau_{zx} & 0 & 0 \end{pmatrix}. \tag{2.15}$$

*Figure 2.3: Schematic illustration of parallel flow from Greve [2018]. $t_{xz}$ corresponds to $\tau_{xz}$.*

Since the flow is solely described by bed parallel shear, the vertical velocity of the ice is assumed to be 0. This means that Glen's flow law (eq. (2.12)) in this case reads
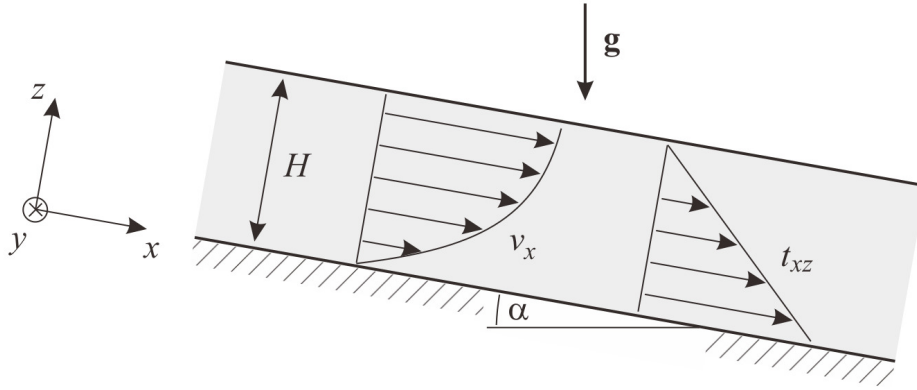
$$\dot{\epsilon}_{xz} = \frac{1}{2}\frac{\mathrm{d}v_x}{\mathrm{d}z} = A\tau_{xz}^n. \tag{2.16}$$

It can be shown that it is reasonable to assume that the shear stress increases linearly with depth [Cuffey and Paterson, 2010]. This means that

$$\tau_{xz} = \tau_b\left(1 - \frac{z}{H}\right), \tag{2.17}$$

with $z$ and $H$ as illustrated in Figure 2.3, which shows a schematic illustration of parallel flow.

Substituting eq. (2.17) into eq. (2.16) and integrating from the bottom ($z = 0$) to $z$ gives the velocity $v(z)$ at depth $H - z$

$$v(z) = v_b + \frac{2A}{n+1}\tau_b^n H\left(1 - \left(1 - \frac{z}{H}\right)^{n+1}\right), \tag{2.18}$$

where $v_b$ is the velocity at the base of the ice. From this the surface velocity, $v_s$ can be found by setting $z = H$

$$v_s = v_b + \frac{2A}{n+1}\tau_b^n H \tag{2.19}$$

An integration from 0 to $H$ of eq. (2.18) gives the ice flux, $Q$, and the depth averaged velocity, $\bar{v}$,

$$Q = v_b H + \frac{2A}{n+2}\tau_b^n H^2 = \bar{v}H \tag{2.20}$$

## 2.2.4 Shallow ice approximation

In parallel flow only flow in the $x$-direction is taken into consideration, which is not very suitable when studying ice caps or ice sheets. By using the same approximation that the ice deforms by

simple bed parallel shear, but in both the $x$- and $y$-directions the deviatoric stress tensor reads

$$\boldsymbol{\tau} = \begin{pmatrix} 0 & 0 & \tau_{xz} \\ 0 & 0 & \tau_{yz} \\ \tau_{zx} & \tau_{zy} & 0 \end{pmatrix}. \tag{2.21}$$

This approximation is called the shallow ice approximation (SIA) and it can be shown that the exact same equations as in parallel flow are also valid here, where $v_s, v_b$ and $\bar{v}$ are the magnitudes of the surface-, basal- and depth averaged velocity respectively. For the SIA to hold it is assumed that the horizontal extent of the ice is much greater than the vertical extent. This assumption is equivalent to assuming that the bed slopes are assumed to be sufficiently small. If this is not the case the SIA breaks down and its predictions can not be trusted.

# 3 Surface velocities from feature tracking

Knowing the surface velocity of the Müller ice cap is essential in the process of deciding upon the drill site location, as high surface velocities can make the process of determining the age of the layers more difficult. Furthermore, if the ice velocity down the ice column is not more or less equal to zero, upstream corrections have to be made, as one cannot assume that the ice in the ice core originates from that specific point on the surface.

For deriving surface velocities from remote sensing data several techniques exist of which feature tracking [Raup et al., 2014] is the technique used in this thesis. Feature tracking can be done both using radar and optical data to find matching features like crevasses, patterns, debris etc. by image correlation. When doing feature tracking of optical data like satellite images, this results in a whole grid of displacements which contains information about the direction and magnitude of the surface flow. In this thesis I am using feature tracking of optical satellite images to find surface velocities of the Müller ice cap. To do so I have used the Image GeoRectification And Feature Tracking for python (pyImGRAFT) which is an open source algorithm developed by Messerli and Grinsted [2014]. In this chapter I will describe how I have used pyImGRAFT, present my results and discuss them briefly.

## 3.1 Deriving surface velocities using pyImGRAFT

ImGRAFT is a feature tracking toolbox created by Messerli and Grinsted [2014] from which I have used the python version of the templatematch toolbox. The templatematch toolbox looks for features in a given template region in an optical image and searches for those same features in a given search region on another image taken at some later time. The feature tracking is done using orientation correlation where the orientation of intensity gradient is calculated in each pixel in the template region, to be matched with similar orientation of intensity gradient in the search region of the second image [Fitch et al., 2002]. Figure 3.1 shows a schematic illustration of the tracking process with template and search region.

The needed size of the template and search region varies from site to site and from what kind of features that can be tracked. On ice caps and ice sheets the template region has to be rather large to capture enough features to be tracked. In faster flowing areas such as outlet glaciers where there are a lot of crevasses and other features that can be tracked, a smaller template region can be used. The optimal search width should have a size where the features in the fastest flowing regions are captured within it. This latter criteria also really depends on the time in between the two images that are being tracked.

In the case of the Müller ice cap the goal is to capture the ice cap well, since that is where
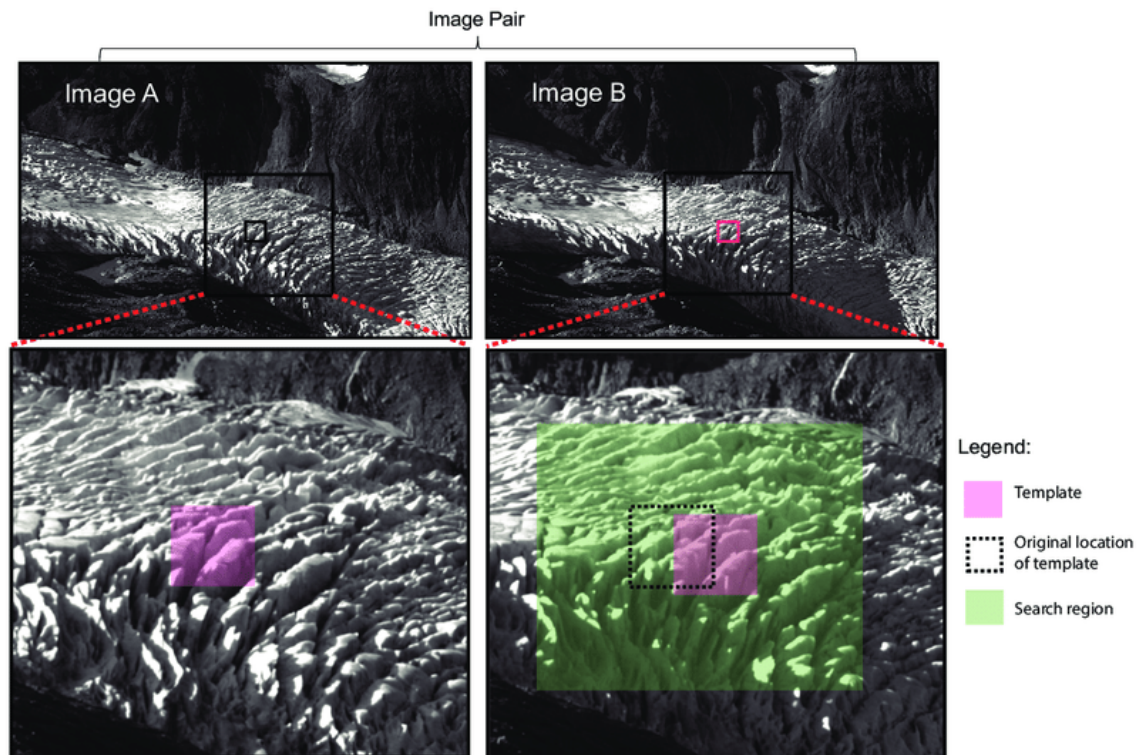
*Figure 3.1: Schematic diagram to show the different components of the templatematch process [Messerli and Grinsted, 2014].*

we want to drill an ice core. Therefore, the template region is chosen to fit the ice cap and not the outlet glaciers in the west (see Figure 1.2). To make sure all velocity maps are on the same grid, one can give a grid as input to the templatematch algorithm, where I have used a 900 $\times$ 900 m grid using UTM 15N (EPSG:32615).

## 3.1.1 Satellite images

The optical data used as input to pyImGRAFT are images from the Landsat 7 and 8 satellites. Landsat 7 was launched in 1999 and is still active today, though the Scan Line Corrector failed in May 2003 [NASA] resulting in stripes of missing pixels in the images which will be explained in Section 3.1.1.1. Landsat 8 was launched in 2013 and the mission is still going flawlessly. For both Landsat 7 and 8 I have used the panchromatic band which essentially is a black and white image, and has a resolution of 15 m for both satellites.

In order to run pyImGRAFT, I need to pair up the different available scenes, whilst taking into account certain criteria. The scenes should be from the same satellite (so either Landsat 7 or 8) and from the same path and row. Furthermore they should be almost cloud free over the ice cap and cover most of it. In the process of choosing the right satellite images I have used

both Landsat 4-5, 7 and 8. I have manually checked which path and row combinations cover most of the ice cap, presented in Table 3.1.

To detect clouds on the ice cap one could use the quality assessment band. However, I found that the computational time to unpack all of the bits and detect whether there where clouds or not on the ice cap was much longer than visually going through all of the images. Some scenes do have a small amount of clouds on the ice cap or on the outlet glaciers. This should not cause any problems with pyImGRAFT since these areas simply will not be tracked by the templatematch. Furthermore, the images should be from the summer months (June-September) to ensure sufficient sun light for the tracking. This requirement was also checked manually. Some scenes are removed due to too little sun light. This is mostly the case for dates from mid to late September.

*Table 3.1: Path and row combinations of scenes that cover the Müller ice cap. Path row combinations marked with (\*) do not cover the entire ice cap.*

| PATH | ROW |
|------|-----|
| 056 | 002 |
| 087 | 242 |
| 055 | 002 (*) |
| 057 | 002 |
| 058 | 002 |
| 054 | 003 (*) |
| 060 | 002 |
| 059 | 002 |

The last criteria for the scenes to become an image pair is the time step between them. To find the sufficient time step, template, and search region, is a matter of trial and error. I found that a time step between the two images of around one year combined with a template region of 208 × 208 pixels and a search region of 208+33 × 208+33 worked rather well on the ice cap. On the ice cap it was not possible for me to do feature tracking between two scenes from the same summer (eg. a scene from June and a scene from late August/early September) since the ice simply had not moved enough to be able, to track it. Thus a time step of around one year was used and I have chosen that any scene from June-September can be paired with any scene from June-September the following year as long as the above mentioned criteria are met. No pairs where made from Landsat 4-5 since the criteria were not met. A total of 71 and 45 pairs were made from Landsat 7 and 8, respectively, ranging from 2004/5 to 2018/19 (see Table 3.2).

*Table 3.2: Number of image pairs per satellite and tracking year.*

| Satellite | Year | Image pairs | Satellite | Year | Image pairs |
|-----------|------|-------------|-----------|------|-------------|
| Landsat 7 | 2004/2005 | 1 | Landsat 7 | 2012/2013 | 5 |
| Landsat 7 | 2005/2006 | 4 | Landsat 7 | 2013/2014 | 9 |
| Landsat 7 | 2006/2007 | 5 | Landsat 8 | 2014/2015 | 16 |
| Landsat 7 | 2007/2008 | 8 | Landsat 8 | 2015/2016 | 17 |
| Landsat 7 | 2008/2009 | 5 | Landsat 8 | 2016/2017 | 3 |
| Landsat 7 | 2009/2010 | 11 | Landsat 8 | 2017/2018 | 4 |
| Landsat 7 | 2010/2011 | 13 | Landsat 8 | 2018/2019 | 5 |
| Landsat 7 | 2011/2012 | 10 | | | |

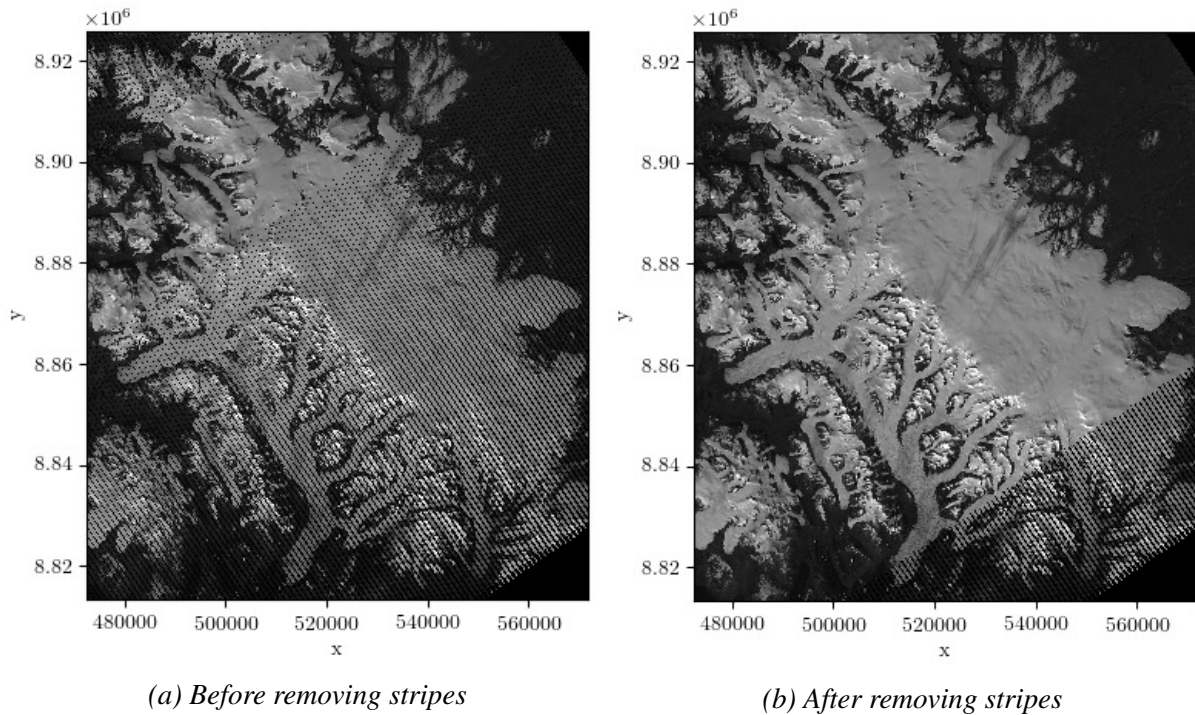*(a) Before removing stripes*                    *(b) After removing stripes*

*Figure 3.2: Removal of stripes on Landsat 7 images using a random number from the gaussian distribution from a 10 pixels radius from the pixel with a missing value.*

### 3.1.1.1 Removing stripes from Landsat 7 scenes

In May 2003 the scan line corrector on Landsat 7 failed [NASA], resulting in stripes with missing values on the satellite images (see Figure 3.2a). In some cases this causes templatematch to track the stripes instead of the ice, see Appendix A for an example of this. To reduce this issue I fill each empty pixel with a random number from the gaussian distribution created from the values of the pixels in a 10 pixels radius from the pixel with a missing value. This also means that if an empty pixel is surrounded by empty pixels in a 10 pixels radius, the pixel will remain empty. With this method a large part of the stripes are taken care of. In order to apply this method to all of the areas with missing values a radius of 30 pixels has to be chosen, corresponding to 450 m. I believe that it would be too crude to assume that the brightness of a point 450 m away is representative for the brightness of that specific point, why I did not use a radius of 30 pixels. Figure 3.2 shows an example of an original satellite image from Landsat 7 with stripes (left) and the same image after the above described method has been applied (right).

## 3.2 Feature tracking

The feature tracking is done using the templatematch function in pyImGRAFT. The inputs to the function are the two satellite images to be tracked (stripe corrected images in the case of

Landsat 7). To ensure that all outputs from the feature tracking process are on the same grid, I use my before mentioned $900 \times 900$ m grid. This is transformed into pixel coordinates, i.e. the pixel coordinates in the first satellite image which you want to track in the second satellite image. Furthermore, the template and search width has to be specified, which were set to be 208 pixels corresponding to 3120 m and 241 pixels (3615 m), respectively. These numbers can seem rather arbitrary. The explanation for that is that the size order was determined by the fact that I wanted to be able to capture the ice cap well, rather than the outlet glaciers. The exact size of the template and search width was a results of a performance test of pyImGRAFT, as the computational time depends strongly on the difference between the size of the template and search width. The reason for that is found in the fast Fourier transformations in pyImGRAFT. Changing the template or search width with just one pixel can potentially double the computational time. Finally, an initial guess of displacement is needed in the feature tracking function, thus if there is any offset between the two satellite images due to the georeferencing of the images, this should be reflected in the initial guess of displacement.

The output from the feature tracking contains the actual pixel centers of the templates in the first satellite image. They might differ slightly from the input of pixel coordinates because of rounding. Furthermore it contains the displacement between the two satellite images. If there is any offset between the image pairs I substract the offset from the displacements. The output also contains the correlation coefficient of the matched template, the mean absolute correlation coefficient over the search region, the signal-to-noise ratio and the feature tracking method. In the case of pyImGRAFT, the only method available is the orientation correlation as mentioned before.

The output is cleaned using the build-in cleaning function in templatematch. Tracked pixels will be replaced by NaNs if the local strain is greater than 0.05 or if the signal-to-noise ratio is less than 1. This cleaning process is done three times for all tracked image pairs. Obviously the signal-to-noise ratio and the strain does not change after cleaning, but in the cleaning function also lies that if a given pixel has a NaN value in one of the 8 neighboring pixels, that given pixel will also be returned as NaN. Hence, after cleaning several times, there will not only be NaNs in areas where the strain is too high or the signal-to-noise ratio is too low, but also in the surroundings of these pixels. It should be noted that the maximum allowed strain and the minimum signal-to-noise ratio used in this thesis is not the same as in the original source code available on GitHub. In the original source code of templatematch the maximum strain and the minimum signal-to-noise ratio are 0.1 and 1.02 respectively, meaning that I have chosen to be more conservative in the cleaning process than implemented in the original source code.

This process of feature tracking is done for all of the 118 image pairs on my personal computer. In the case of Landsat 8 image pairs the computational time is around 2-3 minutes for each pair. With Landsat 7 the computational time is around 5-6 minutes due to the process of

removing stripes.

The displacement output from templatematch is in pixels per time between the two images. This is transformed to m yr$^{-1}$ using 1 year = 365.25 days for all of the image pairs, resulting in 118 velcoity maps on the 900 × 900 m grid with the standard units of m yr$^{-1}$. The velocity maps contains three layers, two layers containing the x- and y-component ($v_x$ and $v_y$) of the velocity vector (**v**) and the third layer containing the magnitude of the velocity ($v$) calculated by

$$v = \sqrt{v_x^2 + v_y^2}. \tag{3.1}$$

Even though the output from templatematch is cleaned, there are still some outliers present in the velocity maps. These outliers are mostly due to melt, clouds, or in the case of Landsat 7, the removal of stripes. The clouds can happen to have the same intensity pattern as the ice, and thus false tracking can be an issue when clouds are present. Melt darkens the intensity of the ice and can thereby have an influence. The story of the stripes sort of writes itself, as "false features" can be created in the process of filling the stripes using the method as described previously.

## 3.3 Velocity map results and discussion

Figure 3.3 and Figure 3.4 show the median of all Landsat 7 and Landsat 8 velocity maps respectively. A figure of the median Landsat 8 velocity map with flow directions can be seen in Appendix B. It can be seen that all areas have been tracked in the Landsat 8 velocity map, with higher velocities on the outlet glaciers in the west and on the ice tongues in the east. The same pattern can be seen in the Landsat 7 velocity map, though not all areas have been captured in the feature tracking process. To have a closer look on why this is the case we look at the yearly median velocity maps which are shown in Figures 3.5, 3.6 and 3.7. In all of the yearly median Landsat 7 velocity maps it can be seen that there are gaps on the ice cap where templatematch has not been able to track anything. Obviously, clouds play a role here, as some of the satellite images do suffer from these, but they cannot be the main factor. In the interior of an ice cap one would assume the surface velocities to be very low, if not almost zero. Therefore, these gaps may be a result of the choice of template and search size together with the time in between the image pairs. Furthermore, the removal of stripes may also cause issues at places with low velocity, as small changes and errors in the brightness of the surface can result in false feature tracking and in no feature tracking at all. Looking at the yearly median Landsat 8 velocity maps in Figure 3.7 it can be seen that there are much fewer gaps where templatematch has not been able to track anything. This suggests that the stripes in the Landsat 7 images are the main factor behind the non trackable areas. From Table 3.2 it should be noted that the difference between the number of image pairs per year does not play a big role since Figures 3.5c, 3.5e, 3.6c and
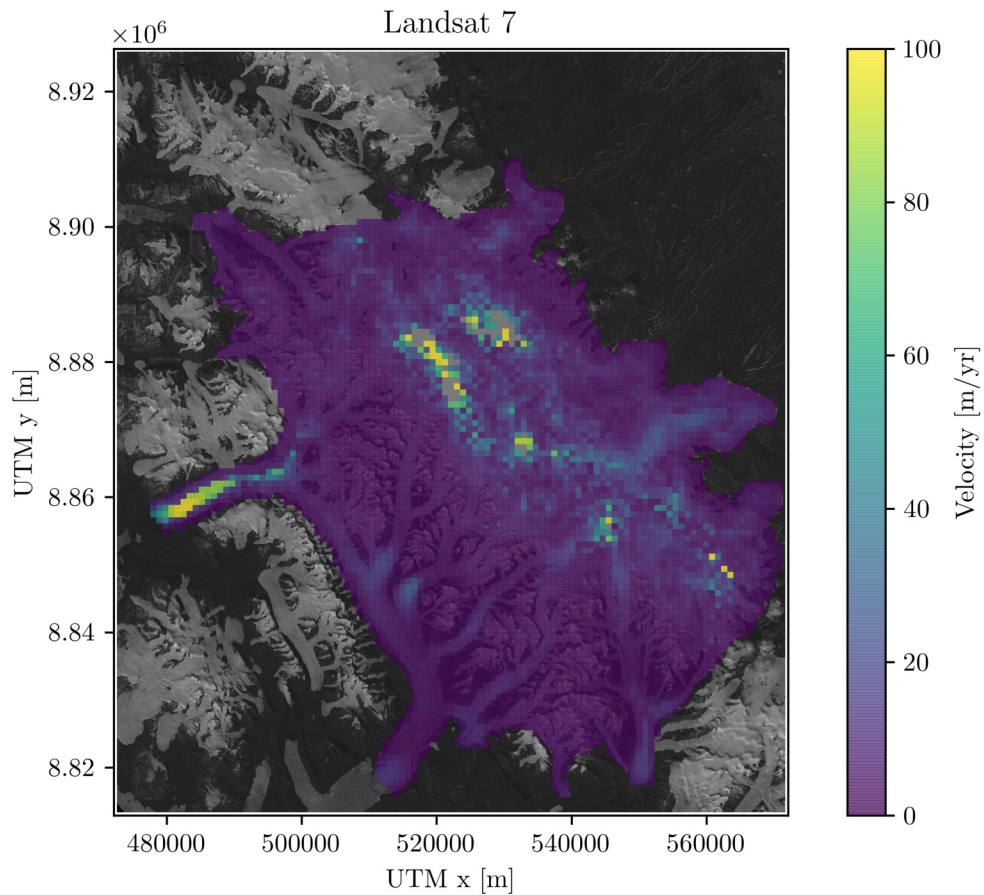
*Figure 3.3: Median of all Landsat 7 velocity maps.*

3.7e are all medians of 5 image pairs. Further, there is clearly a difference between the velocity maps from Landsat 7 and 8.

The Landsat 7 velocity maps does not only suffer from gaps, but also from unrealistic high velocities in the interior of the ice cap. This is mainly due to false feature tracking which very well could be a result of the stripes, or rather the removal of stripes. If I had used a smaller search region it would not have been possible to track such high velocities, or correspondingly, features so far away from the template region (see Figure 3.1). Choosing a smaller search region would have caused problems on the outlet glaciers in the west, as I may not have been able to catch the ice flow. Though the aim of this project is to capture the ice cap well, I still want to be able to catch the outlet glaciers somewhat, why I chose not to decrease the search region.

There are cases of unrealistic high velocities in the interior of the ice cap from the Landsat 8 velocity maps (see Figures 3.7c and 3.7d), though the issue is more pronounced in the Landsat 7 velocity maps. In the Landsat 8 velocity maps it is more a signal of too few image pairs available. This means that false tracking has a higher impact when taking the median of the velocity maps.

The bad coverage and high velocities in the interior of the Landsat 7 velocity maps has lead
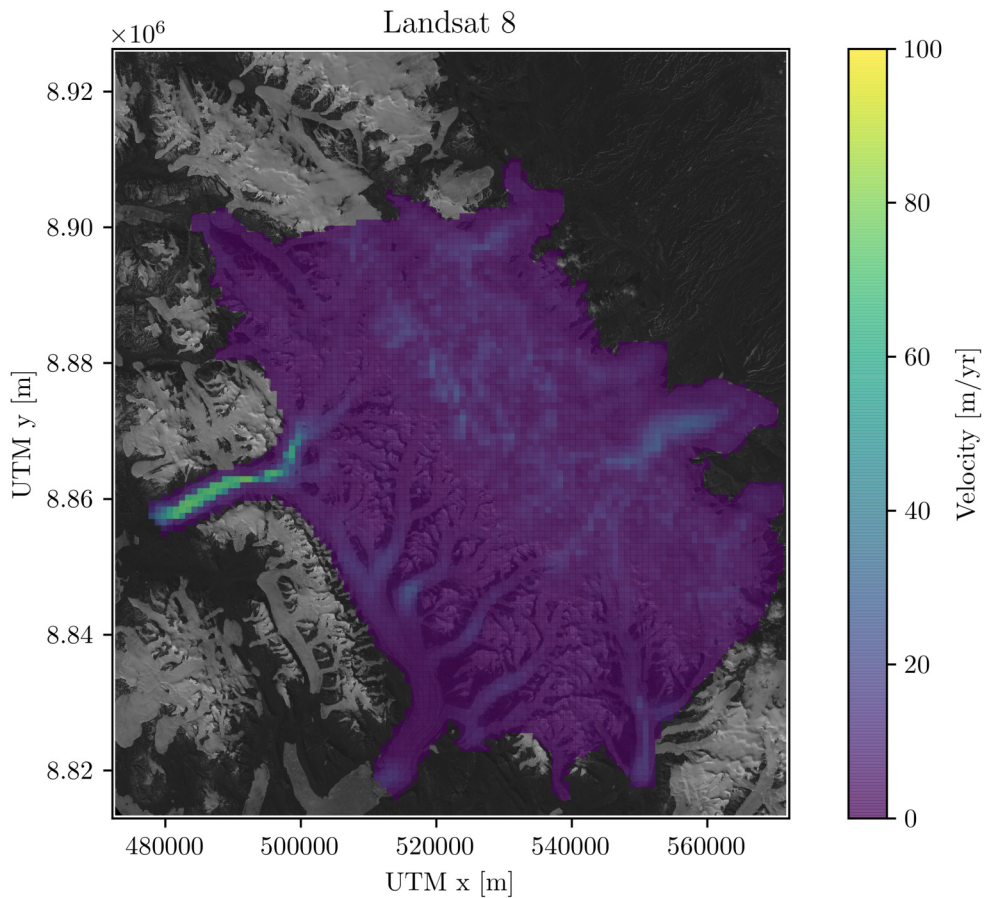
*Figure 3.4: Median of all Landsat 8 velocity maps.*

me to the conclusion of using the Landsat 8 median velocity map in Figure 3.4 as reference frame for this project. It is available as a GeoTIFF on Zenodo (`https://doi.org/10.5281/zenodo.4290041`) alongside with a list of all Landsat 8 images used in the feature tracking process.

To estimate the uncertainty, $\sigma_v$, of the velocity map I have calculated the deviation between the direction of the median Landsat 8 velocity and the slope from the Arctic Digital Elevation Model (ArcticDEM) [Porter et al., 2018]. The ArcticDEM version used in this thesis has been preprocessed such that any gaps has been filled by interpolating over the gaps. In practice there was no gaps in the domain used in this thesis. Furthermore the resolution has been reduced to 130 m. The uncertainty is then calculated using

$$\sigma_v = \text{std}\left(|\mathbf{v} \times \text{norm}(\boldsymbol{\alpha})|\right), \tag{3.2}$$

where std is the standard deviation and norm($\boldsymbol{\alpha}$) is the normalised surface slope in both the x- and y-directions. The uncertainty is being calculated in areas of 5×5 grid cells and can be seen in Figure 3.8.

This way to estimate uncertainty is rather conservative as ice does not always flow down
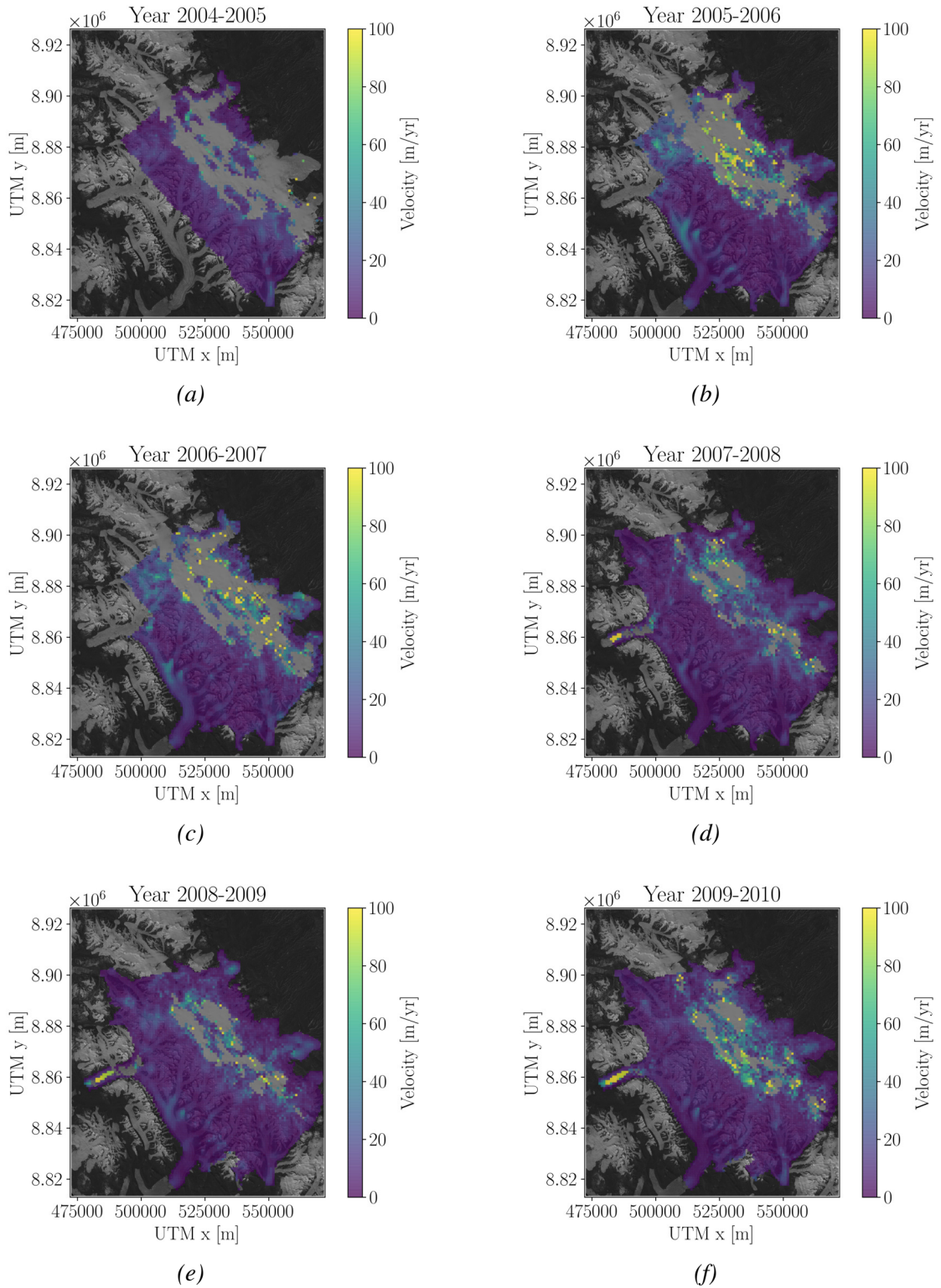
*Figure 3.5: Yearly median of the Landsat 7 velocity maps in the period 2004/2005-2009/2010*
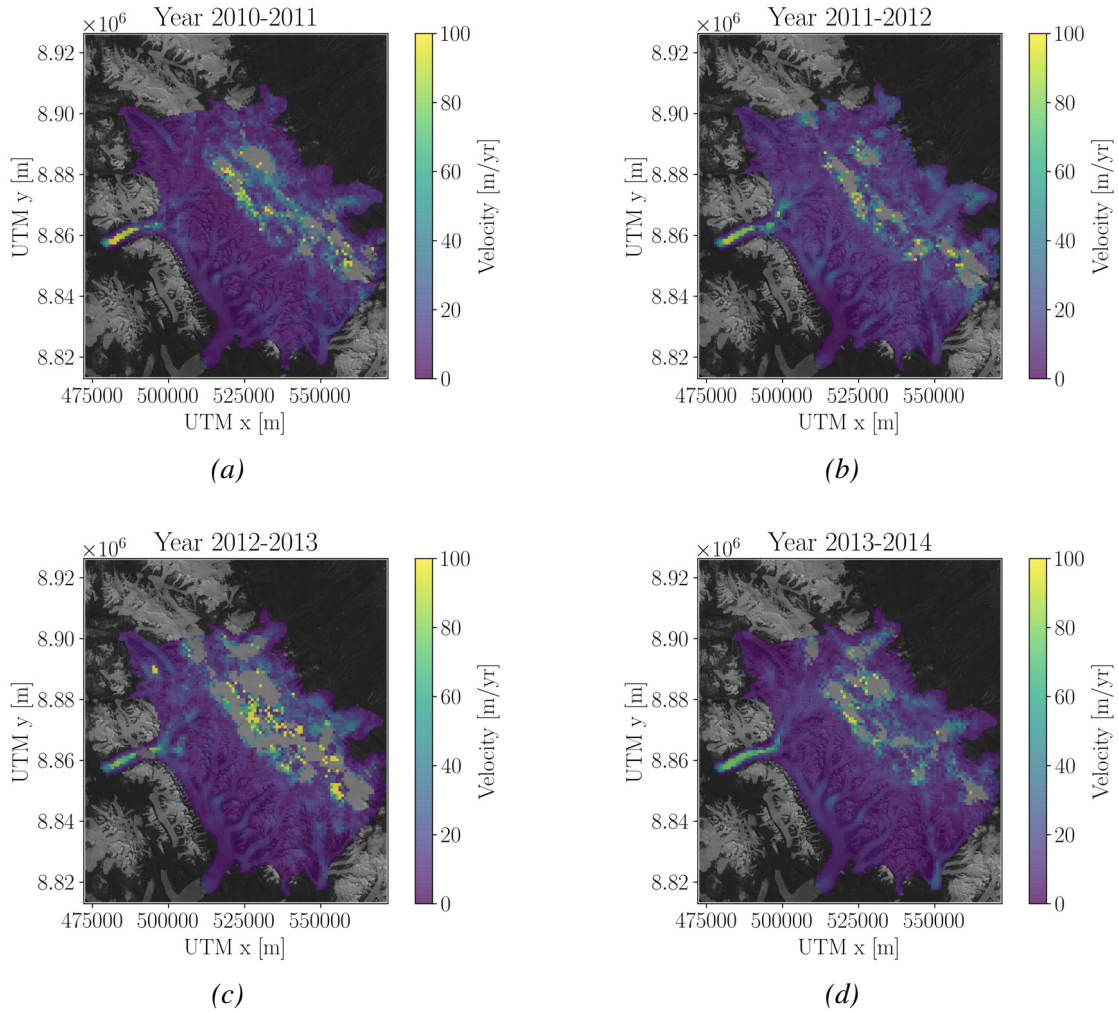
*Figure 3.6: Yearly median of the Landsat 7 velocity maps in the period 2010/2011-2013/2014*

slope, especially not in fast flowing areas such as outlet glaciers where there might be bumps in the bedrock that the ice is flowing over, which also can be seen in Figure 3.8. In general it can be seen that the uncertainty is relatively low except for the above mentioned case. The average uncertainty is 0.9 m yr$^{-1}$ and if I exclude the outlet glacier where the uncertainty reaches 16-28 m yr$^{-1}$, the average uncertainty is 0.7 m yr$^{-1}$.

To compare with existing velocity products of the Müller ice cap, Figure 3.9a shows the median velocity map from 2014-2019 from Van Wychen et al. [2014]. The velocity maps are made using speckle tracking of RADARSAT-2 images with 24 days in between the images and have a mean error along the ice divide of 6.6 m yr$^{-1}$. One image pair from each winter in the period from 2014-2019 is being used to calculate the median. The resolution of the orginal product is 100 m, but in Figure 3.9a I have interpolated it onto my $900 \times 900$ m grid.

Figure 3.9b shows the absolute difference between my median Landsat 8 velocity map (Figure 3.4) and the Van Wychen et al. [2014] median velocity map. Focusing on Figure 3.4 and 3.9a it can be seen the the general pattern and magnitudes of the velocities are the same, es-

*(a)*

*(b)*

*(c)*

*(d)*

*(e)*
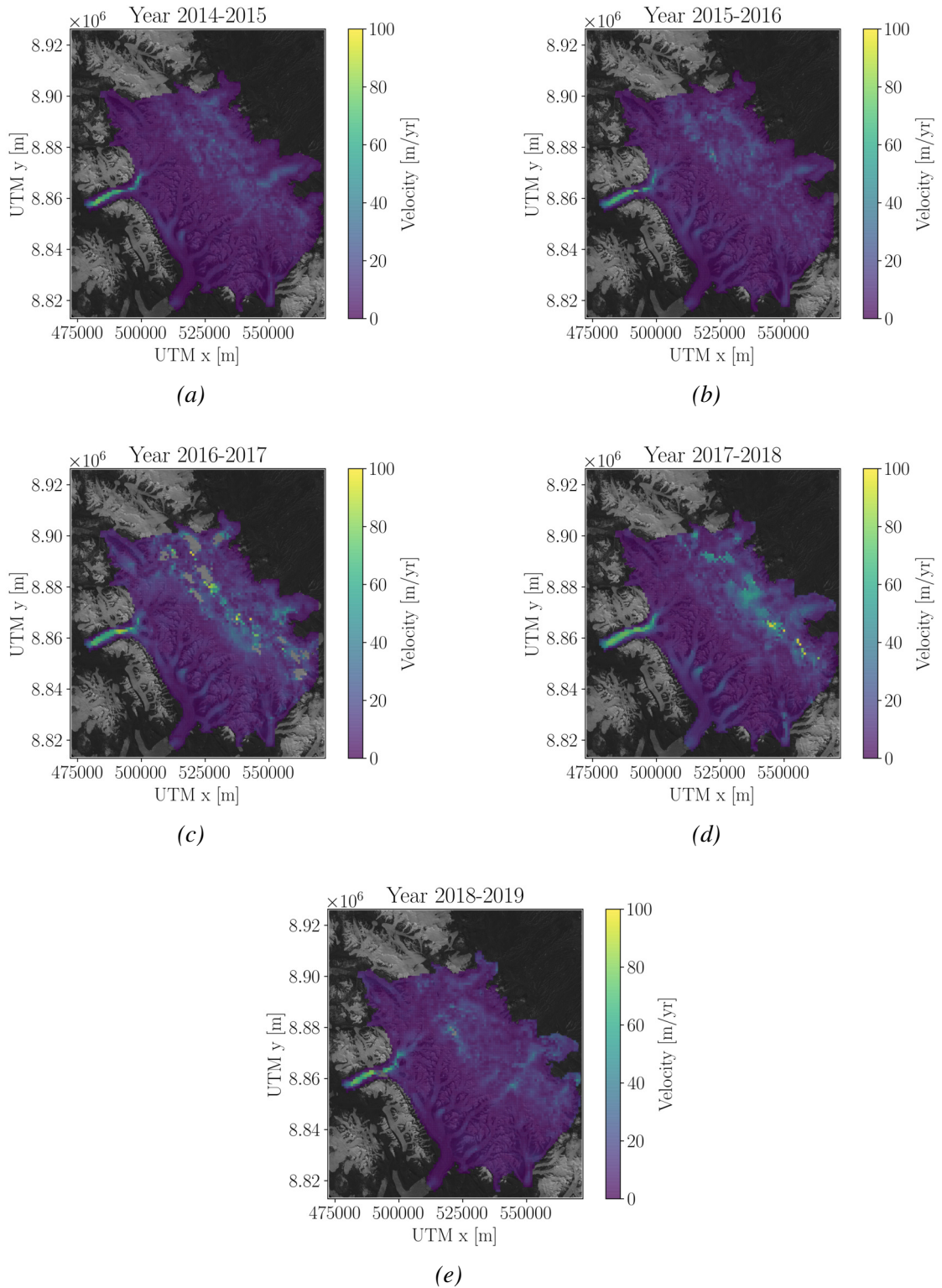
*Figure 3.7: Yearly median of the Landsat 8 velocity maps in the period 2014/2015-2018/2019*
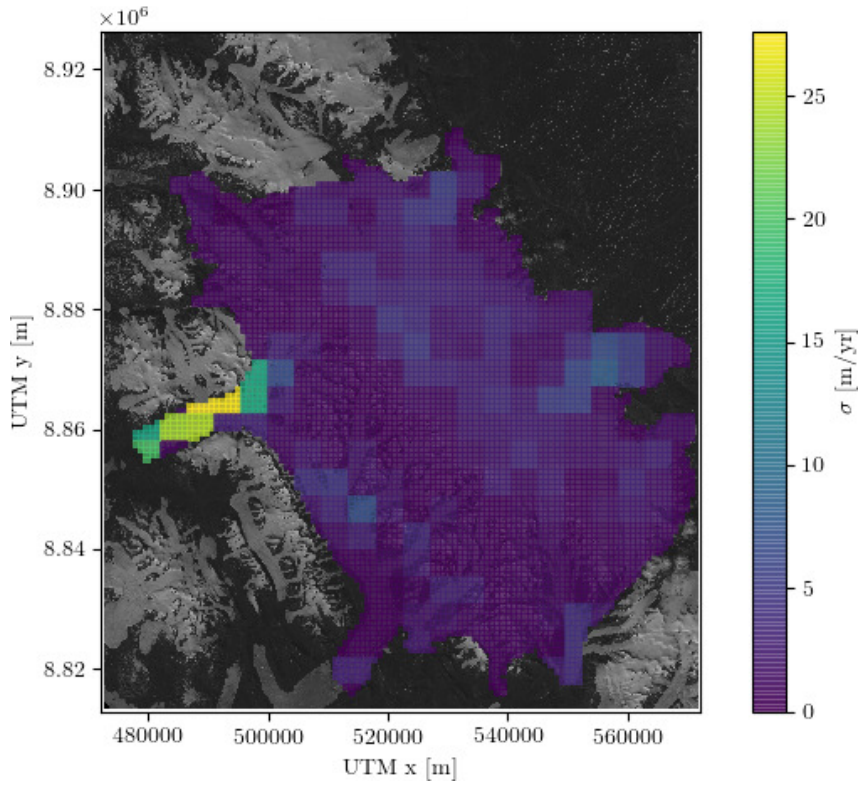
*Figure 3.8: Deviation between the direction of the median Landsat 8 velocity and the slope from ArcticDEM.*



*(a)*        *(b)*
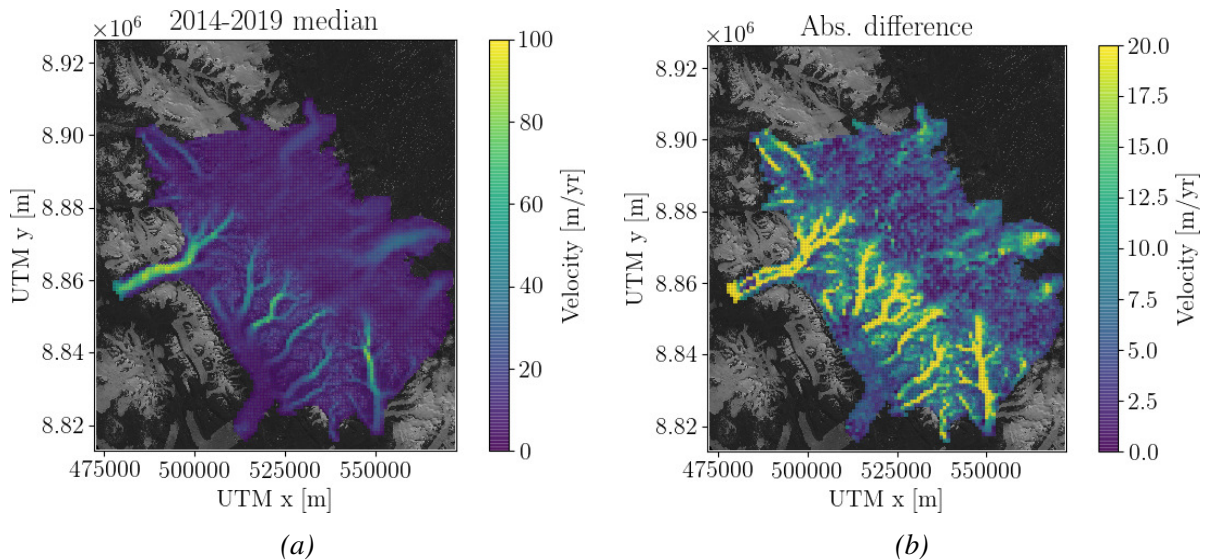
*Figure 3.9: (a) Median velocity map from 2014-2019 using the velocity data from Van Wychen et al. [2014]. (b) Absolute difference of my median Landsat 8 velocity map and the Van Wychen et al. [2014] median velocity map. The absolute difference reaches 86 m yr$^{-1}$ in some of the outlet glaciers.*

pecially on the ice cap. Due to the original greater resolution on the Van Wychen et al. [2014] velocity maps, the smaller outlet glaciers are captured much better. This causes a very high absolute difference between the magnitudes of the velocities in these areas, reaching as high as 86 m yr$^{-1}$. This issue was also mentioned in Section 3.1. If I had chosen a grid and a template and search region that would capture all of the outlet glaciers, I would not have been able to capture the ice cap. To go about this problem I could of course have chosen to run pyImGRAFT twice for every image pair, one capturing the outlet glaciers and one capturing the ice cap and then have combined the results afterwards with different resolutions in the two parts of the domain. Due to my focus being on the tracking of the ice cap, I chose not to pursuit this method.

# 4 Bedrock inversion using the Parallel Ice Sheet Model

Several approaches on estimating the ice thickness are used in this thesis. This chapter presents the first of those methods, and will be followed by chapters presenting the other approaches.

In this chapter I will describe how I have used the Parallel Ice Sheet Model (PISM) to model the Müller ice cap to estimate the bedrock topography. First I will introduce the model (stable version 1.1.4) of PISM [the PISM authors, 2018]. Then I will go through the method used to model the bedrock and conclude with a discussion of my results.

## 4.1 PISM background

PISM is an open source time-dependent thermomechanically coupled ice sheet model that solves an approximated version of the Stokes equations [Bueler and Brown, 2008, the PISM authors, 2018]. Solving the full thermomechanically coupled Stokes equations is computationally costly, which is why many ice flow models attempt to solve different approximated versions of them.

PISM takes advantage of the shallowness of ice sheets to simplify the Stokes equations to the SIA and the Shallow Shelf Approximation (SSA) to save computational time. Furthermore, as the name of P(arallel)ISM indicates, the model is parallelised for optimisation, which is a great advantage if one has access to a supercomputer.

### 4.1.1 The shallow approximations

The SIA, explained in Section 2.2.4, is a good approximation in ice sheets where the horizontal extent is much greater than the vertical. This means that the flow is relatively simply (except at the margin) and can be described by bed-parallel shear.

A sketch of a typical velocity profile using the SIA can be seen in Figure 4.1 to the left. One can add sliding to the SIA by setting the basal velocity equal to some fraction of the surface velocity, which is the case for the lighter grey area of the left figure in Figure 4.1.

In the SIA longitudinal stresses are neglected, but if you for instance think of an ice shelf floating on water, where there no longer is a bedrock to prevent the ice from stretching, the longitudinal stresses are suddenly very important and can not be neglected. In that case one would use the SSA instead of the SIA. In the SSA the ice is assumed to have the same velocity from top to bottom as can be seen in the center of Figure 4.1, since the ocean below the ice can be treated as a "free surface".
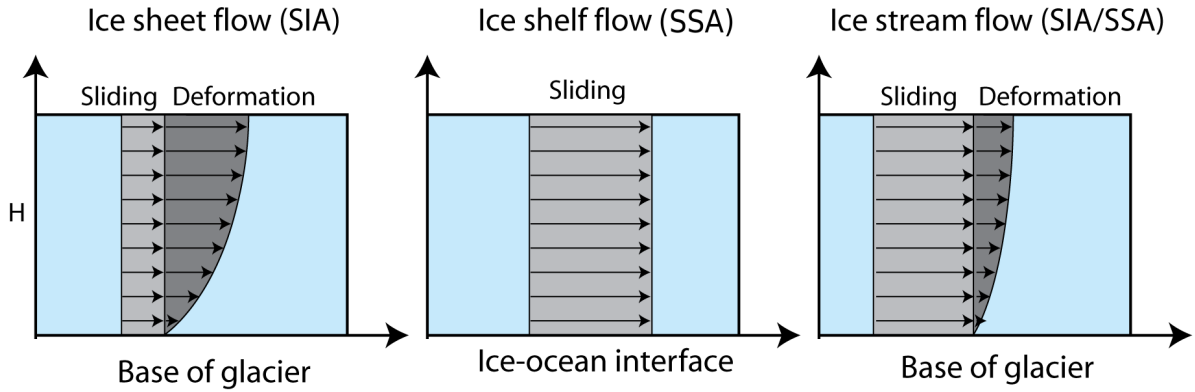
*Figure 4.1: Vertical velocity profiles from AntarcticGlaciers.org and Kirchner et al. [2011].*

Other cases where it is important to take the SSA into account is when the ice is not flowing over hard bedrock, but over soft sediment like subglacial till which is highly deformable. In these cases the basal shear stress will be much lower than that described from the geometry and the overburden load as in the SIA where $\tau_b = \rho g H \alpha$. To describe these cases where there is a deformable bedrock that still causes some basal shear stress one can use a combination of the SIA and SSA. The velocity profile of the combined approximation can be seen to the right in Figure 4.1. This coupled model is also a good approximation in fast flowing outlet glaciers and ice streams.

## 4.1.2   Hybrid model

In PISM one can choose to use the hybrid model [the PISM authors, 2018], which is a combination of the SIA and SSA. The SIA and SSA is run in parallel in every single grid cell and time step, where the SSA is used as a sliding law. It is assumed that the basal shear stress, when sliding occurs, is [Bueler and Brown, 2008, Schoof, 2006]

$$\boldsymbol{\tau_b} = -\tau_c \frac{\mathbf{v_{SSA}}}{\left(v_{SSA_x}^2 + v_{SSA_y}^2\right)^{1/2}}. \tag{4.1}$$

$\mathbf{v_{SSA}}$ is the horizontal velocity using the SSA and $v_{SSA_x}$ and $v_{SSA_y}$ are the two components of the SSA velocity vector. $\tau_c$ is the yield stress, which controls when sliding occurs or not. If the applied stress reaches the yield stress, the ice will start sliding, otherwise the basal shear stress is described by the SIA only. The yield stress is calculated using the Mohr-Columb model [Bueler and Brown, 2008, Cuffey and Paterson, 2010]

$$\tau_c = \tan \phi (\rho g H - p_w), \tag{4.2}$$

where $p_w$ is the pore water pressure and $\phi$ is the till friction angle, which is a strength parameter for the subglacial till.

To couple the SIA and SSA the velocities from the two models are combined such that the final horizontal velocity $\mathbf{v}$ for further computations is

$$\mathbf{v} = f(|\mathbf{v_{SSA}}|)\mathbf{v_{SIA}} + (1 - f(|\mathbf{v_{SSA}}|))\mathbf{v_{SSA}}, \tag{4.3}$$

where

$$f(|\mathbf{v_{SSA}}|) = 1 - \frac{2}{\pi}\arctan\left(\frac{|\mathbf{v_{SSA}}|}{100^2}\right) \tag{4.4}$$

and $\mathbf{v_{SIA}}$ is the horizontal SIA velocity.

This hybrid model is what I have chosen to use when modelling the thickness of the Müller ice cap, since I from satellite images (see Figure 1.2) and velocity maps (see Figures 3.3 and 3.4) know that there are regions with higher velocities where sliding most likely does occur.

## 4.2 Data

To run the coupled SIA+SSA hybrid model in PISM the input file has to contain:

- A grid with x and y coordinates

- Bedrock topography

- Ice thickness

- Surface temperature

- Surface mass balance

- Geothermal heat flux

The grid that I have used to run PISM is the exact same $900 \times 900$ m grid as I have used for my velocity maps. It is used as basis for both input and output data from PISM.

An initial guess for the bedrock topography is needed, and for that I have used Farinotti et al. [2019] (henceforth referred to as the Farinotti bedrock). The Farinotti bedrock is from a global ice thickness estimate of all glaciers and ice caps worldwide and is made from up to five different models [Frey et al., 2014, Fürst et al., 2017, Huss and Farinotti, 2012, Maussion et al., 2019, Ramsankaran et al., 2018]. It is the icing on the cake originating from the Ice Thickness Models Intercomparison eXperiment (ITMIX) [Farinotti et al., 2017], which compares 17 different ice thickness models. The ITMIX results showed that more models would lead to a more robust result, why up to five different models were used in Farinotti et al. [2019].

The Farinotti bedrock has a resolution of approximately 130 m, and is made using flow bands to reduce the problem from 3 to 2 dimensions. The glaciers and ice caps are divided into flow basins, extrapolating the flow band results into the flow basins, thus on some of the borders

*(a)*

*(b)*

*(c)*

*(d)*
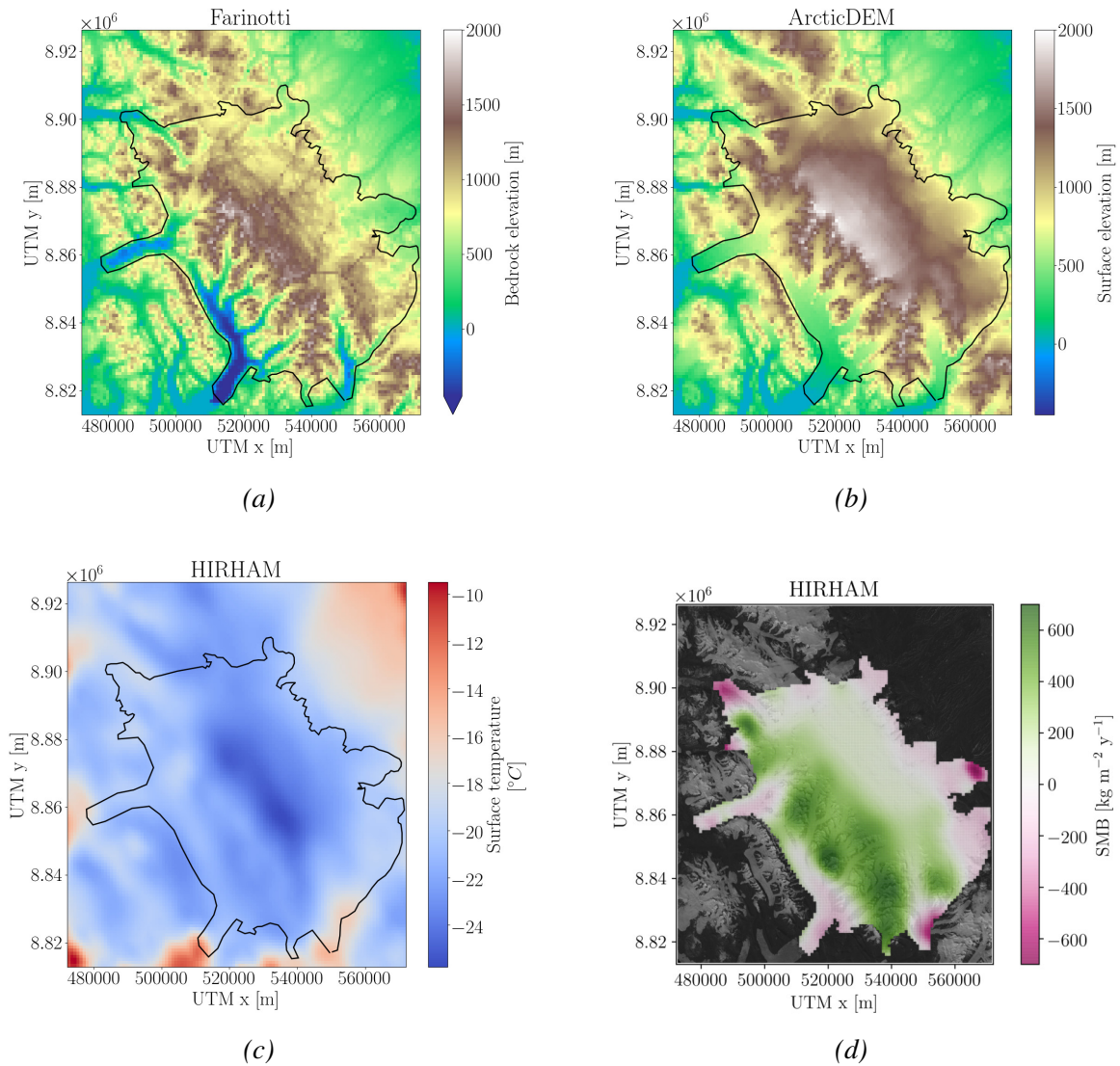
*Figure 4.2: Input data of (a) bedrock topography, (b) surface elevation, (c) surface temperature, and (d) surface mass balance, all on the 900 × 900 m grid.*

between those flow basins, there are NaN values in the data set. These NaN values have been replaced with the value from ArcticDEM in the corresponding position. Places with no ice in the Farinotti bedrock, which are also NaN values, have been treated in the same way. After doing this the bedrock is interpolated onto my grid and can be seen in Figure 4.2a. In hindsight, I should probably have interpolated over the missing values in between the basins, rather than replacing them with values from ArcticDEM. On the other hand it might not have caused much difference since the bedrock is interpolated from a rather fine grid onto my coarser grid.

The initial guess for the ice thickness is simply ArcticDEM substracted by the Farinotti bedrock. It is assumed that ArcticDEM represents the ground truth surface elevation, and it can be seen in Figure 4.2b.

The surface temperature and the surface mass balance (SMB) is obtained from the Regional

Climate Model HIRHAM5 [Langen et al., 2017, Mottram et al., 2017] (henceforth referred to as HIRHAM). I have used the mean value from 1980-2014 and 1980-2016 for the surface temperature and the SMB, respectively. The resolution of HIRHAM is 5 km. The mean SMB on the ice cap from HIRHAM is 72.3 kg m$^{-2}$yr$^{-1}$. I have tried to find in-situ measurements of the SMB of the ice cap, but as mentioned most of the research on Axel Heiberg Island has been focused around White Glacier (see Figure 1.2), which also is the case when it comes to SMB measurements [Cogley et al., 1996, Müller, 1962, Thomson et al., 2016]. Except for Koerner [1979] who did a traverse on the ice cap and found that in the period from 1962-1973 the average yearly accumulation was around 160-200 kg m$^{-2}$ yr$^{-1}$. Due to the sparse SMB measurements from the ice cap I chose to go with HIRHAM. To prevent much ice growth outside of the current ice cap, I have set the SMB to be zero outside of the ice margin. Figure 4.2c and 4.2d shows the HIRHAM surface temperature and HIRHAM SMB on the 900 × 900 m grid, respectively.

Finally, the geothermal heat flux is set to be 0.055 W m$^{-2}$ everywhere on the grid based on Figure 2.4 in Minnick et al. [2018].

## 4.3   Modelling purpose and procedure

To generate a best guess of the ice thickness and thereby also bedrock topography, I have used an iterative inverse method [Koldtoft et al., 2020, Pelt et al., 2013] by tuning to the surface elevation, $S_{DEM}$, from ArcticDEM assuming that the ice cap is in steady state. PISM is used as a forward model in this process, where the bedrock, $B$, and the ice thickness, $H$, is changed after each iteration, $i$, using

$$B_{i+1} = B_i - K(S_i - S_{DEM}) \tag{4.5}$$

$$H_{i+1} = S_{DEM} - B_{i+1}. \tag{4.6}$$

Here $K$ is a relaxation parameter which takes the value 0 below 500 m elevation. It then increases linearly from 500-1000 m elevation, reaching the value of 0.5 at 1000 m elevation. The relaxation parameter is there to prevent overcompensation when changing the bedrock topography. Initially I used a uniform relaxation parameter of 0.5, but that caused the bedrock to lower drastically underneath the outlet glaciers west of the ice cap. Thus, since I am mainly focused at resembling the main ice cap, I chose this linearly increasing relaxation parameter instead, to make sure not to change the bedrock too much underneath the outlet glaciers. The low bedrock (and thereby also great ice thickness) also influenced the flow on the ice cap, since the ice was dragged into the outlet glaciers.

### 4.3.1 Modelling choices

Since the properties of the bedrock are unknown, 12 combinations of till friction angle and enhancement factor, $E$, are modelled. The tested values of till friction angle and enhancement factor are

$$\phi \in \{10, 20, 30, 40\} \tag{4.7}$$

$$E \in \{1, 3, 6\}. \tag{4.8}$$

Every time the bedrock is changed after a forward modelling with PISM, the difference between the modelled surface elevation and ArcticDEM should become smaller with the number of iterations until a minimum is reached. In the ideal world one would continue making iterations until that minimum is reached, but here computational time also needs to be taken into account. Furthermore the closer your initial geometry is to the ground truth, the fewer iterations you need. For this study I have chosen to do 10 iterations based on the results from Koldtoft et al. [2020], resulting in 120 runs of PISM. It should be noted that one is not guaranteed that the misfit between measured surface elevation and modelled surface elevation will reduce after each iteration. However, this iterative inverse method which I am using have shown promising results in other studies [Koldtoft et al., 2020, Pelt et al., 2013].

In the forward PISM modelling, it would be ideal to run the ice cap until steady state in each iteration. Once again, this is not possible due to the computational load. Instead I chose to run PISM for 2000 years with the argument, that if the surface elevation is still off after 2000 years, changes in the bedrock should be made. One might need more iterations than 10 to reach the minimum possible misfit between the modelled surface elevation and ArcticDEM.

I have used two different criteria for the ice margin when running PISM. One where the ice is allowed to grow outside of the current ice margin, and one where the ice is cut off at the current ice margin, by using the `ocean_kill` calving option in PISM. In the latter case I have set the bedrock to -100 m outside of the current ice cap and added a mask to the input file in PISM. At all places where the initial ice thickness $H \neq 0$ the mask is set to grounded ice. At places where $H = 0$ and all 8 surrounding cells also have an ice thickness of $H = 0$ the mask is set to ice free ocean. In all other cases the mask is set to ice free bedrock. Notice that my mask does not contain any floating ice.

## 4.4 Practical concerns when running PISM

As mentioned, PISM is build to run in parallel, why one can speed up the computational time by using more than just one core. The number of optimal cores depends on the size of the modelling domain, though one would think that the more cores the merrier. Because the cores

need to communicate their boundary values of the domains to the other cores, simply increasing the number of cores does not result in a faster calculation. There is a sweet spot, where the communication overload of multiple cores is balanced by the increase in computational power of more cores. The super computer that I have had access to during my thesis has 17 nodes with 16 cores per node (I will call these "small nodes") and 12 nodes with 32 cores per node (these will be called "big nodes"). It has a hard time limit of 12 hours, meaning that a job will be stopped if it is still running after 12 hours.

To find the optimal number of cores to run on I tried different combinations where I would run one forward model of PISM for 2000 years and compare the computational time. The combinations that I tried were 1 small node, 2 small nodes, 1 big node and 2 big nodes. I found that running on 1 big node was the fastest, where running on 2 big nodes was slightly slower. For the small nodes it was faster to run on 2 than on 1, but both slower than running on the big nodes. Due to this test I decided to run on 1 big node when possible.

The time it took a 2000-year forward run of PISM, varied from around 10 minutes to only having reached a couple of hundred years after 12 hours. This is due to the fact that PISM changes the time step continuously depending on how fast the ice flows and deforms. One way to go around the problem of hitting the time limit would be to run much fewer years making sure not to hit the time limit and then do that until 2000 years is reached, change the bedrock and go on from there. The problem about this method is that every time I start a PISM run, the job is put into the queue on the super computer, and would sometimes be in that queue for up to 1-2 weeks before the job would start, due to the high traffic and my low priority on the super computer. If I had to run only 100 years at a time, this would mean that to complete 10 iterations, I would not only be in the queue 10 times but 200 times. In this way I would not be able to complete the runs in time for my final deadline. Luckily, Aslak had an extra stationary computer with 8 cores that he did not use, why I chose to finish the iterations of those simulations that would hit the time limit on that computer. On this stationary computer I obviously had no time limit, hence it did not matter how long time the simulations would take, as long as they would be done within the time frame of my thesis.

## 4.4.1 Deciding on a margin criteria

Due to the long computational time I realised that I would not be able to finish all of the iterations for all parameter combinations for the two different margin criteria previously mentioned. Therefore, I had a look at the results on those runs that I had finished to decide on which method I would complete all runs with.

Figure 4.3a and 4.3b show the velocity maps with streamlines at year 2000 in the 10th iteration of PISM with $\phi = 10$ and $E = 1$ with and without `ocean_kill` respectively. It can be seen that the `ocean_kill` criteria results in high surface velocities at the margin compared
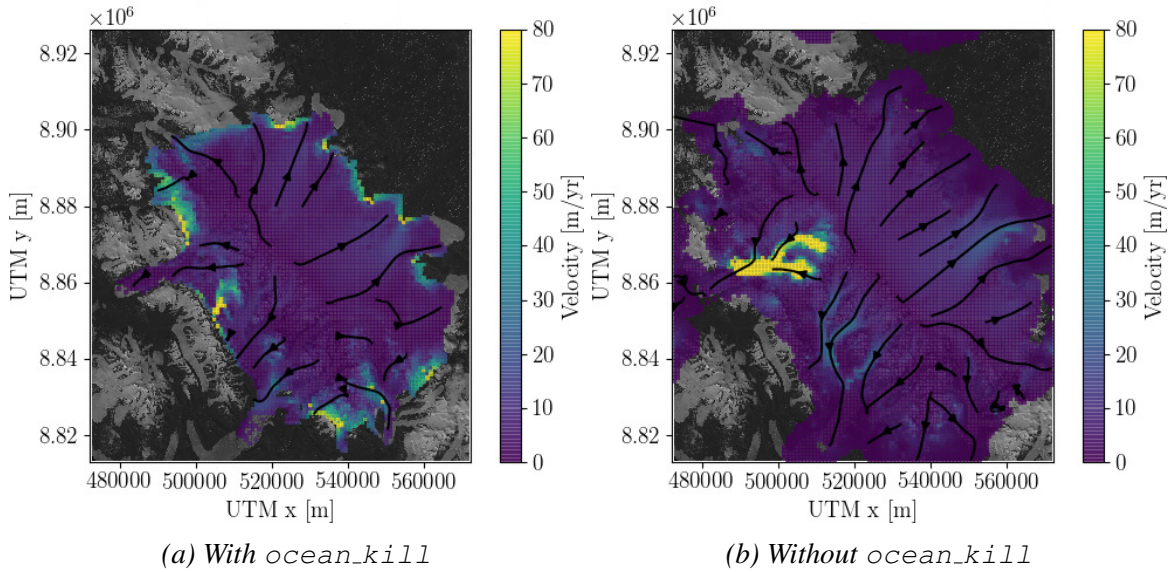
*(a) With* `ocean_kill`    *(b) Without* `ocean_kill`

*Figure 4.3: Velocity maps with streamlines at year 2000 in the 10th iteration of PISM with $\phi = 10$ and $E = 1$ with active* `ocean_kill` *(a) and without active* `ocean_kill` *(b). The upper limit of the colour bar is chosen for easy comparison, the highest velocities are 446 m $yr^{-1}$ and 1259 m $yr^{-1}$ for (a) and (b) respectively.*

to the one with free margins. The high velocities at the margin are a direct result of cutting off ice at the margin using `ocean_kill`. It can be seen that Figure 4.3b shows more similarity with my feature tracked velocities in Figure 3.4.

Figures 4.4a and 4.4b show a cross section of the modelled bedrock topography after each iteration of PISM with and without `ocean_kill` respectively. Like in the velocity maps (Figure 4.3) these cross sections are the result of using a till friction angle of $10°$ and an enhancement factor of 1. The outline of the ice in the figures are based on the surface elevation from Arctic-DEM and the ice thickness measured with radar from Operation IceBridge [Paden et al., 2010, updated 2019] (henceforth referred to as IceBridge). It can be seen that the two models differ the most around $0 - 37$ km and $82 - 110$ km. Figure 4.5 shows the IceBridge flight line, where the red line in the southernmost area of the ice cap is the $0 - 37$ km section, the blue line starting from the south moving north and then west corresponds to the $37 - 82$ km section, and the second red line of the flight line is from $82 - 110$ km. This means that the two models differ mainly at the outlet glaciers and less in the inner part of the ice cap.

I chose to use a margin criteria without an active `ocean_kill` mainly based on the velocity maps in Figure 4.3. This combined with the fact that the runs using `ocean_kill` in general were slower and thereby I would have to rely more on the 8 cores stationary computer than the runs without `ocean_kill`.

*(a) With* `ocean_kill`
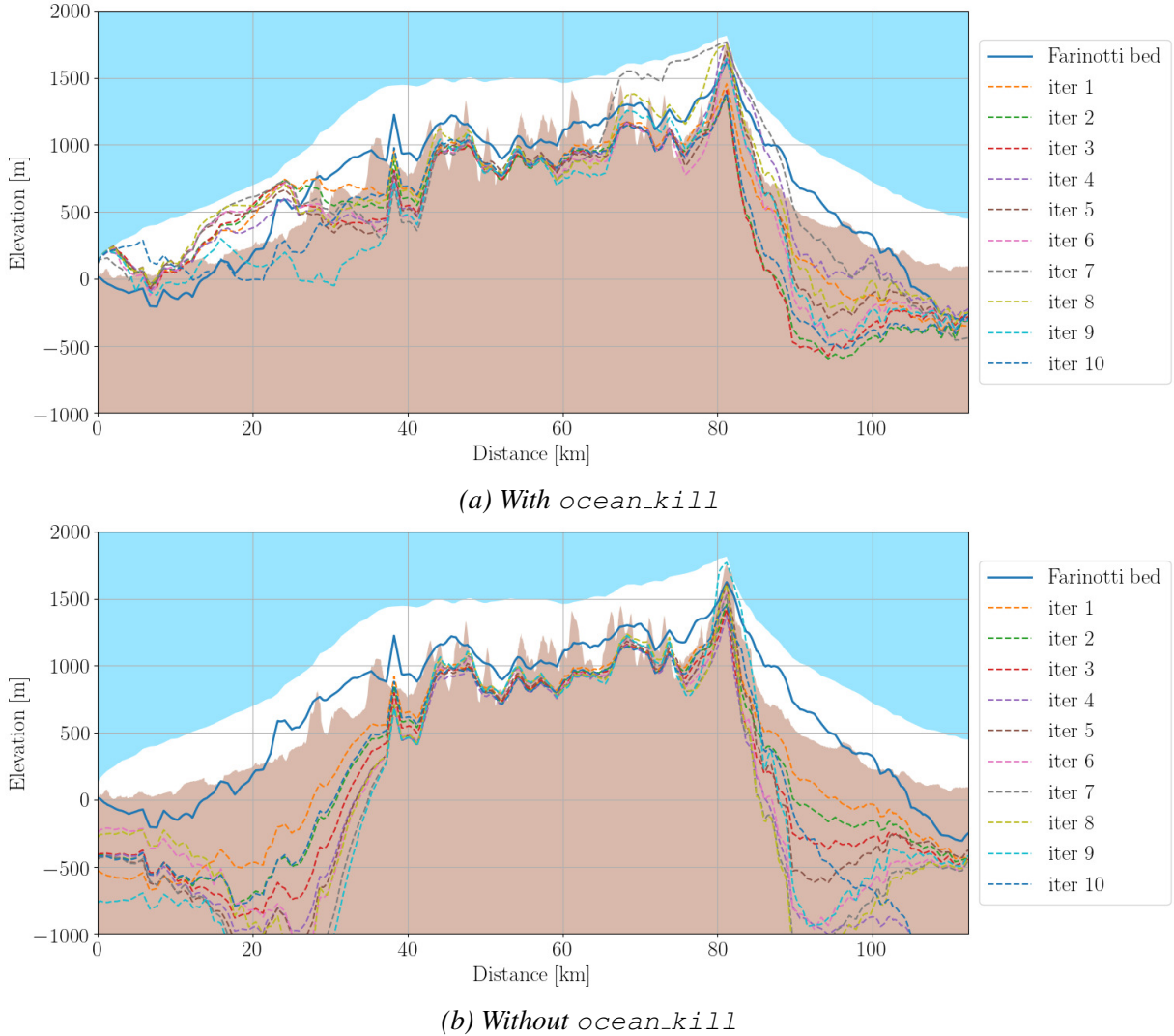


*(b) Without* `ocean_kill`

*Figure 4.4: Cross sections of the modelled bedrock topography after each iteration of PISM with* `ocean_kill` *(a) and without (b) using* $\phi = 10$ *and* $E = 1$.

## 4.4.2 Final PISM setup

The final setup of PISM is in "raw" PISM command as follows

```
pismr −i iter0.nc −bootstrap −y 2000 −Mx 111 −My 126 −Mz 201 −z_spacing equal −Lz
    4000 −sia_e 1 −ssa_e 1 −stress_balance ssa+sia −pseudo_plastic −plastic_phi 10 −
    stress_balance.sia.limit_diffusivity true −extra_file extra_iter0_10_1.nc −
    extra_vars thk,topg,usurf,velsurf,velsurf_mag,tempbase −extra_times 0:100:2000 −
    ts_file ts_iter0_10_1.nc −ts_times 0:10:2000 −o iter0_10_1.nc &> out.iter0_10_1
```

Breaking it into parts `pismr -i iter0.nc -bootstrap` initiates PISM's bootstrapping, meaning that it creates the entire PISM modelling field using what is present in the `iter0.nc` file as described in Section 4.2 and the commands to follow. `-y 2000 -Mx 111 -My 126 -Mz 201 -z_spacing equal -Lz 4000` tells PISM to run for 2000 years using a $111 \times 126$ point grid in the horizontal direction and a 201 point grid in the vertical direction
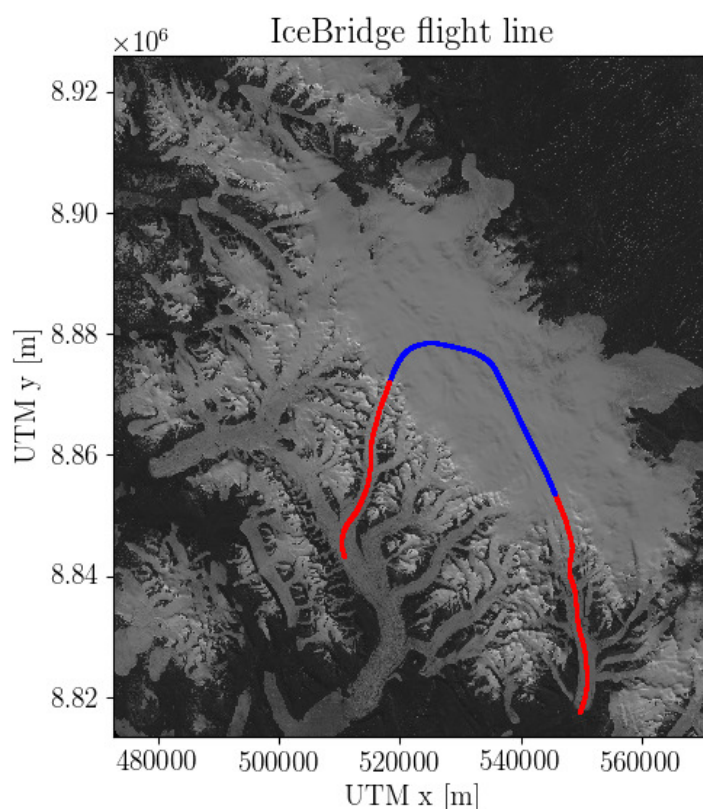
*Figure 4.5: Operation IceBridge flight line. The southernmost red line is from 0-37 km, the blue line is from 37-82 km and the second red line is from 82-110 km.*

with even space in between the grid points to an altitude of 4000 m. `-sia_e 1 -ssa_e 1 -stress_balance ssa+sia -pseudo_plastic -plastic_phi 10` sets the enhancement factor to 1 in both the SIA and SSA, tells PISM to use thy hybrid model (SSA+SIA), enables the pseudo plastic power law (if this is not enabled the flow will be purely plastic) and sets the till friction angle to 10°. Around the outlet glaciers in the west there are areas with high surface slopes where there in reality is no ice as a result of these high surface slopes. When snow/ice is deposited on such sites in PISM it will cause high diffusivity and since the time step in PISM is controlled by the diffusivity, I have to remove the upper diffusivity limit by setting `-stress_balance.sia.limit_diffusivity true`. If this is not done the ice flow in these areas will be too high to be captured in the time step which would otherwise be used and this would cause PISM to fail. Since I am not concerned with capturing the outlet glaciers well I have simply chosen to go about this problem of high diffusivity in this way. Alternatively I could set the SMB highly negative in these areas, which in hindsight could have been computationally advantageous as the time step becomes smaller and smaller with increasing diffusivity. `-extra_file extra_iter0_10_1.nc -extra_vars thk,topg,usurf,velsurf,velsurf_mag,tempbase -extra_times`
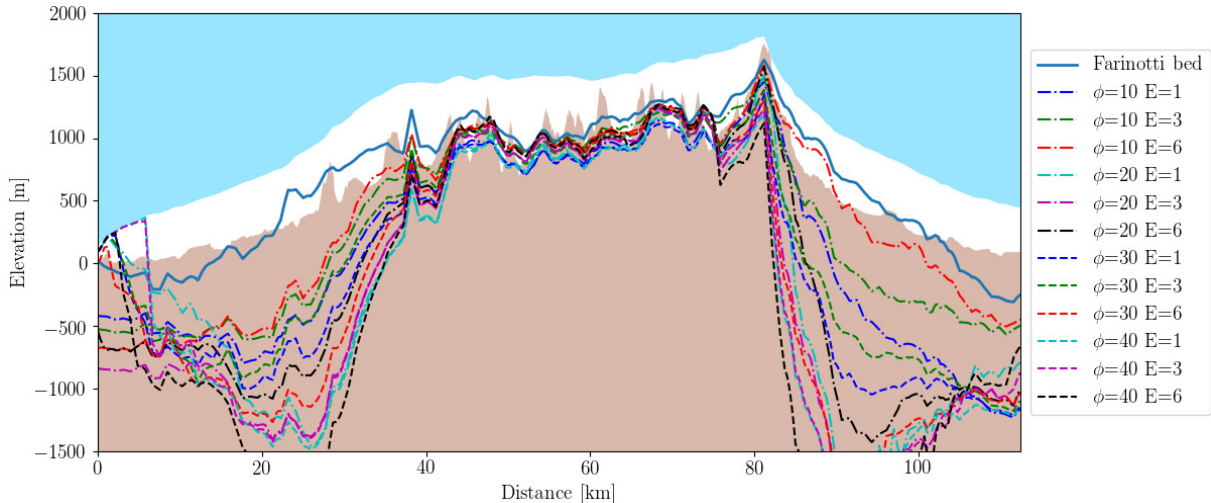
*Figure 4.6: Cross section of the final bedrock topography of all the PISM runs.*

`0:100:2000 -ts_file ts_iter0_10_1.nc -ts_times 0:10:2000 -o`
`iter0_10_1.nc &> out.iter0_10_1` creates all of the output files. First an extra file which contains ice thickness, bedrock topography, surface elevation, surface velocity, magnitude of the surface velocity and the basal temperature at every 100th year from year 0 to year 2000. It should be noted that the bedrock topography does not change at all during a PISM run, as isostasy is not taken into consideration, why it is foolish of me to have added it to the extra file. A file with decadal variables of glacier volume and other features is created and finally the final output of running PISM for 2000 years is created together with an `out.`-file describing each and every time step.

This is how every iteration of PISM is done. The full code including the changing of the bedrock after each iteration can be seen in Appendix C.

## 4.5  PISM results and discussion

Figure 4.6 shows a cross section of the final bedrock topography of all the PISM runs and the Farinotti bedrock topography, with the ice cap outline given by the surface elevation from ArcticDEM and the ice thickness from IceBridge. It should be noted that the output from PISM is interpolated onto the IceBridge flight line which has a resolution of approximately 15 m. In the figure it can be seen that the models differ the most at the outlet glaciers and have more similarities on the ice cap. Furthermore it can be seen that the pattern of the initial guess of bedrock (Farinotti) still is visible in all of the final PISM bedrocks, even though all bedrocks have been changed 10 times according to the surface elevation. At the outlet glaciers it looks like the models with a till friction angle of 10° in general perform better. This is because higher till friction angles in PISM, causes PISM to reduce to a non-sliding SIA. Whereas, low till

friction angles in PISM allows the ice to slide in all radial directions [Bueler and Brown, 2008]. Thus the basal shear stress in eq. (4.1) goes to zero when the till friction angle in the expression of the yield stress (eq. (4.2)) goes to zero, as well. Hence it makes good sense that the models with a low till friction angle performs better at the outlet glaciers. One could argue that it would be interesting to test till friction angles of $5°$ and $15°$ as well.

Figure 4.7 shows the root mean squared error (RMS) of the modelled surface elevation compared to ArcticDEM (upper panel), the modelled ice thickness compared to IceBridge (middle panel) and the modelled ice thickness on the ice cap (blue part in Figure 4.5) compared to the IceBridge thickness (lower panel). Starting at the top, since the model is tuned according to ArcticDEM I would expect a decrease in RMS until some minimum in RMS is reached, where the model cannot be further improved in the setup used. I do see such a decrease in RMS until around iteration 6. The decrease in RMS is smaller than what I would have expected, which might be because the initial guess of bedrock topography actually is a good guess. It could also be because the models are not run until steady state is reached, so further improvement in RMS might be done by running each forward model of PISM until steady state. This would be a place to start if additional computational power were available.

Some of the models tend to get worse around iteration 8-10 than the minimum reached around iteration 6 ($\phi = 10$ $E = 1$, $\phi = 10$ $E = 3$, $\phi = 10$ $E = 6$, $\phi = 30$ $E = 1$ and $\phi = 30$ $E = 3$). A reason for this could be that the bedrock is changed too much after each iteration meaning that a lower relaxation parameter in eq. (4.5) could have been needed. It is clear to see that the models with $\phi = 10$ are doing a much better job than all of the other models with a RMS of around 100 m less than the others.

In the middle and lower panel of the figure we see that the RMS of the modelled ice thickness compared to the IceBridge ice thickness increases with the number of iterations. Except for $\phi = 10$ $E = 1$ that ends up with a lower RMS after the 10th iteration than after the first. The RMS does fluctuate a bit around iteration 4-8, but reaches what one could argue to be a minimum after that. All of the other model runs tend to increase more in RMS and/or fluctuate more. I would not expect a decrease in RMS in these two plots as the models have not been optimised against the IceBridge data at all. Luckily, it can be seen that the RMS is much lower on the main ice cap than when including the outlet glaciers, which emphasises that the models certainly do perform a better job on the ice cap than on the outlet glaciers.

As mentioned in Chapter 3 the outputs from PISM are also to be compared with the Landsat 8 velocity map (Figure 3.4). Since PISM in general is working better at the main ice cap, combined with the fact that I am only interested in the ice cap I have chosen to only use the part of the velocity map which is shown in Figure 4.8. Be aware of the changed limits on the colour bar which represents the minimum and maximum surface velocity in this region. The lowest surface velocity tracked in this region is 9 cm yr$^{-1}$.
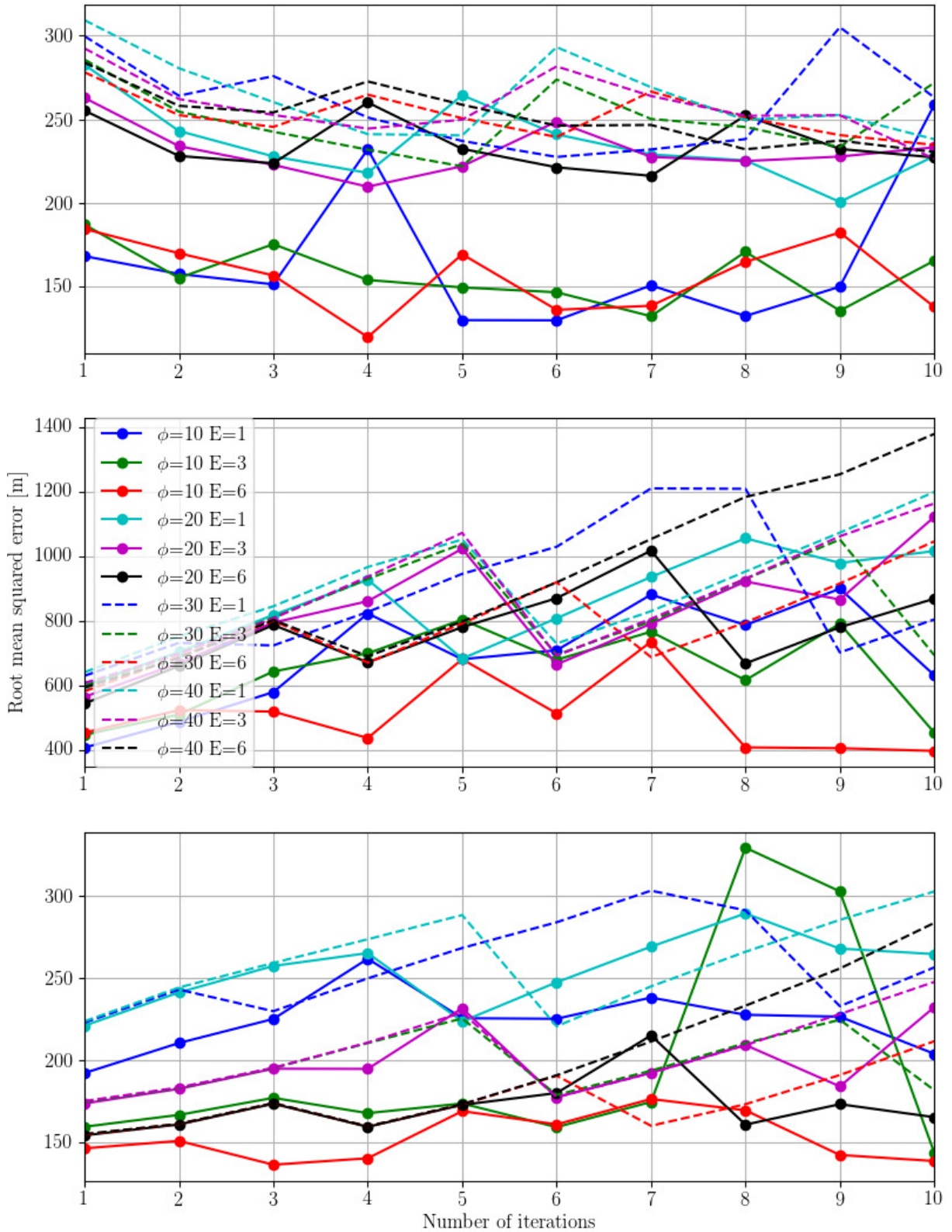
*Figure 4.7:* **Upper panel:** *RMS of the modelled surface elevation compared to ArcticDEM.* **Middle panel:** *RMS of the modelled ice thickness compared to the IceBridge ice thickness.* **Lower panel:** *RMS of the modelled thickness compared to the IceBridge ice thickness on the ice cap marked in blue in Figure 4.5.*
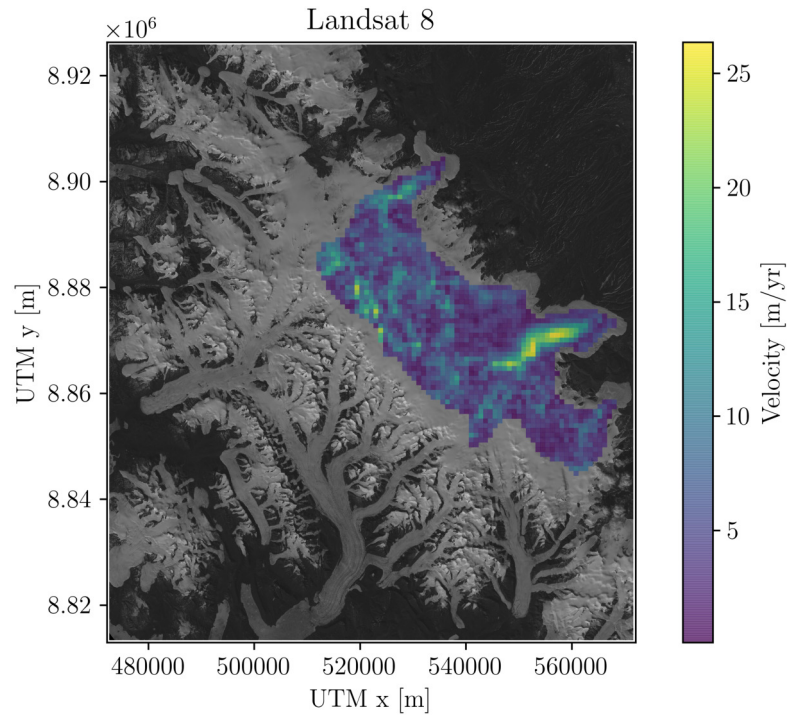
*Figure 4.8: Landsat 8 velocity map of the region to be used in the RMS study.*
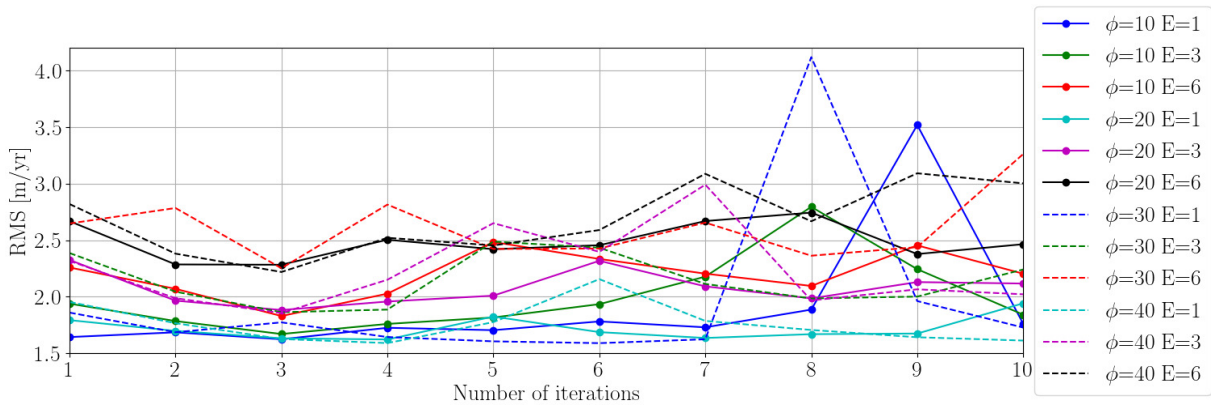


*Figure 4.9: Root mean squared error of the modelled surface velocity compared to the surface velocity from the Landsat 8 median velocity map in Figure 4.8.*

Figure 4.9 shows the RMS of the modelled surface velocity compared to the surface velocity from the Landsat 8 median velocity map as presented in Figure 4.8. It can be seen that the RMS in general only is on the order of 2 m yr$^{-1}$ and that there is no big difference between the RMS after the first and the 10th iteration. The models with $\phi = 20\ E = 6$, $\phi = 30\ E = 6$ and $\phi = 40$ $E = 6$ have the highest RMS in overall and the models with $\phi = 20\ E = 1$ and $\phi = 40\ E = 1$ have the lowest RMS.

Combining the results from Figures 4.6 and 4.7, it is easy to see that the model that performs best is the one using a till friction angle of 10° and an enhancement factor of 6. Taking the RMS

*Figure 4.10: Bedrock topography using $\phi = 10$ and $E = 6$.*

of the surface velocity into account I would still choose that model as my main PISM result of bedrock topography taking the low diverse in RMS of the surface velocity into account.
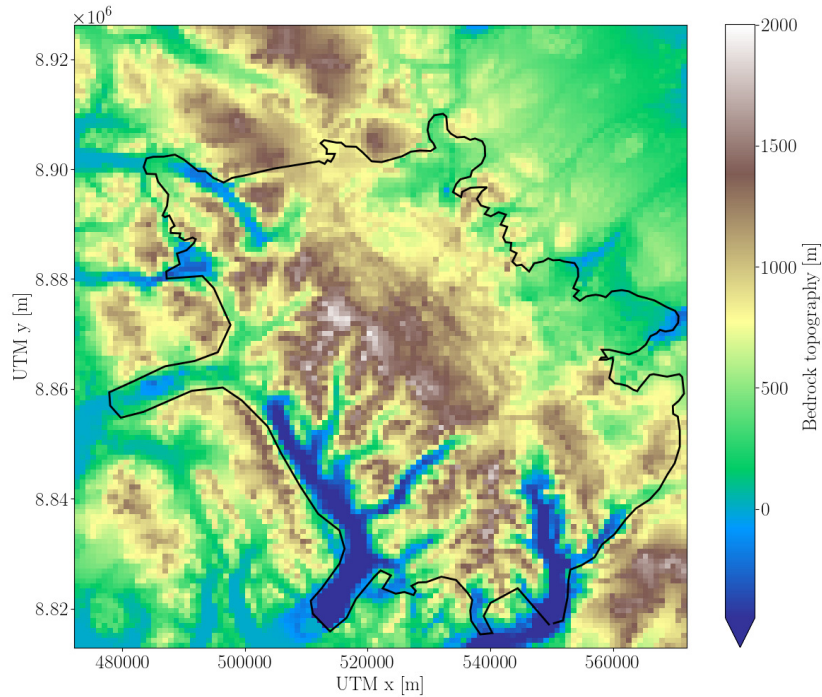
Figure 4.10 shows the bedrock topography (i.e. ArcticDEM subtracted by the PISM ice thickness) of the main PISM result using $\phi = 10$ and $E = 6$. Discontinuity in the bedrock topography can be seen around the outlet glaciers in the southwestern region. This is because PISM builds up ice in the outlet glaciers and I cut off any ice outside of the current ice cap after each iteration, resulting in a very sharp margin. This would have been even worse if the relaxation parameter had not been linearly increasing with altitude as mentioned in Section 4.3.

But why is PISM performing so badly at the outlet glaciers? The mean SMB from HIRHAM is 72.3 kg m$^{-2}$ y$^{-1}$ and from Figure 4.2d it can be seen that the SMB is highly positive over the mountains around the outlet glaciers, hence the massive build up of ice in that region can be described by the SMB. This is probably also why I have had issues with high diffusivity as mentioned in Section 4.4.2. One could argue that it would have been a good idea to subtract the mean SMB from the entire SMB field to reach a mean of zero, to prevent the ice cap from growing, which I also tried. This forced the ice to shrink in the northeastern part of the ice cap, and ice would still build up in the outlet glaciers. That being said, I believe that the only way to avoid this problem would be to create the SMB field myself based on the lapse rate, altitude, temperature, the mass budget data from White Glacier [Cogley et al., 1996, Müller, 1962, Thomson et al., 2016] and the accumulation data from the ice cap by Koerner [1979]. Figure 4.11 shows the SMB as a function of elevation from HIRHAM compared to mean in-
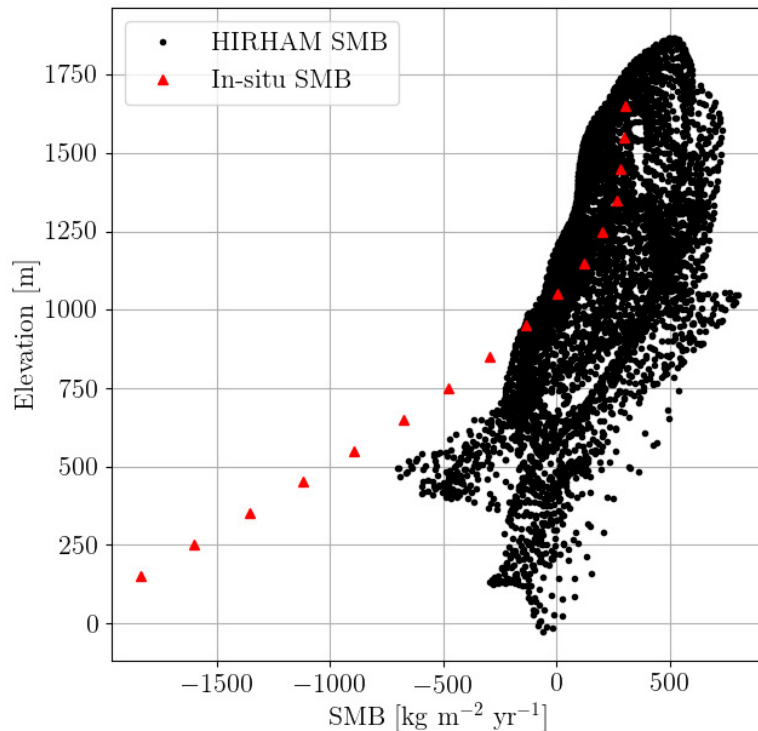
*Figure 4.11: SMB as a function of elevation from HIRHAM (black dots) and mean in-situ measurements from White Glacier from 1961-1990 [Cogley et al., 1996] (red triangles).*

situ measurements from White Glacier from 1961-1990 [Cogley et al., 1996]. It can be seen that HIRHAM in general overestimates the SMB, which is reflected in my results.

A study on HIRHAM's performance over Vatnajökull in Iceland also shows an overestimation of SMB on the upslope in complex terrain [Schmidt et al., 2017], similar to the mountainous region on Axel Heiberg Island. Schmidt et al. [2017] furthermore discussed that the reason for this simply lies in the precipitation scheme of HIRHAM. With that in mind, the HIRHAM SMB certainly is one of the drivers behind the build up of ice on the outlet glaciers.

Another issue could also be that some of the outlet glaciers have been reported as surge-type glaciers [Copland et al., 2003, Short and Gray, 2005, Van Wychen et al., 2014, 2016], which definitely means that the ice cap (or at least the outlet glaciers) is not in steady state in contrast to the assumptions made in this model. This can also be an explanation why PISM performs bad at the outlet glaciers.

Thirdly we should remember that PISM is a simplified model using a coupling of the SIA and the SSA. Whether this approximation has an impact on the issues at the outlet glaciers, is an open question. A full Stokes model like Elmer/Ice [Gagliardini et al., 2013] could potentially perform better, which could be tested in further studies. Nonetheless, I think that it would still
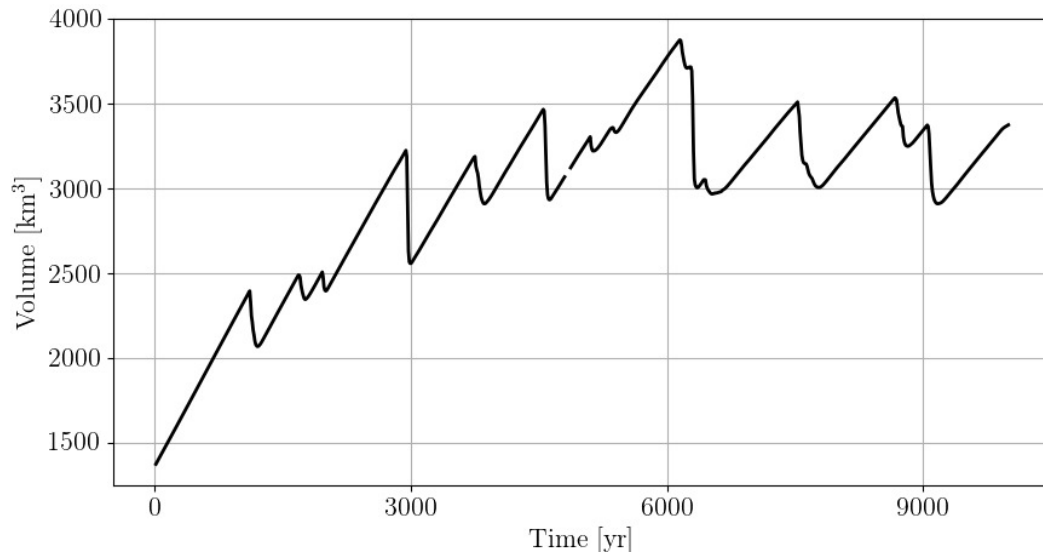
*Figure 4.12: Volume of the ice in glacierised areas as a function of time using iteration 10 of the final model as input to PISM.*

have a problem with the input data not resembling the truth sufficiently. Therefore, I think that this is the main issue.

As seen in Section 4.4.2 I have used the same enhancement factor in the SIA and SSA. If I had used different enhancement factors in the two approximations, I might have been able to capture the outlet glaciers better. I would expect that the enhancement factor differs greatly on the ice cap and on the outlet glaciers, respectively. Hence, it could be beneficial to set a lower enhancement factor on the outlet glaciers, i.e. a lower enhancement factor in the SSA than in the SIA as suggested in Ma et al. [2010].

In my PISM modelling I have used a constant till friction angle everywhere in the domain, even though there are various options in PISM to make it spatially variable. This could of course also have an influence on my results, but since all of the models with $\phi = 10$ in general are performing better (see Figure 4.7) I do not worry to much about this. The most intuitive way to optimise this issue would be testing an even lower till friction angle on the outlet glaciers, or letting PISM reduce to a full SSA on the outlet glaciers. This would definitely be an interesting topic for further study, but it is out of the scope of this thesis.

Focusing on the choice of the best model again, two questions arise. How much do we trust the modelled bedrock topography? Is the ice cap in steady state? To answer these questions I have taken the ice cap geometry after the 10th iteration and let that run for 10,000 years, to test whether it is in fact in steady state or not. Figure 4.12 shows the volume of the ice in the glacierised areas as a function of time. It can be seen that the the volume increases in the first 4000 years before reaching a state where the volume fluctuates around the same value. This

indicates that the model is not in steady state, although close to it. The fluctuations are caused by surging of the outlet glaciers as a result of the SSA, whereas the fluctuations on the main ice cap are smaller.

I only expect the model to perform well enough to come up with suggestions on where to conduct ground based radargrams. Even though the ice cap has been observed not to be in steady state [Thomson et al., 2011, 2016], otherwise assumed in this model, I still do believe that the modelled bedrock does represent the true bedrock to this extent, especially because I can blindly exclude the bedrock at the outlet glaciers from my results. Furthermore, as I am to compare these results with several more models of the ice thickness, the combined result will be more robust than this.

# 5    Thickness inversion of the shallow ice approximation

In this chapter I will describe a method to calculate the ice thickness, when the only known parameters are the surface slope, the outline of the ice cap, the ice flux and a single radar flight line with thickness measurements.

The motivation for applying this method is its simplicity, both theoretically and computationally.

Estimating ice thicknesses from sparse data was studied well in the ITMIX project [Farinotti et al., 2017], where 7 out of 17 models only relied on a digital elevation model (DEM) and a glacier outline. The ice flow equations of all 7 models are less approximated than the SIA. Inspired by this, I test how well the ice thickness can be approximated by doing a simple least squares regression of the SIA.

I will start by describing the model and the parameters needed in the model. This will be followed by a presentation of my results and a discussion of them. The future possibilities of this model will be discussed in a later chapter.

## 5.1    Deriving a thickness model assuming no sliding

Remembering the theory sections 2.2.3 and 2.2.4 on parallel flow and the SIA, we know the average velocity down the ice column from eq. (2.20) which reads

$$\overline{v} = \frac{2A}{n+2}\rho^n g^n \alpha^n H^{n+1} \tag{5.1}$$

$$= c\alpha^n H^{n+1} \tag{5.2}$$

where the constant $c = \frac{2A}{n+2}\rho^n g^n$ is defined. By introducing the constant $c$ the ice flux can be reduced to

$$Q = c\alpha^n H^{n+2}. \tag{5.3}$$

Isolating the ice thickness then results in

$$H = Q^{\frac{1}{n+2}} \cdot \alpha^{\frac{-n}{n+2}} \cdot c^{\frac{-1}{n+2}}. \tag{5.4}$$

Introducing $a = \frac{1}{n+2}$, $b = \frac{-n}{n+2}$ and $k = c^{\frac{-1}{n+2}}$ reduces eq. (5.4) to

$$H = Q^a \cdot \alpha^b \cdot k. \tag{5.5}$$

Taking the logarithm on both sides then gives

$$\log H = a \log Q + b \log \alpha + \log k, \tag{5.6}$$

which is a nice linear relationship between the logarithm of the ice thickness, the ice flux and the surface slope. This allows me to conduct a least squares regression with $a, b$ and $k$ as tuning parameters. The idea then is that if I know the ice flux and the surface slope all over the ice cap I can do a least squares regression using the ice thickness from the IceBridge flight line to obtain $a, b$ and $k$. Assuming that the result from this regression is representative for the entire ice cap, I can calculate the ice thickness everywhere on the ice cap. For this, a grid of 100 × 100 m will be used.

### 5.1.1  Surface elevation

I have used the surface elevation from ArcticDEM, to do so I start by interpolating ArcticDEM onto the 100×100 m grid. Since I know that I will not be able to catch small scale features, I smooth the surface elevation. To do so I use a Gaussian filter with a standard deviation of $\sigma = 2.5$ corresponding to 250 m. To apply the filter I make a mask with ones in areas with ice and zeros in ice free areas. The mask is made from the Farinotti bedrock, but I could also just have made a mask from an optical satellite image, drawing the present day margin. The surface elevation is then smoothed with the Gaussian filter inside the mask. This is illustrated in Figure 5.1, which shows an example of smoothing of a single point with a value of one surrounded by zeros. The figure to the left shows the single point and the figure to the right shows the result after applying the above described smoothing.

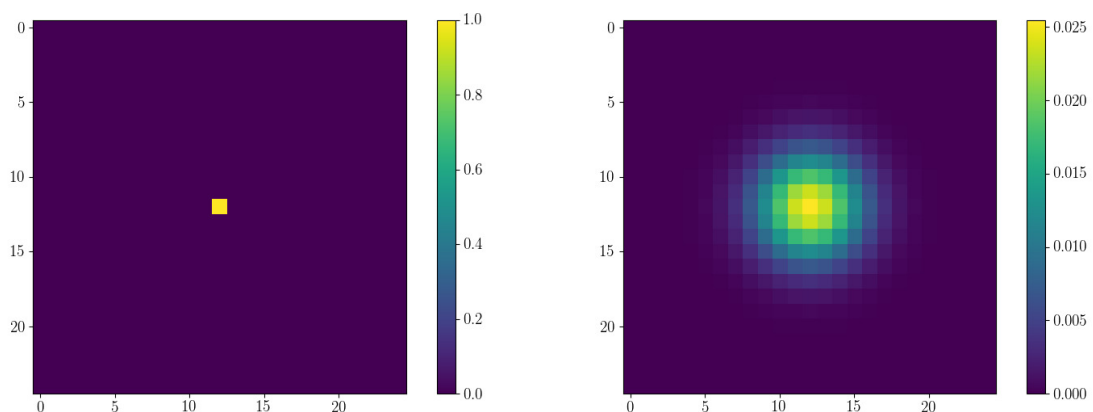The smoothed surface elevation is what will be used throughout this chapter.



*Figure 5.1:* **Left:** *A single point with a value of one surrounded by zeros.* **Right:** *The result after applying the smoothing.*

## 5.1.2 Surface slope

To calculate the slope from the smoothed surface elevation I simply calculate the gradients, $dx$ and $dy$, and from that calculate the surface slope by using

$$\alpha = \sqrt{dx^2 + dy^2} \tag{5.7}$$

Since I need to take the logarithm of the slope (eq. (5.6)) the model breaks in places where $\alpha = 0$ since $\log 0 = -\infty$. This issue would result in an overestimation of ice thickness in these areas. This is a well known issue in these kinds of models [Farinotti et al., 2009, 2017] and the most common way to go around it is to introduce a minimum slope. In the ITMIX project [Farinotti et al., 2017] the minimum slopes used in similar models ranged from $2°$-$5°$. I have chosen to use a minimum slope of 0.01 radians which is $0.6°$ as a higher minimum slope would give the ice flux too much influence on the modelled ice thickness.

## 5.1.3 Ice flux

I have no data for the actual ice flux on the ice cap, thus I need to make a model of it. I have chosen to make a model based on the HIRHAM SMB and the surface slope and assumed that the ice only flows downhill, essentially calculating the balance fluxes. The mean SMB is subtracted in order to simulate steady state. Furthermore the SMB is set to zero outside of the ice cap as defined by the Farinotti bedrock. I sort the surface elevation array by elevation and start with the highest point. In this cell the flux must be equal to the SMB. From that cell I let the ice flow into the surrounding cells according to the surface slope. I assign a weight, $w$, to all of the 8 neighbouring cells such that

$$w = max(0, \alpha)^3, \tag{5.8}$$

where $\alpha$ is the slope between the current cell and the neighbouring cell. This means that if the slope is negative then $w = 0$. Then the ice flows to the neighbouring cells by

$$Q_{neighbour} = Q_{neighbour} + \frac{w_{neighbour}}{\sum w_{allneighbours}} Q_{currentcell} \tag{5.9}$$

I then repeat this process in the second highest elevation cell with the result from before, i.e.

$$Q_{cell} = Q_{cell} + SMB_{cell}. \tag{5.10}$$

To prevent the ice thickness to go towards infinity when taking the logarithm, I introduce a minimum ice flux of $10^{-3}$ m s$^{-1}$ per grid cell area. Note that both the SMB and thereby also the ice flux is measured in m s$^{-1}$ per grid cell area. In the end I have the ice flux in every single grid cell as shown in Figure 5.2. From the figure it can be seen that all the areas outside of the ice cap (as given by the Farinotti bedrock) have the value of the minimum allowed ice flux.
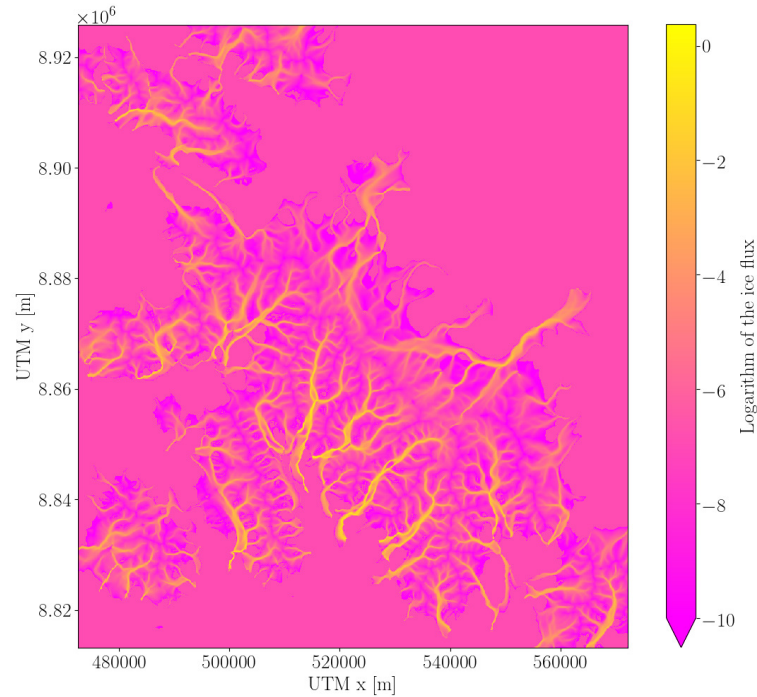
*Figure 5.2: The logarithm of the modelled ice flux.*

## 5.2   SIA inversion results and discussion

With the above described model and data I can do a least squares regression of eq. (5.6) by using the ice thickness from IceBridge, the surface slope and the ice flux to obtain $a, b$ and $k$, and apply the result to the entire ice cap. Since I am mainly interested in the main ice cap I only perform the regression of the IceBridge flight line over the ice cap, shown in blue in Figure 5.3.

Figure 5.4 shows the cross section of the ice cap on the IceBridge flight line. The non-toned part of the figure denotes the data used for the regression in eq. (5.6). The outline of the ice is defined by the smoothed ArcticDEM surface elevation and the the IceBridge ice thickness. The solid black line is the bedrock from my least squares regression where I have subtracted the calculated ice thickness from the smoothed ArcticDEM. It can be seen that in some areas with low surface slope there are some "dips" in the bedrock, especially around 42 km. This is most likely due to taking the logarithm of a very small number (i.e. the slope or ice flux).

The values of $a, b$ and $\log k$ obtained are $a = 0.087$, $b = -0.435$ and $\log k = 5.174$. This results in $n = 9.536$ when using $a = \frac{1}{n+2}$ and $n = 1.540$ when using $b = \frac{-n}{n+2}$. The creep exponent is usually around 2-4 [Cuffey and Paterson, 2010], indicating that this model might be too simplified and that the ice cap is not in steady state as opposed to what is assumed in the calculation of the ice/balance flux.
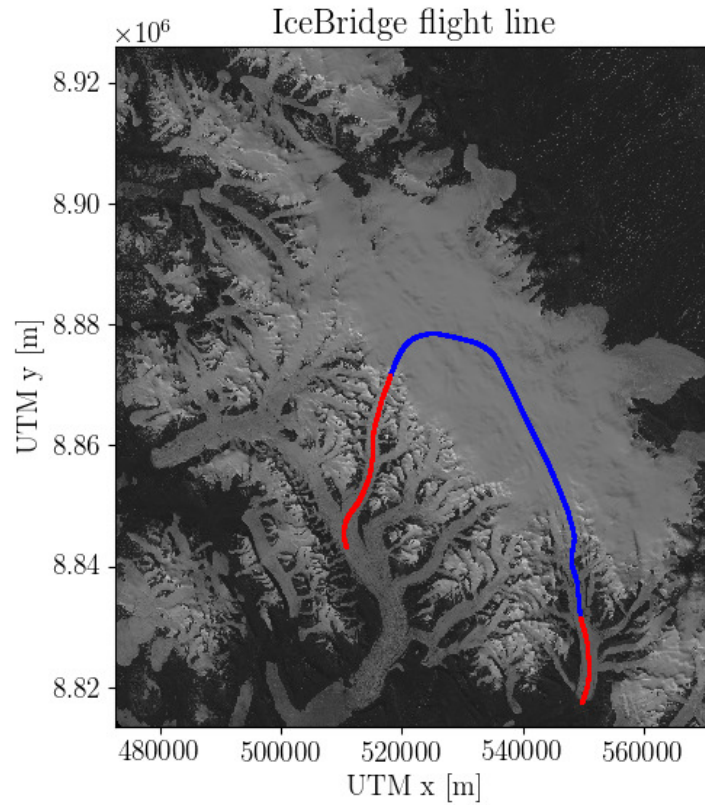
*Figure 5.3: Operation IceBridge fligt line. The blue part of the line is the part used in the SIA inversion.*
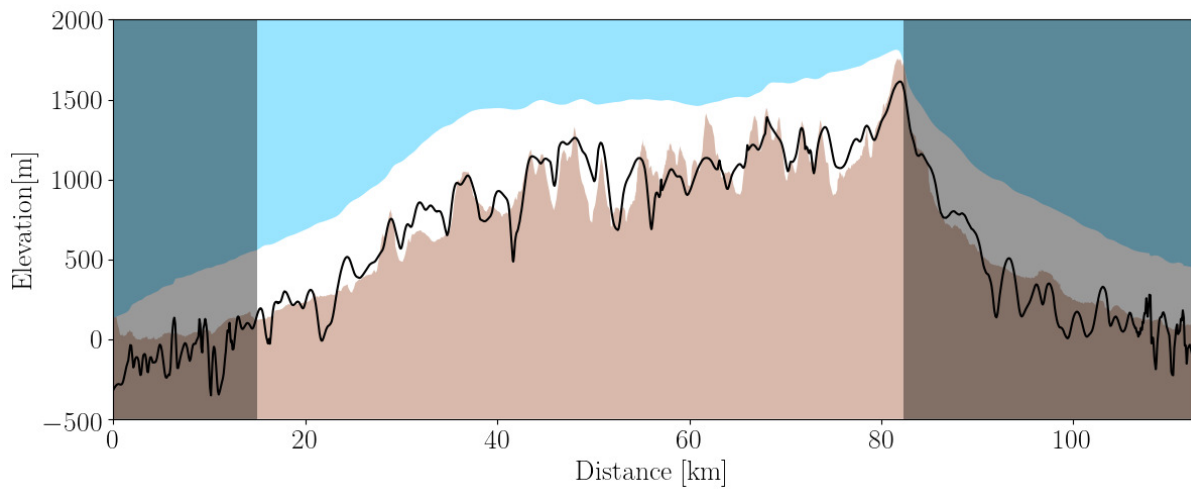


*Figure 5.4: IceBridge flight line cross section with the modelled bedrock using the SIA inversion.*

From the model in eq. (5.6) we know that

$$\log k = \log c^{\frac{-1}{n+2}} \tag{5.11}$$

$$= \log \left( \left( \frac{2A}{n+2} \rho^n g^n \right)^{\frac{-1}{n+2}} \right), \tag{5.12}$$

rearranging and isolating for the rate factor, $A$, gives

$$A = 2^{\frac{-2}{n+2}} \cdot \frac{n+2}{k^2} \rho^{-n} g^{-n} k^{-n} \left( 2^{\frac{1}{n+2}} \right)^{-n}. \tag{5.13}$$

When using $\rho = 917 \, \text{kg m}^{-3}$, $g = 9.8 \, \text{m s}^{-2}$ and $n = 3$ I get a rate factor of $2.06 \cdot 10^{-23} \, \text{s}^{-1} \text{Pa}^{-3}$ which corresponds to a temperature of just above 0°C as seen in Figure 2.2.

Both the values of $n$ and $A$ are in the right order of magnitude, but they are not close to realistic values. Especially because I get two such different values of $n$. I would not expect to obtain correct values of $n$ and $A$ as the SIA is an approximation and the ice flux originates from a model. All errors that there might be in the ice flux, the slope and in the SIA will be captured in these tuning parameters, hence it would be crude to assume that it would result in a true rate factor and a true creep exponent. Furthermore, this model does not take any sliding into account, also affecting the tuning parameters. With the simplicity of this model in mind I am satisfied with these results.

The values of $a, b$ and $k$ from the regression have then been used to calculate the ice thickness of the entire ice cap. Figure 5.5 shows the bedrock topography using this methodology, where I have subtracted the modelled ice thickness from the smoothed ArcticDEM to get the bedrock elevation. It can be seen that there are places scattered across the bedrock where shallow spots and cliffs appear. This again is due to either low ice flux, small surface slope or both. It can also be seen that the stream like pattern from the ice flux in Figure 5.2 has affected the modelled bedrock.

From this ice thickness and the ice flux, I can calculate the average velocity down the ice column using eq. (2.20) and plotted in Figure 5.6. It should be noted that the maximum velocity is 353 m yr$^{-1}$ although the colour bar is capped to 100 m yr$^{-1}$, and the mean velocity is 1.4 m yr$^{-1}$. On the ice cap it can be seen that the flow patterns are roughly the same as in Figure 3.4 with ice flowing out in the two tongues in the eastern and northeastern part. Due to the higher resolution (100 m rather than 900 m), all outlet glaciers in the west are captured better than previously. However, the magnitude of the velocities in general are too high, as compared to Figure 3.9a. The ice divide is well defined and corresponds to what has been found in both Figures 3.4 and 3.9a. This suggests that the modelled ice thickness is not to far off the ground truth.

The advantages of this model are that the only needed variables are the SMB, the surface elevation, an outline of the ice cap margin and a radar line with ice thickness measurements.
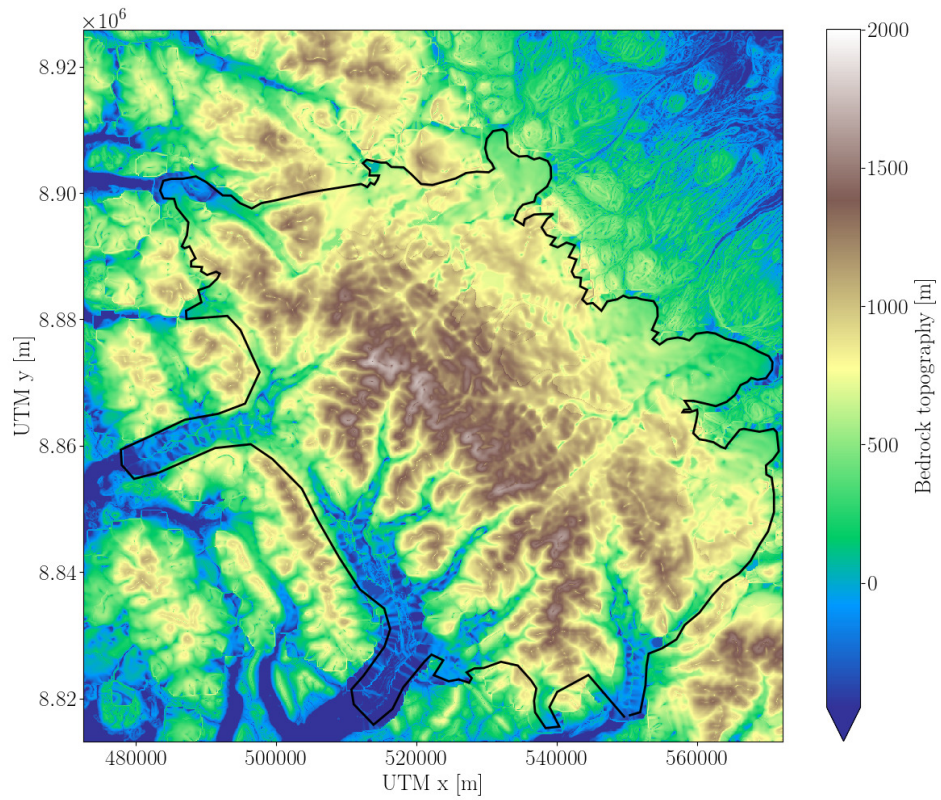
*Figure 5.5: Modelled bedrock topography using the SIA inversion.*
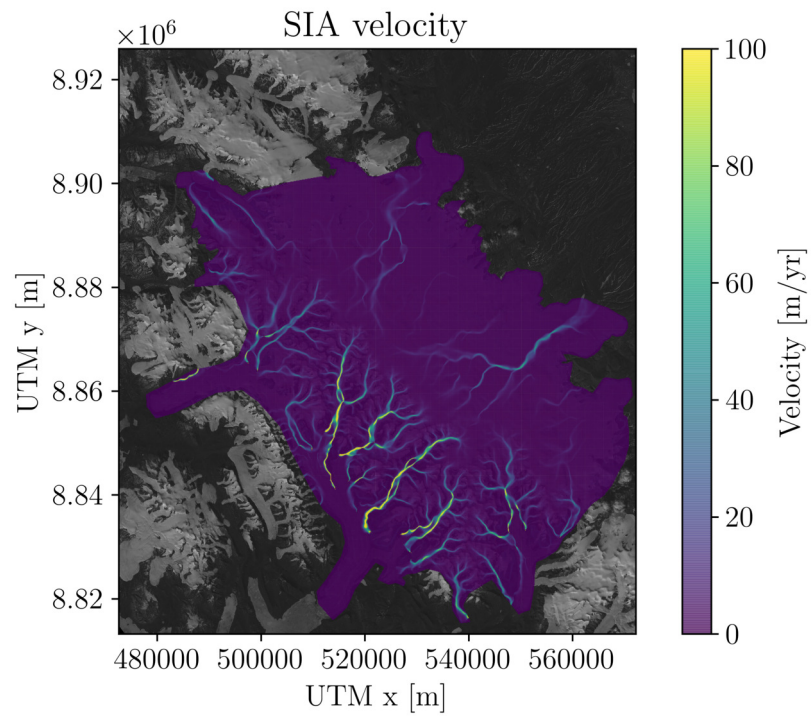


*Figure 5.6: Velocities calculated from the modelled thickness and ice flux.*

Combined with the fact that the model takes no time to run, its performance is very good. With a $100 \times 100$ m grid it takes a bit less than 3 minutes to run the model. Furthermore, it can be shown that the model is not too sensitive towards the SMB. In fact, similar results can be obtained by applying a uniform SMB, as shown in Appendix D. This means that this model can easily be applied to other ice caps and glaciers as long as the surface elevation of the entire ice cap is known, together with an outline of the glacier, and a radar line with ice thickness measurements.

The disadvantages of this model are that no sliding is included, and it can be hard to interpret the tuning constants $a$, $b$ and $k$, because of its simplifications and assumptions. This might very well be the cause of the unphysical values. Furthermore, we do not know how well this model represents the areas outside of the IceBridge flight line. This issue will be treated further in Section 7.1.

# 6 Estimating the ice thickness using Bayesian statistics

In the least squares regression of the SIA inversion in the previous chapter I was able to estimate values of $n$ and $A$ within the right order of magnitude. However, since $n$ and $A$ were only indirectly tuned, I knew that they would not necessarily resemble the truth. Thus, in this chapter I will use a Monte Carlo (MC) sampling method to estimate the ice thickness using the SIA both with and without sliding. Using a MC sampling method will allow me to discard the tuning parameters, $a$, $b$, and $k$, from the SIA inversion and keep the physical expression, further described below.

In glaciology, MC sampling methods have especially been used in estimating mass balance and basal properties [Chandler et al., 2006, Colgan et al., 2012, Gardner et al., 2011, Machguth et al., 2008]. In particular, these methods have been employed on well studied glaciers, where the data quality and quantity resemble that of White Glacier, introduced in Section 1.1.

As a part of the ITMIX project [Farinotti et al., 2017], Brinkerhoff et al. [2016] used a MC sampling method to estimate the ice thickness from the SMB, surface elevation change, and surface velocity. The model solves a much less approximated form of the conservation laws presented in Section 2.1.3 as compared to the SIA.

Werder et al. [2020] have also modelled ice thicknesses from MC sampling methods. They used a combination of mass conservation and the SIA reduced to a 1D model by using elevation bands. Thus, that model is simpler than the one from Brinkerhoff et al. [2016], but not as simple as an inversion of the SIA which is what I will try to conduct within this chapter.

The chapter is structured such that I first will give a brief introduction to MC modelling and present the Python package PyMC3 [Salvatier et al., 2016] which I will be using. Afterwards, I will present the two models one at a time accompanied by their results.

All of the input data in this chapter is the same as in Chapter 5, this also implies that the data is on a $100 \times 100$ m grid, that ArcticDEM is smoothed as described in Section 5.1.1, and that $\rho = 917$ kg m$^{-3}$ and $g = 9.8$ m s$^{-2}$. Furthermore, the models presented here will be trained on the data marked in blue in Figure 5.3.

## 6.1 Markov chain Monte Carlo

In short Markov chain Monte Carlo (MCMC) is one way to encode a Bayesian approach to solve the problem at hand. A completed introduction of MCMC is a vast task outside the scope of this thesis. I will, however, introduce the necessary parts, based on Tarantola [2005].

Imagine we have some data, $\mathbf{d}$ (i.e. the ice thickness), which can be described by some physical relation, $g$ (i.e. the SIA),

$$\mathbf{d} = g(\mathbf{m}), \tag{6.1}$$

based on some model parameters, $\mathbf{m}$ (i.e. creep exponent, rate factor etc.). Bayes theorem reads as follows

$$f(\mathbf{m}|\mathbf{d}) = \frac{f(\mathbf{d}|\mathbf{m})f(\mathbf{m})}{f(\mathbf{d})}, \tag{6.2}$$

where $f(\mathbf{m}|\mathbf{d})$ is the posterior distribution of the model parameters given the data, $f(\mathbf{d}|\mathbf{m})$ is the likelihood of the data given the model parameters, $f(\mathbf{m})$ is the prior distributions of the model parameters and $f(\mathbf{d})$ is the prior distribution of the data. Thus, this theorem states that given a (prior) distribution of the probability of some parameters, one can update these estimates given new data.

Instead of performing this tedious and complex update by hand, one can use a MCMC. What it does is to perform a random walk through the full parameter space of the model, with parameter probabilities given by the priors. In contrast to the approximations normally employed when optimising the parameters by hand, the MCMC deals just as well with non-Gaussian prior distributions as Gaussian and further, the MCMC can keep track of hundreds of parameters simultaneously. The random walk can be performed in several chains resulting in multiple posterior distributions. Sampling in several chains, is a way to ensure that the global and not only the local maximum is found.

PyMC3 is a Python package with a build-in MCMC sampler [Salvatier et al., 2016]. It offers a wide selection of distributions allowing one to build the best model possible for the problem desired to solve. Both the model with and without sliding will be build within PyMC3 and the MCMC sampling method used in this thesis is the No-U-Turn Sampler (NUTS).

## 6.2 MC model without sliding

### 6.2.1 Method without sliding

Combining the parallel flow (eq. (2.20)) and the SIA inversion equations (eq. (5.6)), introduced in Chapters 2 and 5, and implementing an enhancement factor results in

$$\log H = \frac{1}{n_0 + 2} \log Q + \left( \frac{3}{n_1 + 3} - 1 \right) \log \alpha + \log \left( \left( \frac{2EA}{n_2 + 2} \rho^{n_3} g^{n_4} \right)^{\frac{-1}{n_5 + 2}} \right). \tag{6.3}$$

Here $n_0$ to $n_5$ are the creep exponents, which I have chosen to be allowed to differ, further described below. This expression, combined with the same input data of IceBridge ice thickness, surface slope, and ice flux, as in Chapter 5 can then be sampled using PyMC3 by assigning

prior distributions to all parameters. The prior distributions of the creep exponents, enhancement factor and rate factor are chosen to be as follows

$$n_{0...5} \sim \text{Trunc}\mathcal{N}(\mu = 3, \sigma = 3, 1, 10) \tag{6.4}$$

$$E \sim \mathcal{U}(1, 10) \tag{6.5}$$

$$Ak \sim \text{Lognormal}(\mu = \log 3.5, \sigma^2 = 0.5), \tag{6.6}$$

where $A = Ak \cdot 10^{-25}$. The notation $\sim$ means "distributed as". The shape of the prior distributions are a result of trial and error with a combination of theory of the mean values [Cuffey and Paterson, 2010]. Starting from the top with the six creep exponents, I have chosen to use a truncated normal distribution with $\mu = 3$ and $\sigma = 3$ and a cut off at 1 and 10 to prevent too small and too large creep exponents. The prior distribution of the enhancement factor is chosen to be uniform in the range from 1-10. The rate factor has been split into two, to save the model from tuning on parameters on the size of $10^{-25}$. To do so I let $A = Ak \cdot 10^{-25}$. The prior distribution of $Ak$ is described by a log-normal distribution with $\mu = \log(3.5)$ and $\sigma = 0.5$. The choice of the log-normal distribution is done to prevent the rate factor of becoming less or equal to zero.

The prior distributions of the model, $y$, described by eq. (6.3) and of the uncertainty of the data, $\sigma_{data}$, are set to be

$$\sigma_{data} \sim \mathcal{U}(0, 10) \tag{6.7}$$

$$y = \frac{1}{n_0 + 2} \log Q + \left( \frac{3}{n_1 + 3} - 1 \right) \log \alpha + \log \left( \left( \frac{2EA}{n_2 + 2} \rho^{n_3} g^{n_4} \right)^{\frac{-1}{n_5 + 2}} \right) \tag{6.8}$$

$$y \sim \mathcal{N}(\mu = y, \sigma = \sigma_{data}). \tag{6.9}$$

Meaning that a uniform prior distribution ranging from 0-10 is used to describe the uncertainty of the observed data, the observed data being the logarithm of the IceBridge ice thickness. The reason for the uniform distribution was to give the model more freedom than a normal distribution would have allowed. Finally, the prior distribution of the logarithm of the ice thickness as described in eq. (6.3) is assumed to take the shape of a normal distribution with $\mu$ described by eq. (6.3) and $\sigma = \sigma_{data}$. Notice here that I am using the logarithm of the ice thickness rather than the actual ice thickness. This is my way of "normalising" the data, making it easier for PyMC3 to do the sampling.

To do the actual sampling, I use 200 samples in 2 chains, i.e. 200 samples from the prior distributions will be used to create two posterior distributions with 200 samples in each. This will be done for all of the input parameters. The sampling is done after 1000 steps of tuning, reassuring that the sampling is done after the burn-in time [Tarantola, 2005]. The posterior distributions of $n$, $Ak$, $E$ and $\sigma_{data}$ after the sampling can be seen in Figure 6.1. The blue and
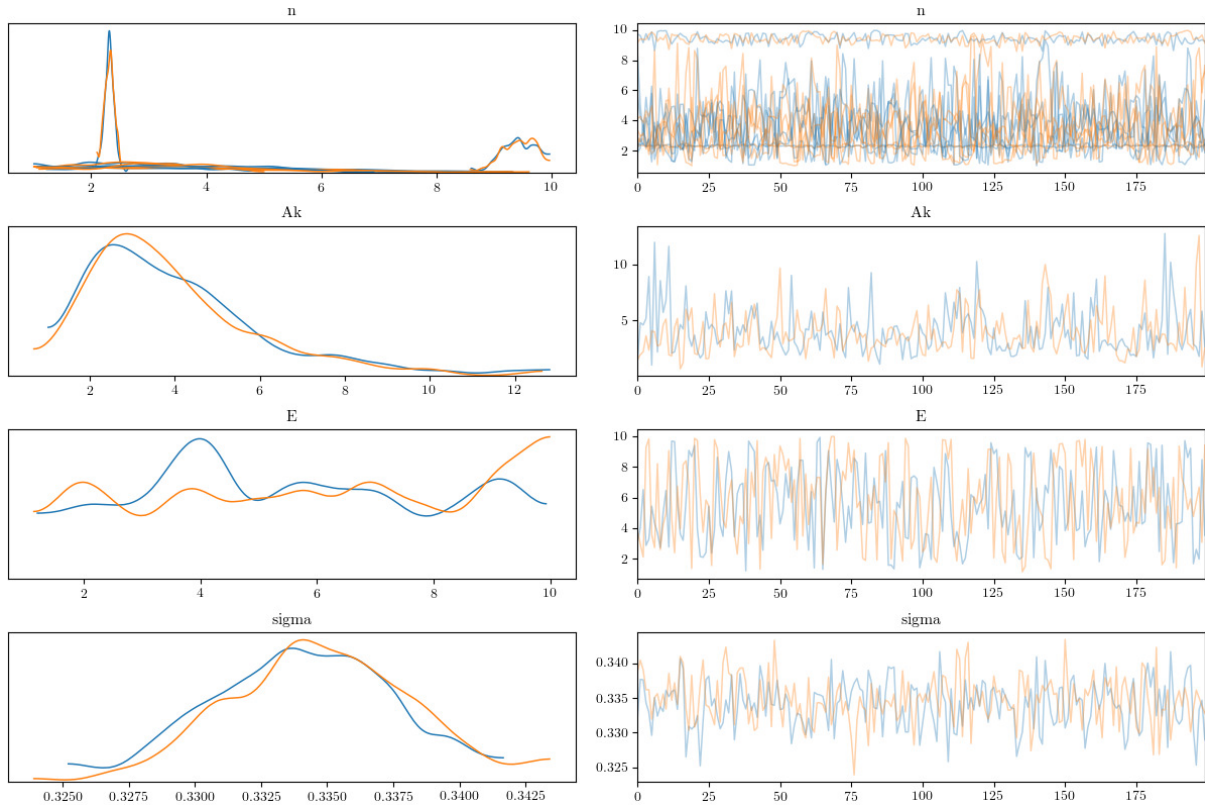
*Figure 6.1: Left: Posterior distributions of $n$, $Ak$, $E$, and $\sigma_{data}$. Right: The variability as a function of number of samples. The two colours represent the two chains.*

orange colours represents the two chains. Looking at the creep exponent it can be seen that two of them have a quite peaked posterior distribution meaning well-located values, whereas the rest of them have quite flat posterior distributions with no clear peak. $Ak$ and $\sigma_{data}$ both have quite well defined posterior distributions. The enhancement factor on the other hand has a quite uniform distribution. It should be noted that the rate factor and the enhancement factor are closely connected, which influences its posterior distribution. It can also been seen that the two chains are more or less similar in all cases, indicating that it is the global maximum which has been found.

The right side of Figure 6.1 shows the value of the different features as a function of samples, and thereby the variability as a function of time. It can be seen that they have all reached a steady state, indicating that I have used enough tuning steps before the sampling starts.

From the posterior distributions in Figure 6.1 one can sample the posterior distribution of the logarithm of the ice thickness. The "best" guess for the ice thickness in the part that has been used for the sampling is thus the mean of the posterior distribution, which I have plotted against the actual IceBridge ice thickness in Figure 6.2a.

Since it shows the mean of the posterior distributions, one can not subtract the values of $n$, $Ak$, $E$ and $\sigma_{data}$ used to get this ice thickness. Thus to find those values I look into the statistics
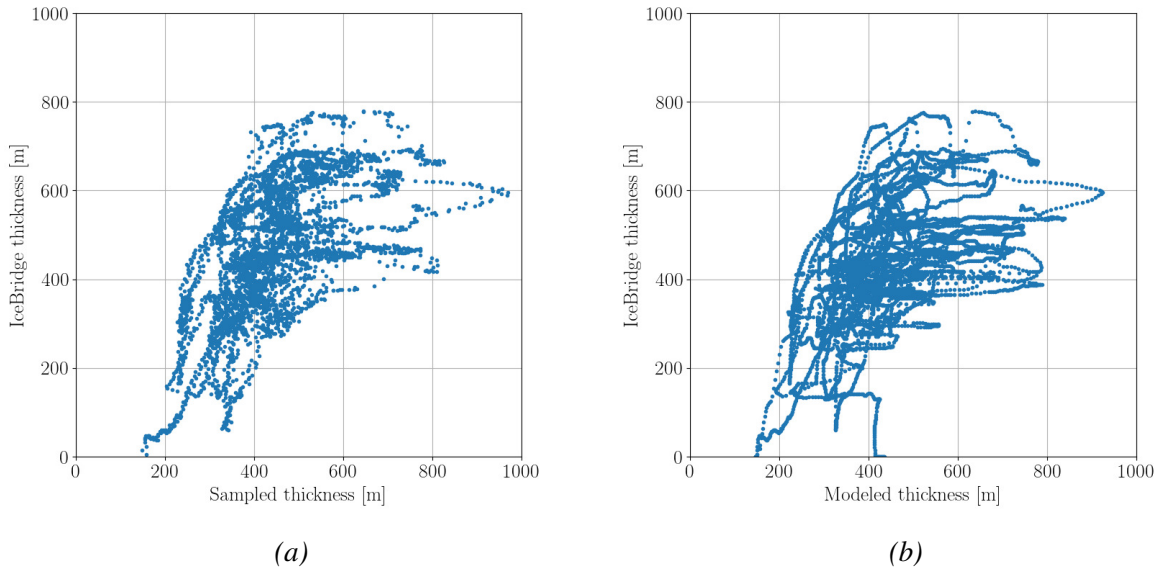
*Figure 6.2: **(a)** Sampled ice thickness versus IceBridge thickness. **(b)** Calculated ice thickness using the mean from Table 6.1 versus IceBridge thickness.*

of Figure 6.1 tabulated in Table 6.1. Here, I have denoted the average of the mean and median as "mean-median" and "std" is the standard deviation. To find the best suited values of $n$, $Ak$, $E$ and $\sigma_{data}$ I simply plotted the same plot as in Figure 6.2a using the mean, median and mean-median values of the parameters and plugged into eq. (6.3), respectively. Instead of just applying the ice flux and the slope from the part of the IceBridge fligt line used in the training (shown in blue in Figure 5.3), I used the entire flight line. After that I interpolated it onto the IceBridge flight line, which then was plotted against the IceBridge ice thickness. By comparing the three different "predicted versus true" plots with Figure 6.2a, I found that the values using the mean resembled Figure 6.2a the most. Figure 6.2b then shows the predicted ice thickness using the mean values in Table 6.1 against the IceBridge ice thickness. These values were then plugged into eq. (6.3) and applied on the entire ice cap.

## 6.2.2 Results and discussion without sliding

Figure 6.3 shows the cross section of the IceBridge flight line with the modelled bedrock in black. The surface elevation is given from the smoothed ArcticDEM. Like in the case of the SIA inversion in Chapter 5, steep dips in the bedrock topography can be seen in some areas with low surface slope. Likewise, higher fluctuations can be seen in the bedrock topography of the outlet glaciers. These discrepancies are expected as the model is only optimised with data from the single flight line shown in blue in Figure 5.3. It catches the broad features of the ice cap but not the details.

*Table 6.1: Summary and statistics of all sampled parameters. The mean-median is the average of the mean and the median.*

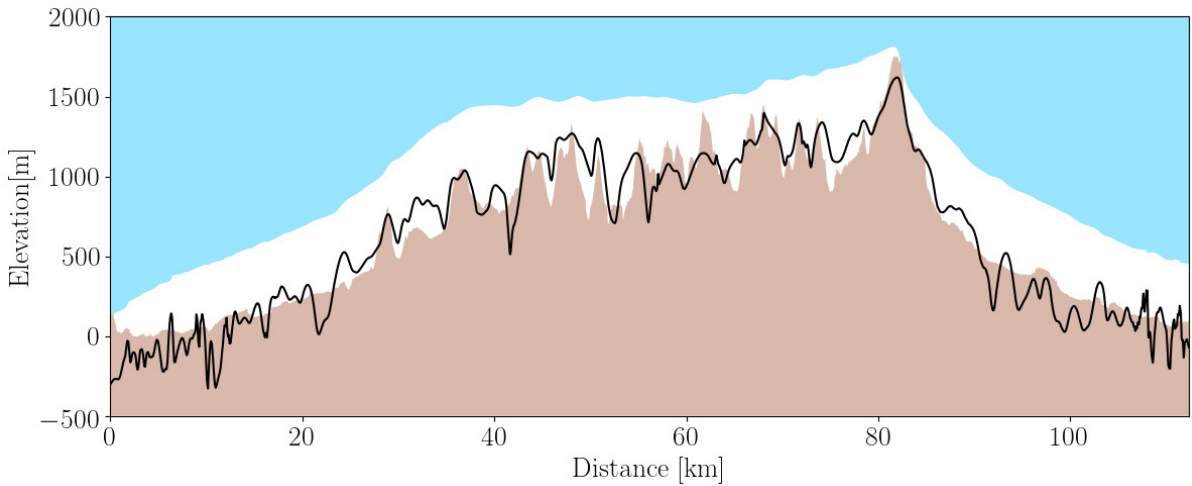|                  | **Mean** | **Median** | **Mean-median** | **Std** |
|------------------|----------|------------|-----------------|---------|
| $n_0$            | 9.42     | 9.43       | 9.43            | 0.29    |
| $n_1$            | 2.32     | 2.32       | 2.32            | 0.09    |
| $n_2$            | 4.17     | 3.97       | 4.07            | 2.04    |
| $n_3$            | 2.71     | 2.65       | 2.68            | 0.94    |
| $n_4$            | 3.69     | 3.40       | 3.54            | 1.86    |
| $n_5$            | 3.58     | 3.49       | 3.53            | 1.24    |
| $Ak$             | 4.00     | 3.51       | 3.76            | 2.05    |
| $E$              | 5.68     | 5.69       | 5.68            | 2.54    |
| $\sigma_{data}$  | 0.334    | 0.334      | 0.334           | 0.003   |



*Figure 6.3: IceBridge flight line cross section with the modelled bedrock as the solid black line.*

The bedrock topography of the entire domain can be seen in Figure 6.4. Here it is a bit more clear to see how the shape of the bedrock is influenced by the flux when comparing to Figure 5.2. It is also interesting to discuss the found values of creep exponent as presented in Table 6.1. $n_1$-$n_5$ all have values between 2 and 4, which is what one would expect from theory [Cuffey and Paterson, 2010]. $n_0$ on the other hand, is 2-3 times larger. Looking at eq. (6.3), $n_0$ is directly influenced by the ice flux. This suggests that the modelled ice flux, as explained in Section 5.1.3, does not represent the actual ice flux of the ice cap. This is to be expected as it is the balance fluxes that I have used under the assumption that the ice cap is in steady state. It could also simply be a signal of the SIA being too crude of an assumption for the Müller ice cap. Remembering the results from Chapter 5, the creep exponent related to the ice flux was 9.54. Exactly the differences in creep exponents were the reason for me not to collapse them into one parameter, which in contrast is expected from theory.

The rate and enhancement factors were found to be $4.00 \cdot 10^{-25}$ s$^{-1}$Pa$^{-3}$ and 5.68, respec-
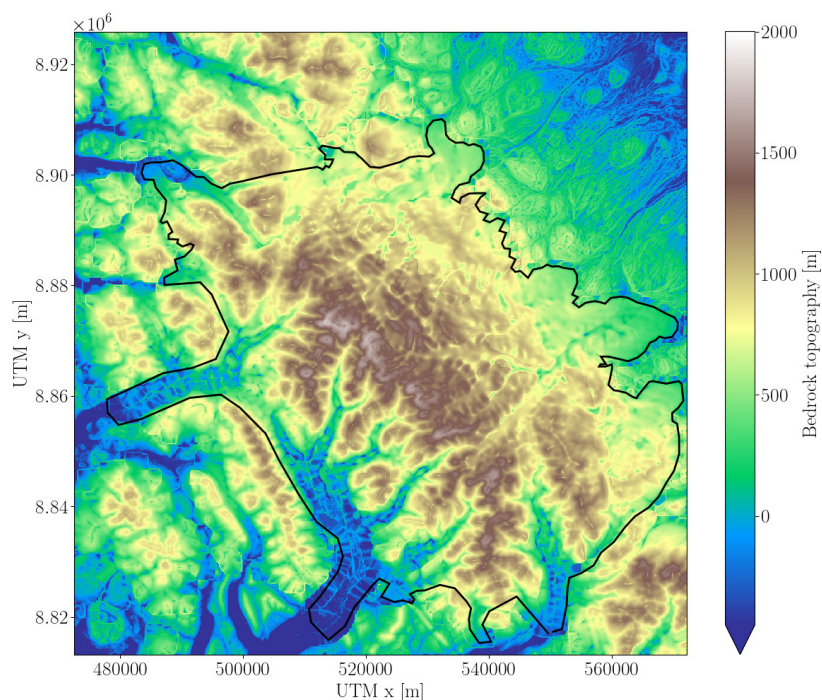
*Figure 6.4: Modelled bedrock topography.*

tively. This corresponds to a temperature of just above $-25°$C. Notice, that $A$ and $E$ are directly related, thus if I had not introduced an enhancement factor, the value of the rate factor would have increased. The new rate factor would thereby increase the corresponding temperature (see Figure 2.2). This indicates that the enhancement factor on the Müller ice cap is greater than 1. It should be noted that the unit of the rate factor depends on the creep exponent, such that the unit of $A$ is $s^{-1}Pa^{-n}$. Thus, to prevent a very complicated unit of $A$ now that the creep exponent has been split into six, I choose to capture it in the enhancement factor. This means that the enhancement factor is no more unitless. This shows the disadvantage of splitting the creep exponent.

Investigating the ice flux brings us back to one of the key assumptions in the model of the ice flux in Section 5.1.3. Namely the assumption that all ice flows downhill. This might not always be the case, i.e. bumps in the bedrock topography may be visible in the surface topography, causing the ice to flow uphill [Cuffey and Paterson, 2010]. Looking at the cross section in Figure 6.3, this may very well be the case.

Remembering Figure 6.2b it can be seen that the model in general overestimates the ice thickness. This is the case in places with small observed ice thicknesses. There is also a clear pattern that some observed ice thicknesses around 400-600 m are overestimated. If we look at the cross section in Figure 6.3, it seems that the overestimation of very small ice thicknesses mostly takes place on the ice cap where the observed bedrock topography has some shallow peaks above the modelled one. Furthermore the model has clearly overestimated the ice thick-

ness at the very summit, where the observed ice thickness almost goes to zero. The overestimation of the observed ice thicknesses of around 400-600 m can mainly be attributed to the two outlet glaciers. Especially in the area around 90-110 km. This overestimation could very well be due to the fact that the model is not trained to perform well in these areas, combined with no sliding being modelled in this model of the SIA.

The advantages of this model are the same as in the SIA inversion in Chapter 5, including the fact that the modelled ice thickness depends little on the SMB. Appendix E shows an example of the results when using a uniform SMB with ones in every grid cell.

In contrast to the SIA inversion I have managed to resolve one of the disadvantages, namely the interpretation of the tuning constants, since I am able to use eq. (6.3) as it is. Even so, the values of $n$ seem to be a bit off. In the following section it is tested whether this issue can be resolved by adding sliding.

## 6.3   MC model with sliding

### 6.3.1   Method with sliding

As mentioned, the advantage of using PyMC3, is that it allows one to sample over any given equation. Hence it gives me the possibility of including sliding. Recalling eq. (2.20) from the definition of parallel flow and plugging in the basal shear stress the ice flux is given by

$$Q = v_b H + \frac{2EA}{n+2}\rho^n g^n \alpha^n H^{n+2}. \tag{6.10}$$

The basal velocity is given by

$$v_b = f v_s, \tag{6.11}$$

where $v_s$ is obtained by the median Landsat 8 velocity map (see Figure 3.4).

When sliding is included it is not possible to isolate the ice thickness directly, which is why I have to sample over something else than the ice thickness, if I want to use PyMC3. Thus I will be sampling over the ice flux calculated in Section 5.1.3. From the ice flux an estimate for the ice thickness can be found by minimising the difference between the left and right hand side of eq. (6.10), which will be further described later on.

The PyMC3 model, $y$, using eq. (6.10) with eq. (6.11) to describe the basal velocity is then

expressed by the following prior distributions

$$n \sim \mathrm{Trunc}\mathcal{N}(\mu = 3, \sigma = 3, 1, 10) \tag{6.12}$$

$$E \sim \mathcal{U}(1, 10) \tag{6.13}$$

$$Ak \sim \mathrm{Lognormal}(\mu = \log 3.5, \sigma^2 = 0.5) \tag{6.14}$$

$$f \sim \mathcal{U}(0, 1) \tag{6.15}$$

$$\sigma_{data} \sim \mathcal{U}(0, 1000) \tag{6.16}$$

$$y = \log\left(fv_sH + \frac{2EA}{n+2}\rho^n g^n \alpha^n H^{n+2}\right) \tag{6.17}$$

$$y \sim \mathcal{N}(\mu = y, \sigma = \sigma_{data}). \tag{6.18}$$

The prior distributions for $n$, $Ak$ and $E$ are the same as in the model without sliding, but only using one value for all creep exponents. This also implies that $A = Ak \cdot 10^{-25}$. The prior distribution of the uncertainty, $\sigma_{data}$, of the logarithm of the "observed" ice flux is described by a uniform distribution from 0 to 1000. The prior distribution of $f$ from eq. 6.11 is uniform from zero to one, allowing the basal velocity to be in the range from 0 to $v_s$. Like in the model without sliding I use the logarithm of the ice flux as a "normalisation" in the sampling.

*Table 6.2: Summary and statistics of all sampled parameters. The mean-median is the average of the mean and the median.*

|  | **Mean** | **Median** | **Mean-median** | **Std** |
|---|---|---|---|---|
| $n$ | 3.03 | 3.02 | 3.03 | 0.07 |
| $Ak$ | 3.68 | 3.14 | 3.41 | 2.06 |
| $E$ | 5.11 | 4.89 | 5.00 | 2.48 |
| $f$ | $3.55 \cdot 10^{-7}$ | $3.55 \cdot 10^{-7}$ | $3.55 \cdot 10^{-7}$ | $1.52 \cdot 10^{-8}$ |
| $\sigma_{data}$ | 1.67 | 1.67 | 1.67 | 0.02 |

The sampling is done in the same way as in the non-sliding model, with 200 samples and 2 chains. Once again 1000 steps are used in the tuning process before the actual sampling is being done. The posterior distributions of $n$, $Ak$, $E$, $f$ and $\sigma_{data}$ can be seen in Figure 6.5 with the statistics presented in Table 6.2. It should be noted that to prevent very small numbers, the surface velocity is kept in m yr$^{-1}$, thus rescaling the size of $f$. The shape and the statistics of the posterior distributions will be discussed further in the next section. As in the case without sliding it can be seen that the number of tuning steps is large enough to be past the burn-in time, and that the two chains have rather similar posterior distributions.

From the posterior distributions of $n$, $Ak$, $E$, and, $f$, posterior distributions of the logarithm of the ice flux are sampled. Using the same method as in the case without sliding the "best" guess of the ice flux is plotted in Figure 6.6a against the modelled ice flux from Section 5.1.3. Following the same line of argumentation as above I found that using the mean in eq. (6.10)
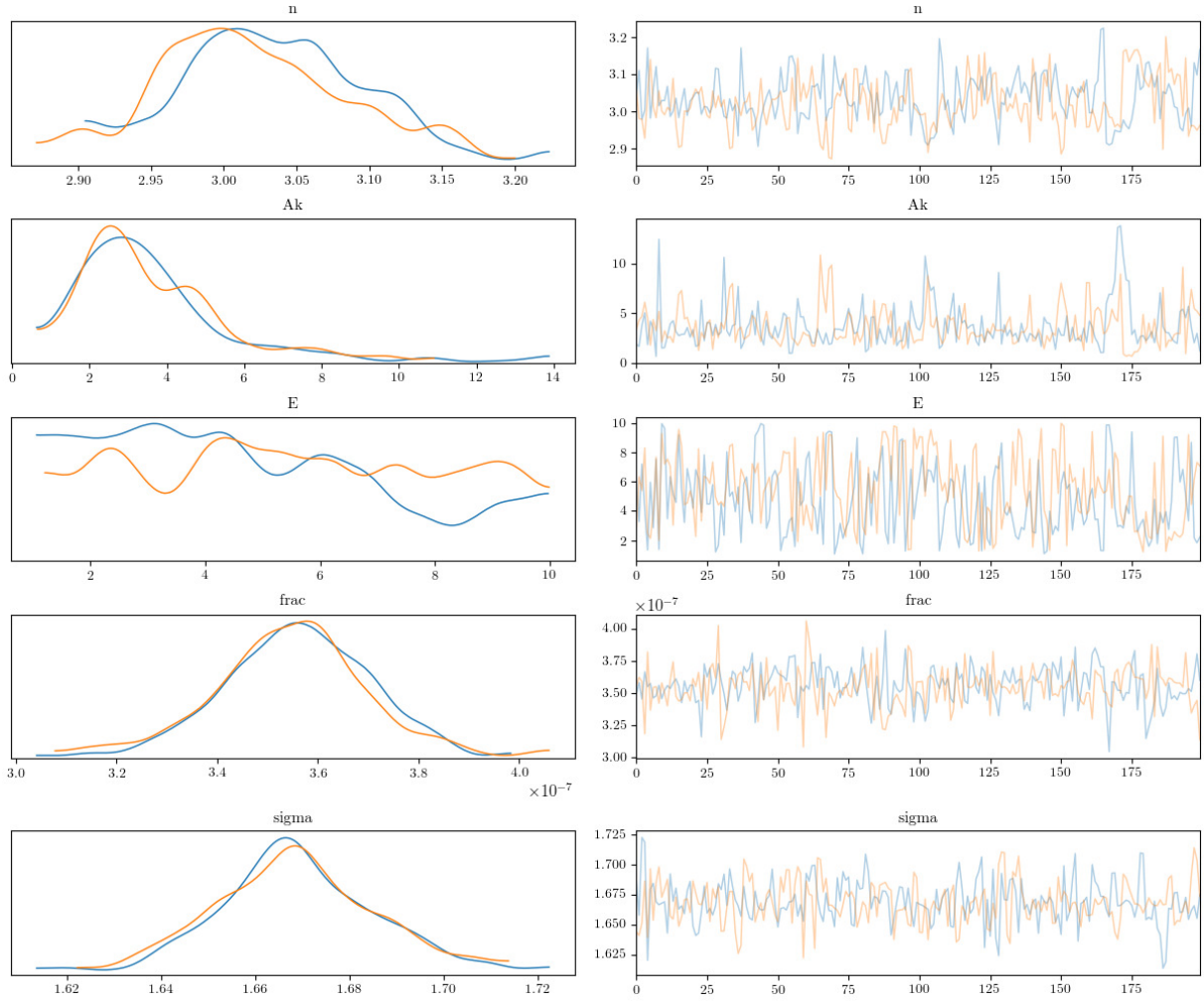
*Figure 6.5: Left: Posterior distributions of $n$, $Ak$, $E$, $f$, and $\sigma_{data}$. Right: The variability as a function of number of samples. The two colours represent the two chains.*

resembled the sampled ice flux the most, which can be seen in Figure 6.6b. Notice that I have used the entire IceBridge flight line in the latter figure.

With $n$, $Ak$, $E$ and $f$ found, these values are inserted into eq. (6.10) and (6.11), leaving the ice thickness as the only unknown parameter. To estimate the ice thickness I use `scipy.optimize.fsolve` which searches for the roots needed to make some expression equal to zero. This means that I feed it with an expression which is equal to the left side of eq. (6.10) minus the right side of eq. (6.10), i.e.

$$0 = \log Q - \log \left( f v_s H + \frac{2EA}{n+2} \rho^n g^n \alpha^n H^{n+2} \right). \tag{6.19}$$

Notice here that I have taken the logarithm on both sides of eq. (6.10). A first guess of the ice thickness also needs to be fed into `scipy.optimize.fsolve`, where I have chosen to use the ice thickness from the SIA inversion in Chapter 5. In the ideal world I would be able to run this and get an estimate of the ice thickness with sliding on my $100 \times 100$ m grid. Due to the

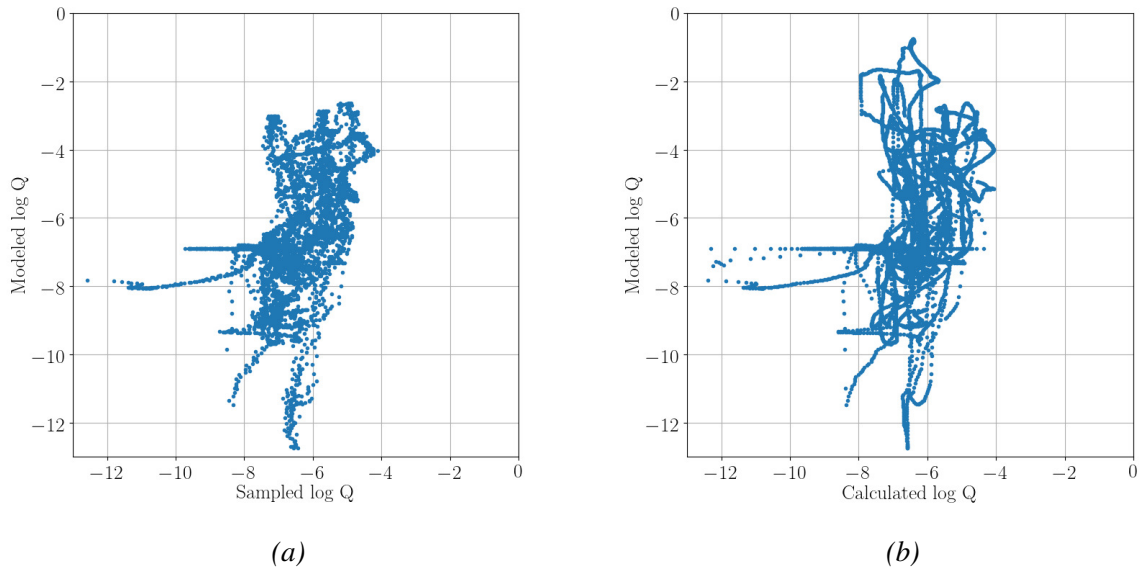*(a)*                                             *(b)*

*Figure 6.6:* **(a)** *Sampled ice flux versus modelled ice flux.* **(b)** *Calculated ice flux using the mean from Table 6.2 versus modelled ice flux.*

amount of memory needed to do this, it was not possible. Therefore I chose to interpolate the data onto my $900 \times 900$ m grid, which was also used in Chapter 3 and 4. Notice here that the velocity obviously already is on the right grid which is why only the ice flux, slope, and SIA inversion ice thickness were interpolated.

## 6.3.2   Results and discussion with sliding

Figure 6.7 shows the IceBridge cross section with the modelled bedrock as the black line. It can be seen that even though the model has not been trained with data from the outlet glaciers, it performs rather well in these areas. The bedrock topography on the ice cap is also captured quite well, and resembles the true bedrock quite well, though not to the same detail. There is only one significant dip in bedrock topography around 10 km, but that cannot be explained by the slope or the ice flux and is believed to be an outlier. All in all this model does a quite good job even in areas with low surface slope and flux in contrast to the model without sliding.

One could argue that since sliding has been included, it could make sense to use the entire flight line in the training of the model. I have chosen not to do that since the main goal is, as mentioned, to capture the ice cap as well as possible. Furthermore, I would expect a completely different basal velocity on the outlet glaciers as on the main ice cap, like in the discussion of the enhancement factor in Section 4.5 [Cuffey and Paterson, 2010, Ma et al., 2010].

The bedrock topography of the entire ice cap can be seen in Figure 6.8. The first thing that becomes apparent when looking at this figure, is how pixelated it is due to the coarser resolution.
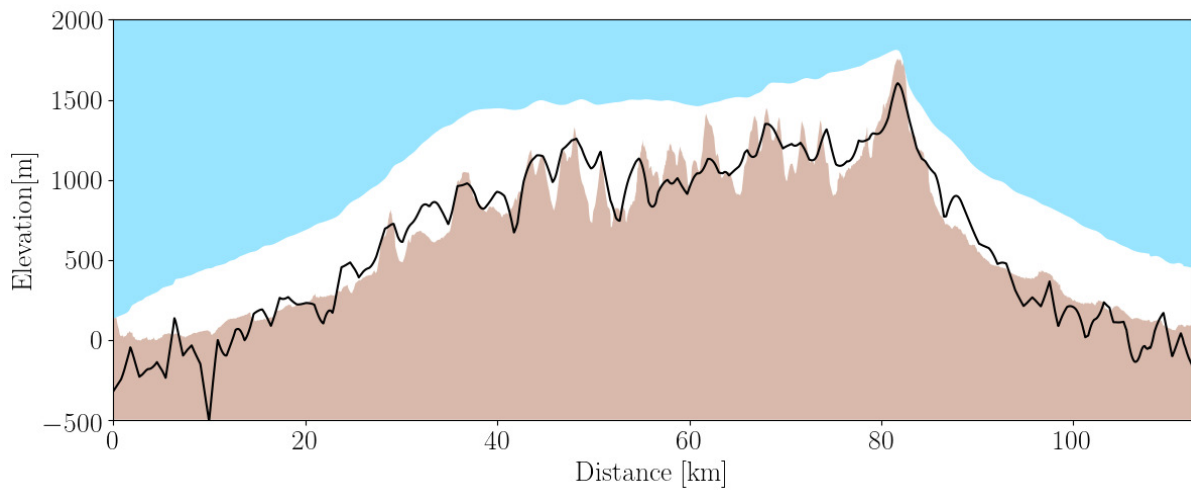
*Figure 6.7: IceBridge cross section with the modelled bedrock topography as the black solid line.*
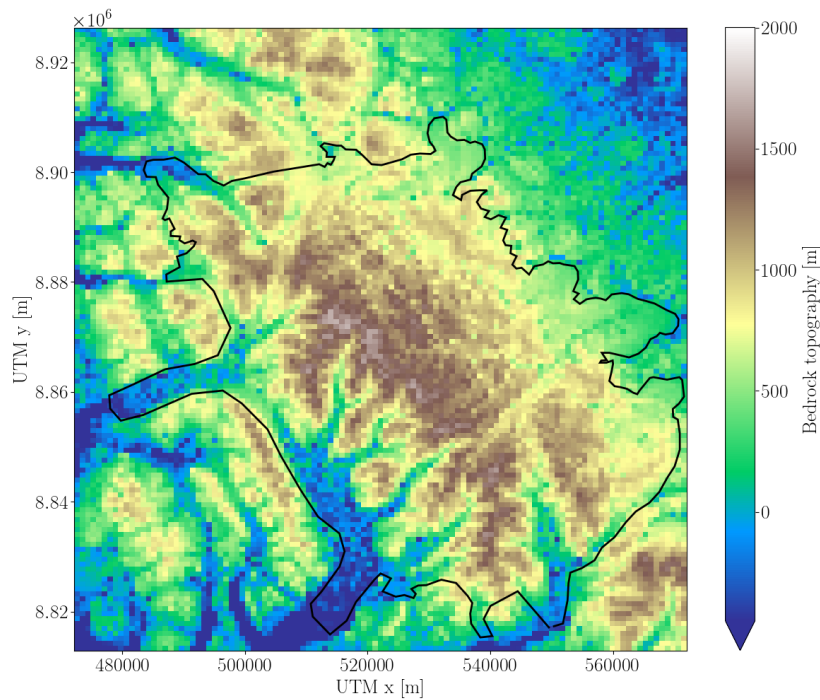


*Figure 6.8: Modelled bedrock topography*

This would definitely be one of the first things to work on if I were to continue on this project. Obviously an "easy" fix would be to run on the supercomputer. Though I think that one of the advantages of this model is that it can be run on a regular laptop, which is why I would rather try to make that possible. A way to do it, would be to look into the options of parallelisation, or to somehow do the minimisation in batches.

Returning to the posterior distributions of $n$, $Ak$, $E$, $f$ and $\sigma_{data}$ in Figure 6.5 and Table 6.2, it can be seen that the mean of the posterior distribution of the creep exponent and the rate
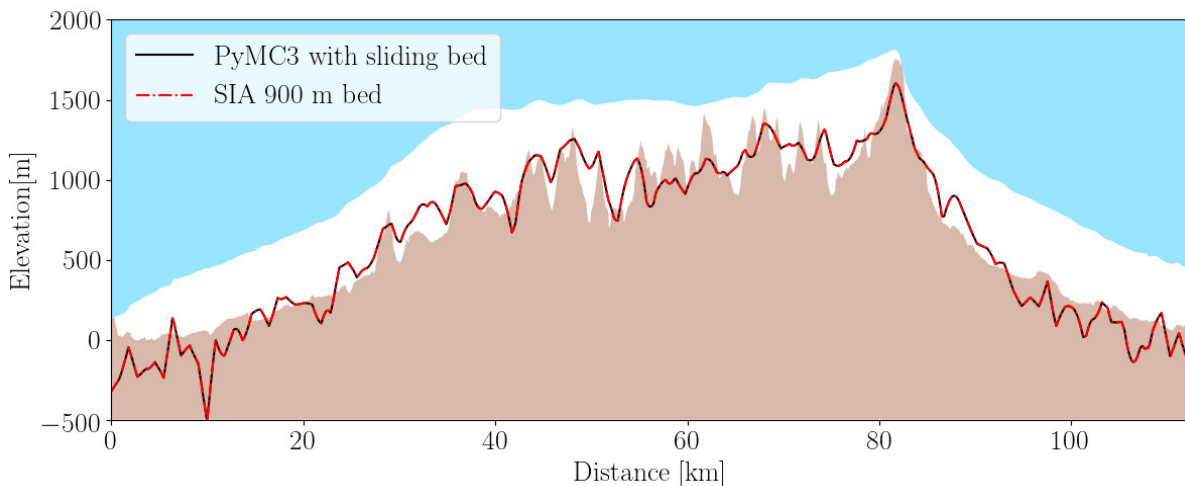
*Figure 6.9: Modelled MC bedrock with sliding in black and the SIA inversion bedrock interpolated onto the $900 \times 900$ m grid and then onto the flight line in dashed red.*

factor is 3.03 and $3.68 \cdot 10^{-25}$ s$^{-1}$Pa$^{-3}$ with a standard deviation of 0.07 and $2.06 \cdot 10^{-25}$ s$^{-1}$Pa$^{-3}$, respectively. This corresponds very well with theory [Cuffey and Paterson, 2010]. Note here that the true unit of the rate factor is in fact s$^{-1}$Pa$^{-3.03}$ because of $n = 3.03$, but since it is so close to 3, I chose to round the unit.

The enhancement factor is found to be around 5, which physically is possible. Do notice that in this model (see eq. (6.10)), it is not possible to really distinguish between $E$ and $A$. Either way, they both seem to have the right order of magnitude as one would expect [Cuffey and Paterson, 2010].

As it turns out, the output from the MC sampling has almost no influence on the estimated ice thickness, if it even has any influence at all. In Appendix F the modelled bedrock topography is shown when using a uniform SMB with ones everywhere. Here it is found that the output from `scipy.optimize.fsolve` is the exact same as when using the HIRHAM SMB. Therefore I tried to change the initial guess of ice thickness to a uniform one with ones in every single grid cell, to see how much `scipy.optimize.fsolve` relies on the initial guess. Unfortunately I found that the ice thickness then became equal to one in every single grid cell. This caused my alarm bells to ring; what if the MC bedrock with sliding is only a result of interpolating the SIA inversion ice thickness from a 100 m to 900 m grid? To investigate this I plotted both the MC bedrock interpolated onto the IceBridge flight line together with the SIA inversion bedrock which first has been interpolated onto the $900 \times 900$ m grid, and after that interpolated onto the IceBridge flight line as shown in Figure 6.9. It can be seen that `scipy.optimize.fsolve` unfortunately comes up with the exact same result as the initial guess.

This means that I have not successfully been able to add sliding to my model as I in reality have just smoothed the SIA inversion bedrock due to the interpolation. Thus the biggest disad-

vantage of this model is that I cannot do the sampling of the ice thickness, and have to use a function like `scipy.optimize.fsolve`. Thus I think it would be worthwhile to set up a new ice flow model where it is possible to sample the ice thickness itself. To do so I could have a further look into the methods presented by Brinkerhoff et al. [2016] and Werder et al. [2020]. This would most likely also imply that much of the simplicity from the model presented here would vanish, and the computational power needed would increase. However, as my studies only represent the tip of the iceberg, there is definitely a lot of potential of using MC algorithms to estimate ice thicknesses.

That being said, I will still use this result in my investigations of possible drill site areas. It will be referred to as the MC model with sliding, but do keep in mind that it really just is a smoothing of the SIA inversion.

# 7 Model merging and discussion

In this chapter I will bring all of the pieces together into one big picture. First I will combine Chapters 4 and 5 in order to create a last estimate of bedrock topography. Then I will compare all modelled bedrock topographies/ice thicknesses, so that I can identify possible drill areas and present ideas for future research.

## 7.1 Using the SIA inversion ice thickness in PISM

To test the validity of the SIA inversion model outside of the IceBridge flight line I will apply the PISM methodology, in which the SIA inversion bed, see Figure 5.5, is used as an initial bedrock topography guess. For future reference I will call this model the SIA+PISM model. The bedrock topography is interpolated onto the $900 \times 900$ m grid. The algorithm is then run for 10 iterations, updating the bedrock as described in Section 4.3. I will, however, not scan all till friction angles and enhancement factors but rather use the optimal parameters, $10°$ and 6, respectively, from Section 4.5. Note here that I use ArcticDEM as described in Chapter 4, and not the smoothed version as described in Section 5.1.1. In hindsight, I should have used the smoothed bedrock as of Section 5.1.1 instead of that of Chapter 4 throughout the thesis. This was unfortunately not possible as the simulations were already underway as this revolution came about. Running all of the PISM runs again was not an option due to the computational time.

Figure 7.1 shows the RMS of the modelled surface elevation compared to ArcticDEM, the modelled ice thickness compared to the entire IceBridge flight line and the IceBridge fligt line on the ice cap (marked in blue in Figure 4.5) and of the modelled surface velocity compared to the surface velocity marked in Figure 4.8. It can be seen that the general minimum RMS is found
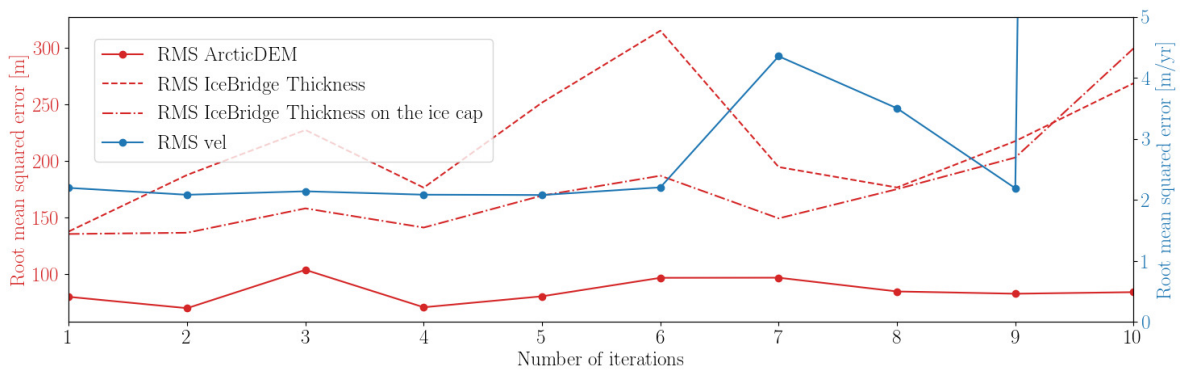


*Figure 7.1: Root mean squared error of the surface elevation, ice thickness and surface velocity as a function of iterations.*
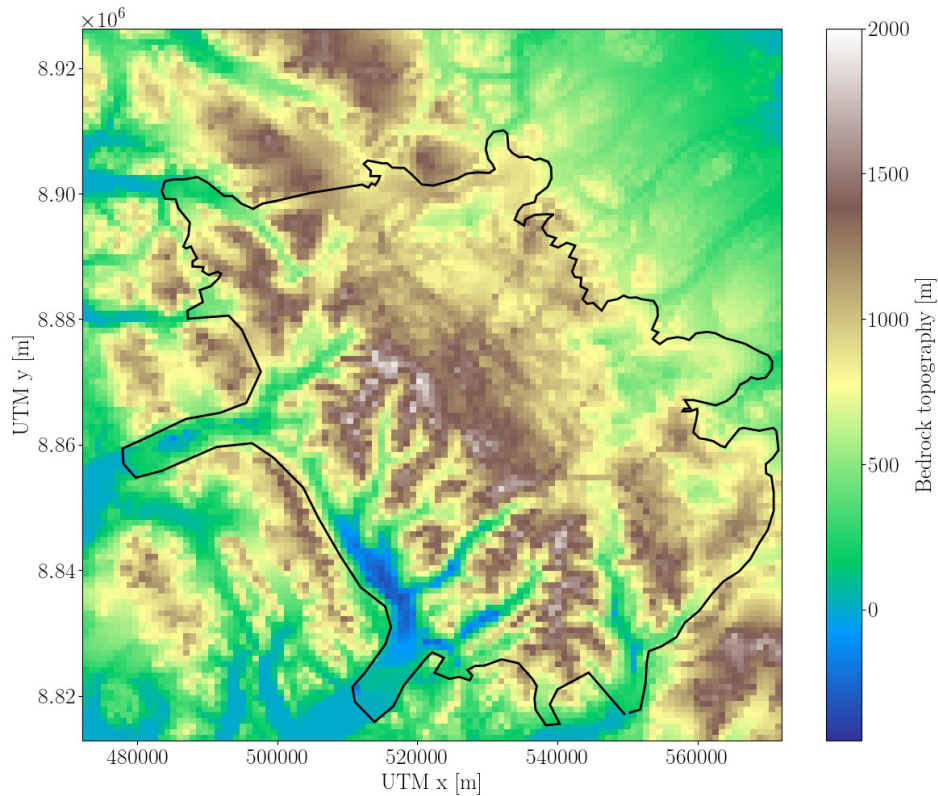
71

*Figure 7.2: Modelled bedrock topography from iteration 1.*

around iteration 1-2 and that the RMSs of the surface elevation and the ice thickness are very low compared to the runs where the Farinotti bedrock has been used (see Figure 4.7). The RMS of the surface elevation compared to ArcticDEM is more or less steady throughout the runs, suggesting that the minimum RMS has already been reached from the beginning. Furthermore it can be seen that the RMS of the surface velocity is in the same order of magnitude as when using the Farinotti bedrock as seen in Figure 4.9, except for the very last iteration where it reaches more than 100 m yr$^{-1}$. This suggests that my simple SIA inversion model performs well also outside of the IceBridge flight line, and that my guess for bedrock topography using this methodology actually is better than the Farinotti bedrock. This would most likely also be the case if I had used one of the MC bedrocks as initial guess.

Figure 7.2 shows the modelled bedrock topography from iteration 1 (i.e. ArcticDEM subtracted by the ice thickness at the end of iteration 1), the iteration with the lowest RMSs when all parameters are taken into consideration.

Because the SIA inversion bedrock is interpolated onto a coarser grid and run in PISM, I also get rid of the big dips in bedrock topography caused by the low surface slope. All of this results in a smoother bedrock topography, as seen in Figure 7.3 which shows the IceBridge cross section at iteration 1. It can be seen that the ice thickness is underestimated on the main outlet glacier, probably due to the high enhancement factor. Using two different enhancement
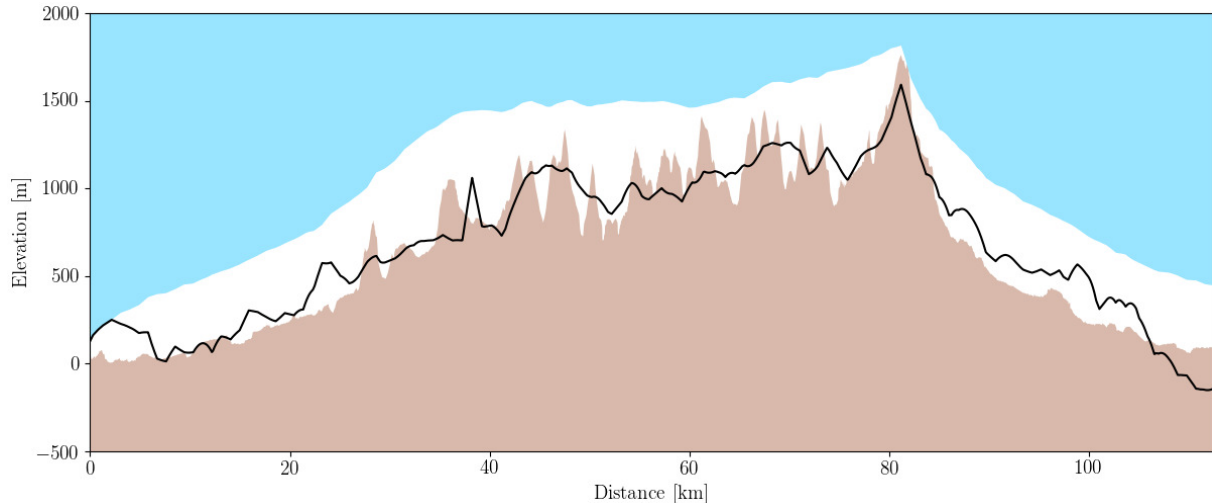
*Figure 7.3: Cross section of the IceBridge flight line with the modelled bedrock topography at iteration 1.*

factors for the SIA and the SSA might improve the results. Future simulations should be similar to the ones I have performed, with the only change of different enhancement factors in the SIA and SSA, where the value for the latter is to be found. I believe this would improve the results on the outlet glaciers without compromising those on the main ice cap.

## 7.2 Comparing all modelled ice thicknesses

Figure 7.4 shows the full IceBridge flight line cross section with all modelled bedrocks and the Farinotti bedrock. Notice that I have used the smoothed version of ArcticDEM as surface elevation. Not surprisingly, the biggest differences are found on the outlet glaciers, where especially the PISM bedrock stands out. However, on the main ice cap not much difference is to be seen between the SIA and the two MC models. In the case of MC without sliding, this is obviously because they are based on the same equation but with different tuning parameters. In the case of MC with sliding, the models are similar as the MC with sliding only represents a smoothed version of the SIA inversion.

A close up of the modelled bedrocks on the ice cap can be seen in Figure 7.5. The Farinotti bedrock alongside the two bedrocks that have been through PISM (PISM and SIA+PISM) show many similarities in the pattern of the bedrock. The fact that the PISM bedrock shares similarities with the Farinotti bedrock is not surprising as the latter was used as an initial guess in PISM, but the fact that the SIA+PISM bedrock also shares the same similarities on the ice strikes me. This pattern also showed up in all of the PISM models (i.e. Figure 4.6), indicating that it might just reflect the ice dynamics in PISM, rather than the initial guess of bedrock topography.

Focusing on the bedrock on the ice cap from the SIA inversion and MC without sliding, it
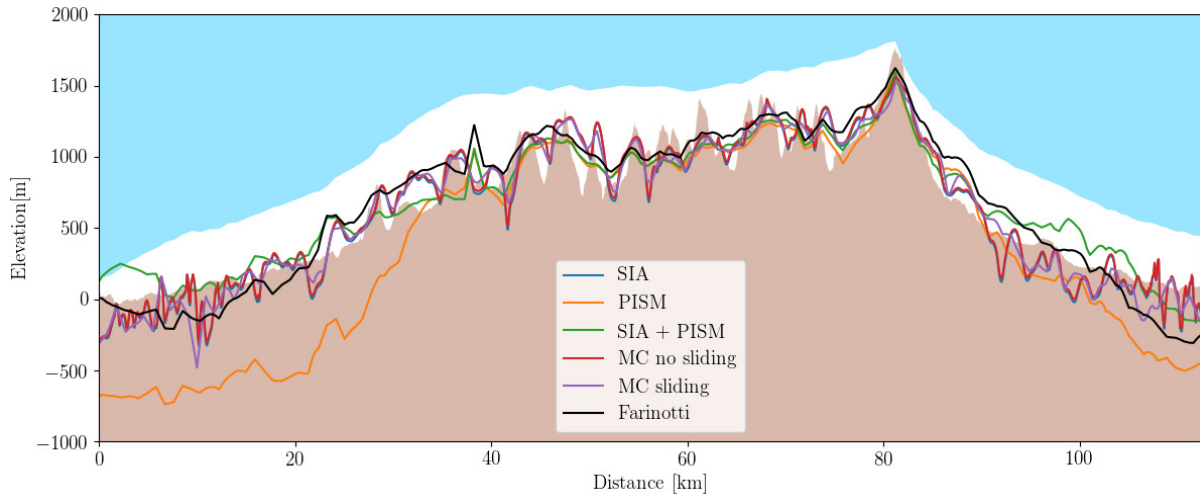
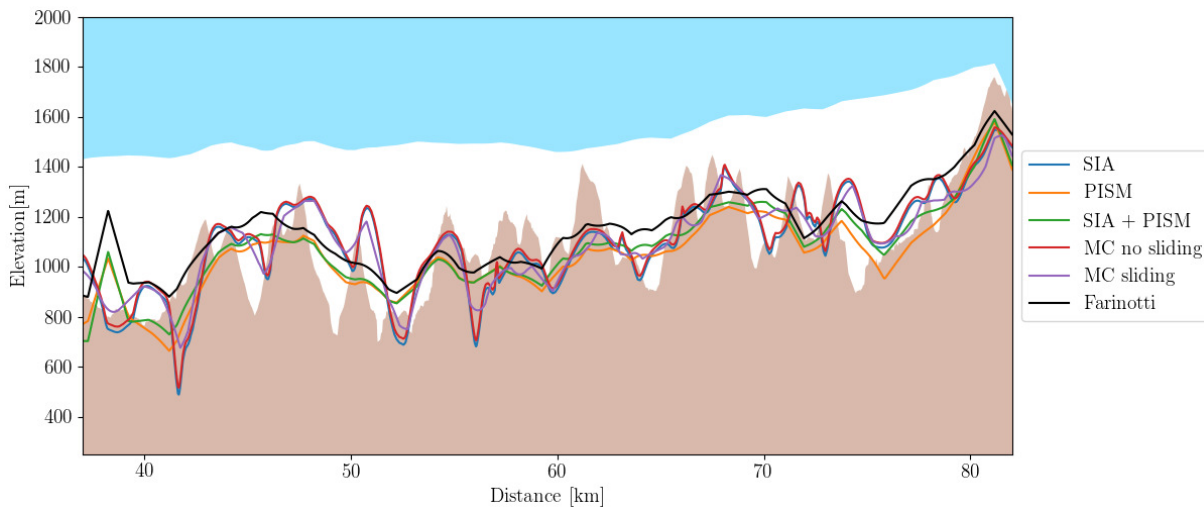*Figure 7.4: IceBridge cross section of all modelled bedrocks.*



*Figure 7.5: IceBridge cross section as marked in blue in Figure 4.5 of all modelled bedrocks.*

becomes even more apparent how closely related they are, with the SIA inversion tending to reach lower elevations. The MC with sliding bedrock shows the same features only smoother, and thus does not reach as low or as high elevations compared to the other two.

To be able to compare all modelled bedrocks of the entire ice cap I have plotted them together in Figure 7.6 including the Farinotti bedrock for comparison. I will only compare the models within the outline of the ice cap, shown in black. Notice, that the SIA inversion and MC without sliding are on a $100 \times 100$ m grid, the Farinotti on its original 130 m grid, and the rest are on the $900 \times 900$ m grid. All of the bedrocks share many of the same features, except for the irregularities on the outlet glaciers in Figures 7.6c, 7.6d and 7.6e, the very low bedrock on the southern outlet glacier in 7.6b, and its elevated northern part. Thus in the areas of interest regarding drilling a full depth ice core, the bedrocks are quite similar.

Now that all ice thicknesses have been presented together, I want to just have a brief dis-

*(a) Farinotti et al. [2019]*

*(b) PISM*

*(c) SIA inversion*

*(d) MC without sliding*

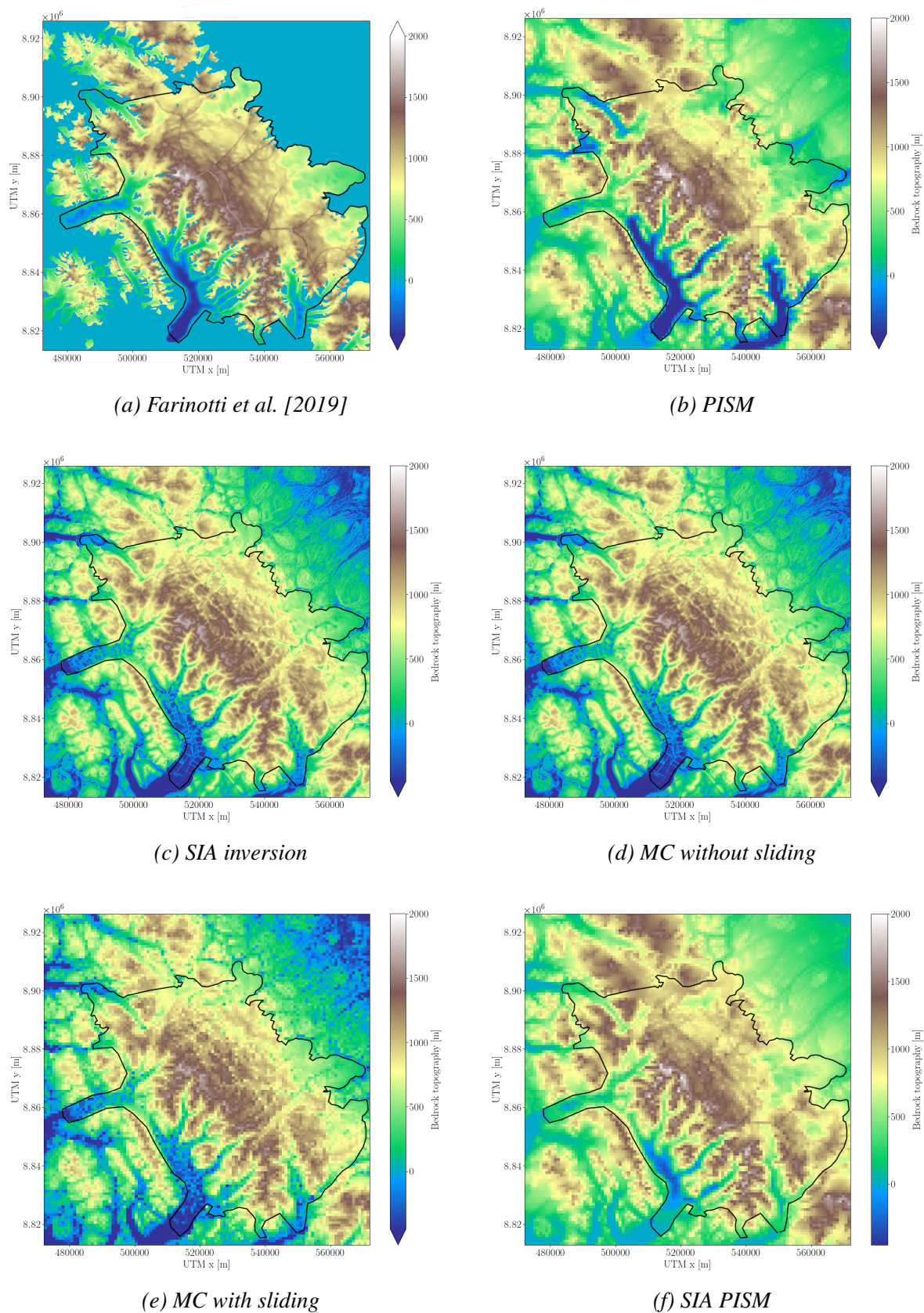*(e) MC with sliding*

*(f) SIA PISM*

*Figure 7.6: All modelled bedrocks including the bedrock by Farinotti et al. [2019] for comparison. The black line represents the outline of the ice cap.*

cussion on the rate factors (and thereby also enhancement factors) found in the SIA inversion and in the two MC models. In the SIA inversion $A$ was found to be $2.06 \cdot 10^{-23}$ s$^{-1}$Pa$^{-3}$, and no enhancement factor was used. In MC without sliding the rate and enhancement factors were found to be $4.00 \cdot 10^{-25}$ s$^{-1}$Pa$^{-3}$ and 5.68, respectively. Substituting the enhancement factor into the rate factor, gives a rate factor of $2.27 \cdot 10^{-24}$ s$^{-1}$Pa$^{-3}$. Doing the same in MC with sliding, substituting the enhancement factor into the rate factor gives $1.88 \cdot 10^{-24}$ s$^{-1}$Pa$^{-3}$. The standard deviation of $A$ from the two latter models is around $2 \cdot 10^{-25}$ s$^{-1}$Pa$^{-3}$ and the standard deviation of the enhancement factor is around 2-3. Taking these uncertainties into consideration, the rate factor in the three models are more or less the same and corresponds to an unrealistic high ice temperature just above 0 °C when no enhancement factor is taken into consideration (see Figure 2.2). This is of course an unrealistic high ice temperature. However, this does not take the enhancement factor into account, but doing so results in an ice temperature well below -10 °C. All of this indicates that the enhancement factor on the Müller ice cap is somewhere between 4 and 6, in agreement with my PISM results.

A summary of the RMS results is tabulated in Table 7.1. The RMS on the ice cap is calculated using the part marked in blue in Figure 4.5. It can be seen that all models perform better than Farinotti on the ice cap and that the MC model with sliding performs the best.

*Table 7.1: Comparison of all ice thickness products on the entire IceBridge flight line and on the ice cap marked with blue in Figure 4.5.*

| RMS | Farinotti | PISM | SIA inversion | MC no sliding | MC sliding | SIA+PISM |
|---|---|---|---|---|---|---|
| **All [m]** | 169.1 | 396.2 | 136.1 | 132.6 | 137.9 | 137.9 |
| **Ice cap [m]** | 146.3 | 138.9 | 131.4 | 132.1 | 129.9 | 135.4 |

If I had to decide on a best model, I am in doubt whether I would choose the SIA inversion or the MC without sliding. The reason is that I really like the simplicity of the SIA inversion combined with the fact that it takes around 3 minutes to run and ends up with roughly the same RMSs as MC without sliding. MC without sliding does give one an insight into the tuning parameters as compared to the SIA inversion, but it takes roughly 18 minutes to run, and ends up with approximately equally good results. Both models have shown not to depend on the SMB (see Appendices D and E). This is a huge advantage when the data is sparse. That being said, they are both very unsmooth where SIA+PISM does offer a much smoother result with approximately the same RMS.

All of the modelled ice thicknesses alongside with the corresponding bedrock topographies and surface elevations are available as GeoTIFFs on Zenodo (`https://doi.org/10.5281/zenodo.4290039`).

# 7.3 Suggestion for possible drilling areas

The goal of this thesis is to suggest areas where ground based radar should be performed in preparation of drilling a full depth ice core. The optimal drilling site should fulfill a handful of criteria: The site should have the thickest possible ice, have a minimal horizontal velocity and be of highest possible elevation to reduce melting. To quantify this I made a scoring system based on studies of equilibrium line [Cogley et al., 1996] and a discussion with Associate Professor Bo Møllesøe Vinther, one of the leading scientists in the Müller ice core drilling project.

I used the $900 \times 900$ m grid as it has been used in the most models. Thus, all other data is interpolated onto this grid. In addition to the modelled ice thicknesses (PISM, SIA inversion, MC without sliding, MC with sliding and SIA+PISM), the scoring system is based on elevation data from ArcticDEM and the Landsat 8 median velocity map (see Figure 3.4).

The score of every single grid cell is determined as follows:

| | |
|---|---|
| Surface velocity $< 5$ m yr$^{-1}$ | *1 point* |
| Surface velocity $< 2$ m yr$^{-1}$ | *1 point* |
| Surface elevation $> 1600$ m | *1 point* |
| Surface elevation $> 1700$ m | *1 point* |
| PISM ice thickness $> 500$ m | *1 point* |
| SIA ice thickness $> 500$ m | *1 point* |
| MC no sliding ice thickness $> 500$ m | *1 point* |
| MC with sliding ice thickness $> 500$ m | *1 point* |
| SIA+PISM ice thickness $> 500$ m | *1 point* |

Furthermore, if either the surface velocity exceeds 10 m yr$^{-1}$, the surface elevation is below 1500 m or all modelled ice thicknesses are below 500 m, the total score in that grid cell will be zero. This means that it is possible to get a total score of 9 points.

Figure 7.7a shows the Müller ice cap with scores and elevation contour lines every 100 m from 1400-1700 m. It can be seen that grid cells with scores $\geq 1$ are scattered in the western part of the ice cap along the mountain range, besides from a few patches just northeast of the southernmost outlet glacier. As this results in a rather large area to conduct ground based radar, I have chosen to also make a figure only showing scores $\geq 7$ (see Figure 7.7b). This results in more or less one cluster at the very top of the ice cap. In the scoring system, the ice thickness is essentially weighted higher than the surface velocity and elevation. It can be shown that the pattern of interesting sites is more or less the same if the scores are weighted, so that the final suggestion is not influenced significantly by the fact that the ice thickness ice weighted higher. Furthermore, one could argue that weighting the ice thickness higher in the search of a full depth ice core drilling site is reasonable.
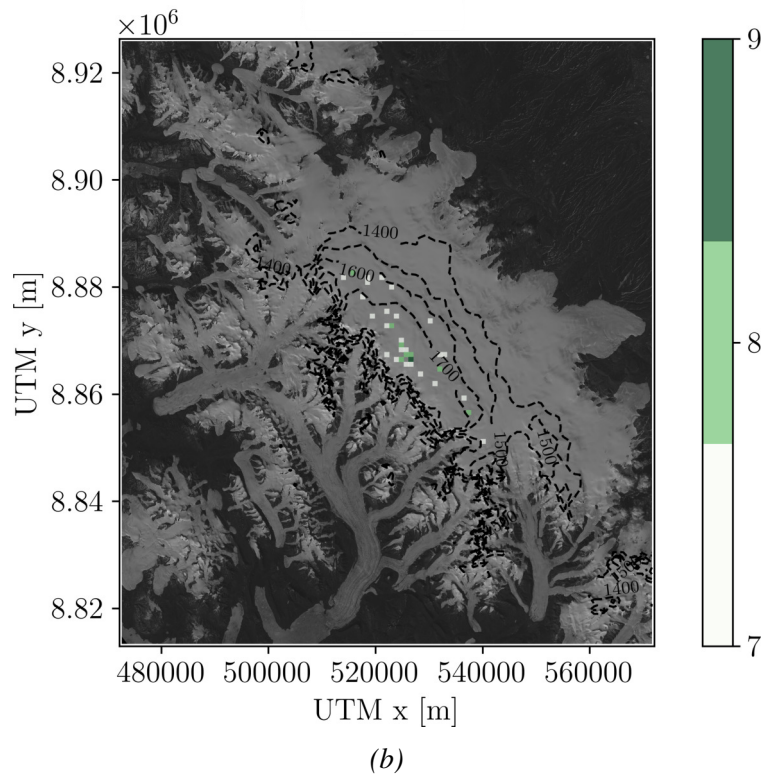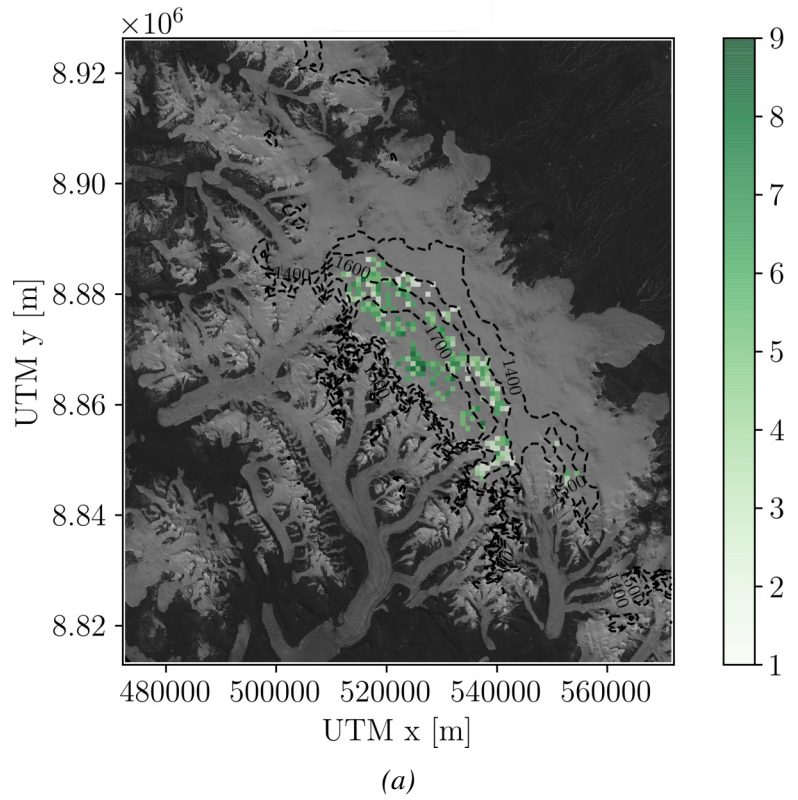
*(a)*



*(b)*

*Figure 7.7:* **Top:** *Map of suggested drill sites with scores and a contour of the surface elevation with contour lines every 100 m from 1400-1700 m.* **Bottom:** *Map of suggested drill sites with a score of at least 7 and a contour of the surface elevation with contour lines every 100 m from 1400-1700 m.*
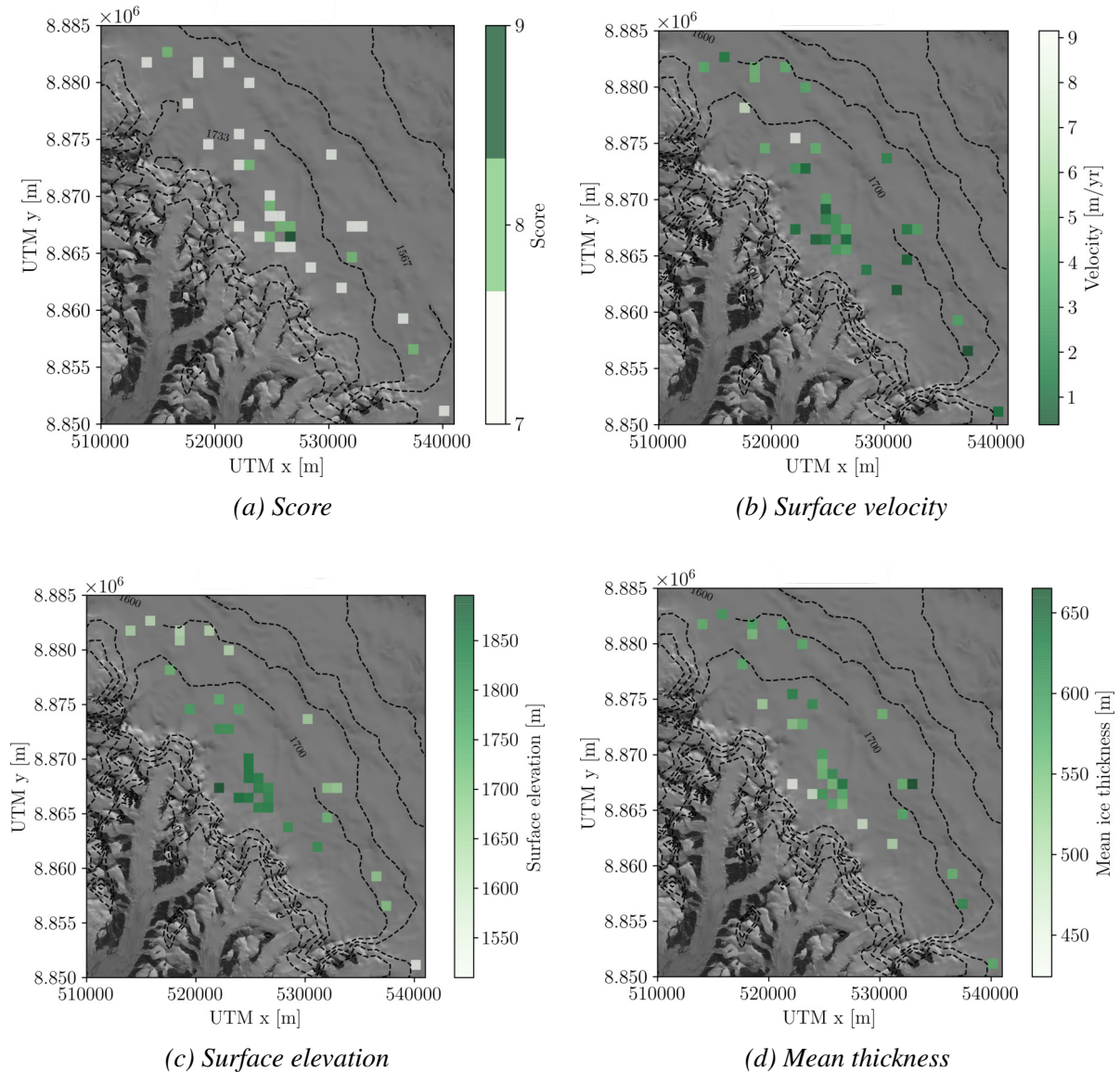
*(a) Score*

*(b) Surface velocity*

*(c) Surface elevation*

*(d) Mean thickness*

*Figure 7.8: Zoom-in of score (a), surface velocity (b), surface elevation (c) and mean ice thickness (d) in the area of interest.*

A zoom-in in Figure 7.8a shows that the biggest cluster of high scored pixels can be found around UTMx:525700, UTMy:8867000 (EPSG:32615). Here it can be seen that only one pixel reaches a score of 9 (henceforth referred to as site #1), but the pixels in the area around it, also have relatively high scores.

To see what this means in terms of surface velocity, surface elevation and ice thicknesses, the Figures 7.8b, 7.8c and 7.8d show these fields, respectively. The ice thickness is the mean of all modelled ice thicknesses. Notice, the colour bar is chosen such that dark green corresponds to the most suitable drilling area in all subfigures in Figure 7.8, i.e. the velocity map is inverted. Individual values for site #1 are given in Table 7.2. The difference in ice thickness originating from all of the models varies quite a lot. Had I based my scoring solely on one model, the result

*Table 7.2: Surface velocity, elevation and modelled ice thicknesses for site #1.*

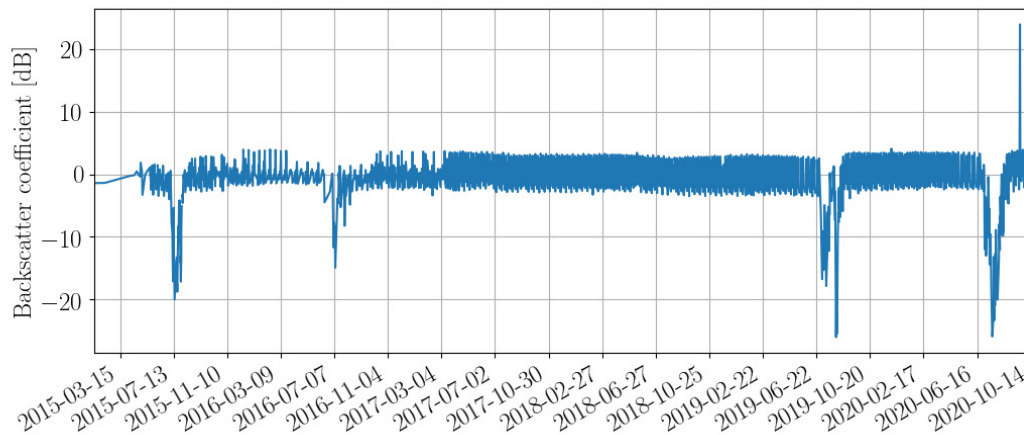| Site #1 | |
|---|---|
| **Surface velocity [m yr$^{-1}$]** | 1.2 |
| **Surface elevation [m]** | 1804 |
| **PISM thickness [m]** | 535 |
| **SIA thickness [m]** | 579 |
| **SIA+PISM thickness [m]** | 562 |
| **MC without sliding thickness [m]** | 560 |
| **MC with sliding thickness [m]** | 579 |



*Figure 7.9: Backscatter coefficient as a function of time at site #1, UTMx: 526629, UTMy: 8866463, EPSG:32615.*

might be biased, but using the average makes my prediction more robust. However, this shows how much variance there is in the results which is why the highlighted points in Figure 7.8a are only suggested locations for additional measurements.

As mentioned it is also important to know how much melt is taking place, as one would preferably do the drilling in a place with as little as possible. Alternatively, one could perform the drilling prior to the onset of melting, but after the sun has returned obviously. Sentinel-1 measures the backscattering of light on the surface, and since water reflects approximately four times more than ice, it can be used as a proxy for melt. Figure 7.9 shows the backscatter data, treated with the Sentinel-1 Toolbox [Veci et al., 2014], as a function of time a the midpoint of site #1 (UTMx: 526629, UTMy: 8866463, EPSG:32615). The backscatter showed here is only from the HH band (Horizontal Transmit - Horizontal Receive Polarisation), which is why there is noise around zero as the radar does not necessarily detect what is right below it. It should be noted that I have used a ready made script on Google Earth Engine, where by choosing a point on the Earth I could download the data from that specific point, which then is what I have plotted.
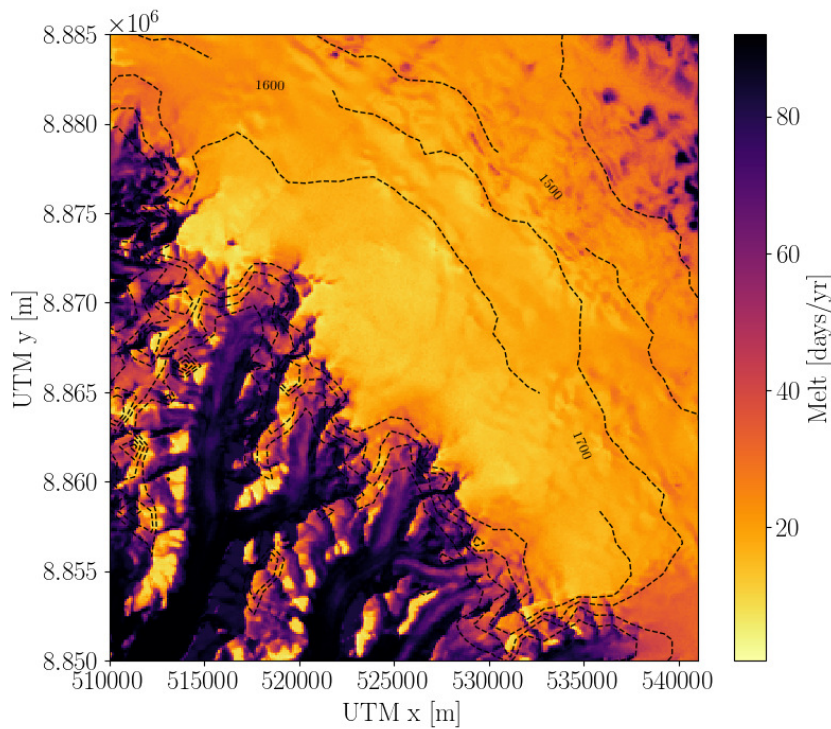
*Figure 7.10: Average melt days per year in the period of 2016-2020. If the backscatter coefficient < -5 dB, it is considered a melt day.*

From Figure 7.9 it can be seen that melt has occurred four out of six summers in the past six years. In the years with the most melt, the melt kicked in at the end of June. This means that a melt-free drilling season would start when sunlight permits it around March/April and end in the middle of June worst case scenario. Figure 7.10 shows the average melt days per year in the area of interest on the ice cap. In these calculations it is considered a melt day if the backscatter coefficient < -5 dB, and only scenes from June-August are taken into consideration. Here it can be seen that in the area with the highest scores the average number of melt days per year is less than 20, which is on the lower limit that can be observed on the ice cap.

## 7.4  Outlook

With the SIA inversion and the MC without sliding I was able to estimate the ice thickness only using the surface elevation (and thereby the slope), the glacier outline and one radar line with ice thicknesses. It was shown that the SMB had very little influence on the final estimate of ice thickness, thus these two methods rely only on remote sensing data.

Imagine that one of these two methods were applied to all glaciers with an available DEM and at least one line of thickness measurements, for instance using the glacier thickness database (GlaThiDA). Then one would be able to obtain tuning parameters for all of these glaciers.

Those tuning parameters could then be compared with data, such as location on Earth, average temperature, elevation etc., allowing one to do statistics on the relationship between these and the tuning parameters. Especially the rate factor dependents strongly on temperature, thus the chance of getting useful relationships out of the statistical studies, certainly is present. Thus if a clear pattern shows up, this would allow one to make a global glacier estimate only using a DEM and an outline of the glaciers. With these parameters it would be possible, and even quite fast, to perform a SIA inversion of all glaciers and ice caps around the globe.

Most global glacier estimates, excluding the polar ice sheets, only provide the volume of the glaciers [Dyurgerov and Meier, 2004, Grinsted, 2013, Radić and Hock, 2010, Radić et al., 2014]. Only two global glacier estimates with ice thicknesses exists [Farinotti et al., 2019, Huss and Farinotti, 2012], one of which is the Farinotti bedrock used in this thesis. One of the ITMIX [Farinotti et al., 2017] main results was that averaging over many models resulted in more robust results, which makes the future perspectives of the SIA inversion and the MC without sliding even more interesting. In the future they could be a part of an even more robust global glacier thickness estimate. In the end this would also lead to a better estimate of the potential contribution to sea level rise, from all glaciers and ice caps around the world.

In terms of the Müller ice cap an even better estimate for the ice thickness could be made after retrieval of ground based radar measurements. The SIA inversion and/or the MC without sliding could then be applied again using not only the IceBridge data, but also the ground based radar data. Depending on the amount of measurements one could also investigate the possibilities of applying machine learning to such data. That is, one could use the radar measurements as training data with input features such as surface elevation, slope, SMB etc.

Thus the methods and results from this thesis arise various ideas for interesting future research. Especially studies of potential contribution to sea level rise from the glaciers, ice caps and ice sheets are of great importance in these times of climate change.

# 8    Conclusion

In this thesis, surface velocities and ice thicknesses of the Müller ice cap have been studied, for the purpose of deciding where to conduct ground based radar in preparation for the drilling of a full depth ice core.

Surface velocity maps with a resolution of 900 m have been made of all cloud free Landsat 7 and 8 scenes covering the ice cap. The main result is a median velocity map of all Landsat 8 maps. Due to the coarse resolution the surface velocity is not captured well on all of the outlet glaciers, as the focus has been on the actual ice cap. The Landsat 8 median velocity map is available as a GeoTIFF on Zenodo (`https://doi.org/10.5281/zenodo.4290041`) alongside with a list of all satellite images used to create the velocity map.

In the process of estimating the ice thickness, five models have been used. All modelled ice thicknesses are compared with the ice thickness measured from Operation IceBridge by calculating the root mean squared error. Quickly summing up the models one by one. The PISM model performs badly on the outlet glaciers, but it offers a smooth output of the ice thickness. It takes a long time to run, and one might get better use of PISM in cases where more parameters are known. Different combinations of till frictions angles and enhancement factors are tested, and it was found that using a till friction angle of $10°$ and an enhancement factor of 6 resulted in the lowest root mean squared error. The SIA inversion and the MC model without sliding offer a fast procedure to estimate the ice thickness with a relatively low root mean squared error. They both suffer from overestimation of ice thicknesses in areas with low surface slopes. The MC model without sliding offers an insight into the physical parameters of the model in contrast to the SIA inversion. In the second MC model, sliding was added in the SIA. Due to the adding of sliding in the SIA, it was not possible to sample the ice thickness why the ice flux was sampled instead. To estimate the ice thickness from the sampled parameters a minimisation function was used. When the results from the MC model with sliding were investigated further, it became clear that they were merely a smoothed version of the SIA inversion. In the final estimate of the ice thickness, the result from the SIA inversion was used as initial guess of geometry in PISM. As compared to the initial PISM runs, there was no overestimation of ice thickness on the outlet glaciers. Furthermore, it was found that the root mean squared error in general was smaller than in the initial PISM runs, suggesting that the SIA inversion geometry is closer to the true geometry than the Farinotti geometry. All of the modelled ice thicknesses alongside with the corresponding bedrock topographies and surface elevations are available as GeoTIFFs on Zenodo (`https://doi.org/10.5281/zenodo.4290039`).

From the surface velocity map, the modelled ice thicknesses and the surface elevation from ArcticDEM, a scoring system was created in order to suggest areas on where to conduct ground

based radar as preparation for drilling a full depth ice core. The optimal drill site should have a great ice thickness, low surface velocity and have a high surface elevation to ensure the least possible amount of melt. The position of the center of the grid cell with the highest possible score is at 526629 m easting and 8866463 m northing in UTM zone 15N. In that cell the modelled ice thicknesses are within the range of 535-579 m, the surface velocity is 1.2 m yr$^{-1}$ and the surface elevation is 1804 m. Furthermore, the average number of melt days per year in the 2015-2020 period was found to be less than 20.

This work shows how much one can actually do solely with remote sensing data, and will hopefully save the Müller project group valuable time in the field searching for an optimal drill site location. Furthermore, it might even improve the choice of drill site, as such thorough pre-drilling investigations as presented here, are usually not done outside of the polar ice sheets.

# Bibliography

P. Adams. Fritz Müller's legacy on Axel Heiberg Island, Nunavut, Canada. *Annals of Glaciology*, 31:1–9, 01 2000. doi: 10.3189/172756400781819798.

AntarcticGlaciers.org. An introduction to the hierarchy of ice-sheet models. URL `http://www.antarcticglaciers.org/glaciers-and-climate/numerical-ice-sheet-models/hierarchy-ice-sheet-models-introduction/`.

D. J. Brinkerhoff, A. Aschwanden, and M. Truffer. Bayesian Inference of Subglacial Topography Using Mass Conservation. *Frontiers in Earth Science*, 4:8, 2016. ISSN 2296-6463. doi: 10.3389/feart.2016.00008.

E. Bueler and J. Brown. Shallow shelf approximation as a "sliding law" in a thermomechanically coupled ice sheet model. *Journal of Geophysical Research*, 10 2008. doi: 10.1029/2008JF001179.

D. Chandler, A. Hubbard, B. Hubbard, and P. Nienow. A Monte Carlo error analysis for basal sliding velocity calculations. *Journal of Geophysical Research*, 111, 10 2006. doi: 10.1029/2006JF000476.

J. Cogley and W. P. Adams. Remote-sensing Resources for Monitoring Glacier Fluctuations on Axel Heiberg Island. *ARCTIC*, 53, 09 2000. doi: 10.14430/arctic856.

J. Cogley, W. P. Adams, M. A. Ecclestone, F. Jung-Rothenhäusler, and C. S. L. Ommanney. Mass balance of White Glacier, Axel Heiberg Island, N.W.T., Canada, 1960–91. *Journal of Glaciology*, 42(142):548–563, 1996. doi: 10.3189/S0022143000003531.

J. G. Cogley, W. P. Adams, and M. A. Ecclestone. Half a Century of Measurements of Glaciers on Axel Heiberg Island, Nunavut, Canada. *ARCTIC*, 64:371–375, 09 2011. doi: 10.14430/arctic4127.

W. Colgan, W. Pfeffer, H. Rajaram, W. Abdalati, and J. Balog. Monte Carlo ice flow modeling projects a new stable configuration for Columbia Glacier, Alaska, c. 2020. *The Cryosphere, Volume 6, Issue 6, 2012, pp.1395-1409*, 6:1395–1409, 11 2012. doi: 10.5194/tc-6-1395-2012.

L. Copland, M. J. Sharp, and J. A. Dowdeswell. The distribution and flow characteristics of surge-type glaciers in the Canadian High Arctic. *Annals of Glaciology*, 36:73–81, 2003. doi: 10.3189/172756403781816301.

K. M. Cuffey and W. S. B. Paterson. *The Physics of Glaciers*. Elsevier, 2010.

M. Dyurgerov and M. Meier. Glaciers and the Changing Earth System: A 2004 Snapshot. *Institute of Arctic and Alpine Research Occasional Paper*, 58, 01 2004.

J. England, N. Atkinson, J. M. Bednarski, A. Dyke, D. A. Hodgson, and C. O. Cofaigh. The Innuitian Ice Sheet: Configuration, dynamics and chronology. *Quaternary Science Reviews*, 25:689–703, 04 2006. doi: 10.1016/j.quascirev.2005.08.007.

D. Farinotti, M. Huss, A. Bauder, M. Funk, and M. Truffer. A method to estimate ice volume and ice thickness distribution of alpine glaciers. *Journal of Glaciology*, 55:422–430, 06 2009. doi: 10.3189/002214309788816759.

D. Farinotti, D. Brinkerhoff, G. Clarke, J. Fürst, H. Frey, P. Gantayat, F. Gillet-Chaulet, C. Girard, M. Huss, P. Leclercq, A. Linsbauer, H. Machguth, C. Martin, F. Maussion, M. Morlighem, C. Mosbeux, A. Pandit, A. Portmann, A. Rabatel, and L. M. Andreassen. How accurate are estimates of glacier ice thickness? Results from ITMIX, the Ice Thickness Models Intercomparison eXperiment. *The Cryosphere*, 11:949–970, 04 2017. doi: 10.5194/tc-11-949-2017.

D. Farinotti, M. Huss, J. Fürst, J. Landmann, H. Machguth, F. Maussion, and A. Pandit. A consensus estimate for the ice thickness distribution of all glaciers on Earth. *Nature Geoscience*, 12, 03 2019. doi: 10.1038/s41561-019-0300-3.

A. Fitch, A. Kadyrov, W. Christmas, and J. Kittler. Orientation Correlation. volume 1, 01 2002. doi: 10.5244/C.16.11.

H. Frey, H. Machguth, M. Huss, C. Huggel, S. Bajracharya, T. Bolch, A. Kulkarni, A. Linsbauer, N. Salzmann, and M. Stoffel. Estimating the volume of glaciers in the Himalayan-Karakoram region using different methods. *The Cryosphere*, 8(6):2313–2333, 2014. doi: 10.5194/tc-8-2313-2014. URL `https://tc.copernicus.org/articles/8/2313/2014/`.

J. J. Fürst, F. Gillet-Chaulet, T. J. Benham, J. A. Dowdeswell, M. Grabiec, F. Navarro, R. Pettersson, G. Moholdt, C. Nuth, B. Sass, K. Aas, X. Fettweis, C. Lang, T. Seehaus, and M. Braun. Application of a two-step approach for mapping ice thickness to various glacier types on Svalbard. *The Cryosphere*, 11(5):2003–2032, 2017. doi: 10.5194/tc-11-2003-2017. URL `https://tc.copernicus.org/articles/11/2003/2017/`.

O. Gagliardini, T. Zwinger, F. Gillet-Chaulet, G. Durand, L. Favier, B. Fleurian, R. Greve, M. Malinen, C. Martin, P. Råback, J. Ruokolainen, M. Sacchettini, M. Schäfer, H. Seddik,

and J. Thies. Capabilities and performance of Elmer/Ice, a new-generation ice sheet model. *Geoscientific Model Development*, 6, 08 2013. doi: 10.5194/gmd-6-1299-2013.

A. Gardner, G. Moholdt, B. Wouters, G. J. Wolken, D. Burgess, M. Sharp, J. Cogley, C. Braun, and C. Labine. Sharply increased mass loss from glaciers and ice caps in the Canadian Arctic Archipelago. *Nature*, 473:357–60, 05 2011. doi: 10.1038/nature10089.

J. W. Glen. The creep of polycrystalline ice. *Proceedings of the Royal Society of London. Series A. Mathematical and Physical Sciences*, 228:519 – 538, 1955.

R. Greve. Advanced Course in Theoretical Glaciology. *Institute of Low Temperature Science Hokkaido University*, 2018.

A. Grinsted. An estimate of global glacier volume. *The Cryosphere*, 7(1):141–151, 2013. doi: 10.5194/tc-7-141-2013. URL https://tc.copernicus.org/articles/7/141/2013/.

M. Hambrey and F. Müller. Structures and Ice Deformation in the White Glacier, Axel Heiberg Island, Northwest Territories, Canada. *Journal of Glaciology*, 20(82):41–66, 1978. doi: 10.3189/S0022143000021213.

M. Huss and D. Farinotti. Distributed ice thickness and volume of all glaciers around the globe. *Journal of Geophysical Research: Earth Surface*, 117(F4), 2012. doi: 10.1029/2012JF002523. URL https://agupubs.onlinelibrary.wiley.com/doi/abs/10.1029/2012JF002523.

R. Jagels, B. LePage, and M. Jiang. Definitive identification of Larix (Pinaceae) wood based on anatomy from the middle Eocene, Axel Heiberg Island, Canadian High Arctic. *IAWA Journal*, 22:73–83, 01 2001. doi: 10.1163/22941932-90000270.

N. Kirchner, C. Hutter, M. Jakobsson, and R. Gyllencreutz. Capabilities and limitations of numerical ice sheet models: A discussion for Earth-scientists and modelers. *Quaternary Science Reviews - QUATERNARY SCI REV*, 30, 12 2011. doi: 10.1016/j.quascirev.2011.09.012.

R. M. Koerner. Accumulation, Ablation, and Oxygen Isotope Variations on the Queen Elizabeth Islands Ice Caps, canada. *Journal of Glaciology*, 22(86):25–41, 1979. doi: 10.3189/S0022143000014039.

I. Koldtoft, A. Grinsted, B. Vinther, and C. Hvidberg. Ice thickness and volume of Renland Ice Cap, East Greenland. *Submitted*, 2020.

P. L. Langen, R. S. Fausto, B. Vandecrux, R. H. Mottram, and J. E. Box. Liquid Water Flow and Retention on the Greenland Ice Sheet in the Regional Climate Model HIRHAM5: Local and Large-Scale Impacts. *Frontiers in Earth Science*, 4:110, 2017. ISSN 2296-6463. doi: 10.3389/feart.2016.00110. URL `https://www.frontiersin.org/article/10.3389/feart.2016.00110`.

Y. Ma, O. Gagliardini, C. Ritz, F. Gillet-Chaulet, G. Durand, and M. Montagnat. Enhancement factors for grounded ice and ice shelves inferred from an anisotropic ice-flow model. *Journal of Glaciology*, 56(199):805–812, 2010. doi: 10.3189/002214310794457209.

H. Machguth, R. Purves, J. Oerlemans, M. Hoelzle, and F. Paul. Exploring uncertainty in glacier mass balance modelling with Monte Carlo simulation. *The Cryosphere*, 2, 12 2008. doi: 10.5194/tcd-2-447-2008.

F. Maussion, A. Butenko, N. Champollion, M. Dusch, J. Eis, K. Fourteau, P. Gregor, A. H. Jarosch, J. Landmann, F. Oesterle, B. Recinos, T. Rothenpieler, A. Vlug, C. T. Wild, and B. Marzeion. The Open Global Glacier Model (OGGM) v1.1. *Geoscientific Model Development*, 12(3):909–931, 2019. doi: 10.5194/gmd-12-909-2019. URL `https://gmd.copernicus.org/articles/12/909/2019/`.

A. Messerli and A. Grinsted. Image GeoRectification And Feature Tracking toolbox: Im-GRAFT. *Geoscientific Instrumentation, Methods and Data Systems Discussions*, 4, 08 2014. doi: 10.5194/gid-4-491-2014.

M. Minnick, D. Shewfelt, C. Hickson, J. Majorowicz, and T. Rowe. Nunavut geothermal feasibility study. *Topical report RSI-2828, Quilliq Energy Corporation*, 06 2018.

R. Mottram, F. Boberg, P. Langen, S. Yang, C. Rodehacke, J. Christensen, and M. Madsen. Surface mass balance of the Greenland ice sheet in the regional climate model HIRHAM5: Present state and future prospects. *Low Temperature Science. Series A. Physical Science*, 75: 105–115, 2017. ISSN 0439-3538. doi: 10.14943/lowtemsci.75.105.

F. Müller. Zonation in the Accumulation Area of the Glaciers of Axel Heiberg Island, N.W.T., Canada. *Journal of Glaciology*, 4(33):302–311, 1962. doi: 10.3189/S0022143000027623.

NASA. Landsat 7. URL `https://landsat.gsfc.nasa.gov/landsat-7/`.

J. Paden, J. Li, C. Leuschen, F. Rodriguez-Morales, and R. Hale. IceBridge MCoRDS L2 Ice Thickness, Version 1, IRMCR2 20170330 02, 2010, updated 2019.

W. Pelt, J. Oerlemans, C. Reijmer, R. Pettersson, V. Pohjola, E. Isaksson, and D. Divine. An iterative inverse method to estimate basal topography and initialize ice flow models. *The Cryosphere*, 7, 06 2013. doi: 10.5194/tc-7-987-2013.

C. Porter, P. Morin, I. Howat, M.-J. Noh, B. Bates, K. Peterman, S. Keesey, M. Schlenk, J. Gardiner, K. Tomko, M. Willis, C. Kelleher, M. Cloutier, E. Husby, S. Foga, H. Nakamura, M. Platson, J. Wethington, Michael, C. Williamson, G. Bauer, J. Enos, G. Arnold, W. Kramer, P. Becker, A. Doshi, C. D'Souza, P. Cummens, F. Laurier, and M. Bojesen. ArcticDEM, 2018. URL https://doi.org/10.7910/DVN/OHHUKH.

V. Radić and R. Hock. Regional and global volumes of glaciers derived from statistical upscaling of glacier inventory data. *Journal of Geophysical Research: Earth Surface*, 115 (F1), 2010. doi: 10.1029/2009JF001373. URL https://agupubs.onlinelibrary.wiley.com/doi/abs/10.1029/2009JF001373.

V. Radić, A. Bliss, A. C. Beedlow, R. Hock, E. Miles, and J. G. Cogley. Regional and global projections of twenty-first century glacier mass changes in response to climate scenarios from global climate models. *Climate Dynamics*, 42(1-2):37–58, Jan. 2014. doi: 10.1007/s00382-013-1719-7.

R. Ramsankaran, A. Pandit, and M. F. Azam. Spatially distributed ice-thickness modelling for Chhota Shigri Glacier in western Himalayas, India. *International Journal of Remote Sensing*, 39:3320–3343, 05 2018. doi: 10.1080/01431161.2018.1441563.

B. H. Raup, L. M. Andreassen, T. Bolch, and S. Bevan. Remote sensing of glaciers. In *Remote Sensing of the Cryosphere*, chapter 7, pages 123–156. 2014. ISBN 9781118368909. doi: 10.1002/9781118368909.ch7. URL https://onlinelibrary.wiley.com/doi/abs/10.1002/9781118368909.ch7.

J. Salvatier, T. Wiecki, and C. Fonnesbeck. Probabilistic programming in Python using PyMC3. 01 2016. doi: 10.7287/PEERJ.PREPRINTS.1686V1.

L. S. Schmidt, G. Adalgeirsdóttir, S. Gudmundsson, P. L. Langen, F. Pálsson, R. Mottram, S. Gascoin, and H. Björnsson. The importance of accurate glacier albedo for estimates of surface mass balance on Vatnajökull: evaluating the surface energy budget in a regional climate model with automatic weather station observations. *The Cryosphere*, 11(4):1665–1684, 2017. doi: 10.5194/tc-11-1665-2017. URL https://tc.copernicus.org/articles/11/1665/2017/.

C. Schoof. A variational approach to ice stream flow. *Journal of Fluid Mechanics*, 556:227–251, 06 2006. doi: 10.1017/S0022112006009591.

N. Short and L. Gray. Glacier dynamics in the Canadian High Arctic from RADARSAT-1 speckle tracking. *Canadian Journal of Remote Sensing*, 31:225–239, 06 2005. doi: 10.5589/m05-010.

A. Tarantola. *Inverse Problem Theory and Methods for Model Parameter Estimation*. Society for Industrial and Applied Mathematics, 2005. doi: 10.1137/1.9780898717921. URL `https://epubs.siam.org/doi/abs/10.1137/1.9780898717921`.

the PISM authors. PISM, a Parallel Ice Sheet Model, 2018. URL `http://www.pism-docs.org`.

L. Thomson, G. Osinski, and C. Ommanney. Glacier change on Axel Heiberg Island, Nunavut, Canada. *Journal of Glaciology*, 57:1079–1086, 12 2011. doi: 10.3189/002214311798843287.

L. Thomson, M. Zemp, L. Copland, J. Cogley, and M. Ecclestone. Comparison of geodetic and glaciological mass budgets for White Glacier, Axel Heiberg Island, Canada. *Journal of Glaciology*, 63:1–12, 10 2016. doi: 10.1017/jog.2016.112.

W. Van Wychen, D. Burgess, L. Gray, L. Copland, M. Sharp, J. Dowdeswell, and T. Benham. Glacier velocities and dynamic ice discharge from the Queen Elizabeth Islands, Nunavut, Canada. *Geophysical Research Letters*, 41:484–490, 01 2014. doi: 10.1002/2013GL058558.

W. Van Wychen, J. Davis, D. O. Burgess, L. Copland, L. Gray, M. Sharp, and C. Mortimer. Characterizing interannual variability of glacier dynamics and dynamic discharge (1999–2015) for the ice masses of Ellesmere and Axel Heiberg Islands, Nunavut, Canada. *Journal of Geophysical Research: Earth Surface*, 121(1):39–63, 2016. doi: 10.1002/2015JF003708. URL `https://agupubs.onlinelibrary.wiley.com/doi/abs/10.1002/2015JF003708`.

L. Veci, P. Prats-Iraola, R. Scheiber, F. Collard, N. Fomferra, and M. Engdahl. The sentinel-1 toolbox. pages 1–3, 07 2014.

M. A. Werder, M. Huss, F. Paul, A. Dehecq, and D. Farinotti. A Bayesian ice thickness estimation model for large-scale applications. *Journal of Glaciology*, 66(255):137–152, 2020. doi: 10.1017/jog.2019.93.

# Appendices

# A   Stripes in Landsat 7

An example of the output from templatematch when using the original Landsat 7 scenes with stripes can be seen in Figure A.1a. It can easily be seen how templatematch matches the black stripes rather than the ice underneath in several places. Even the outlet glacier in the northwest cannot be tracked as we can see the arrows pointing in the opposite direction of the flow. It should be noted that the colour bar is in pixels per passed time in between the two images. Figure A.1b shows the feature tracking of the same image pair, but after the removal of stripes.
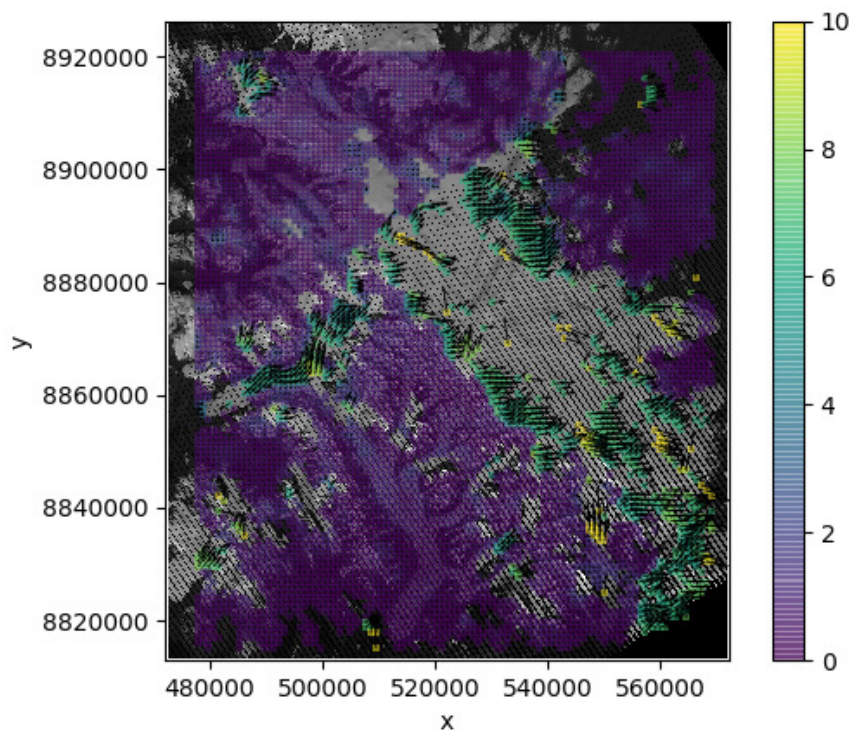
*(a) Before removing stripes*
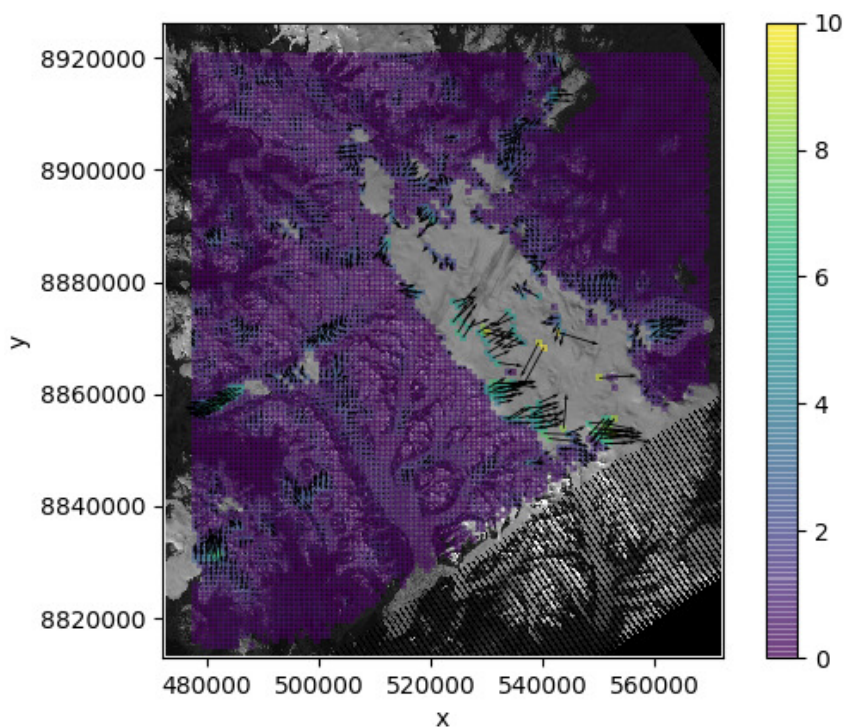


*(b) After removing stripes*

*Figure A.1: Difference in feature tracking before and after the removal of stripes in Landsat 7.*

# B  Streamplot of the Landsat 8 velocity map

Figure B.1 shows a streamplot of the median Landsat 8 velocity map. It can be seen that in areas with low velocity the directions of flow are a bit off.
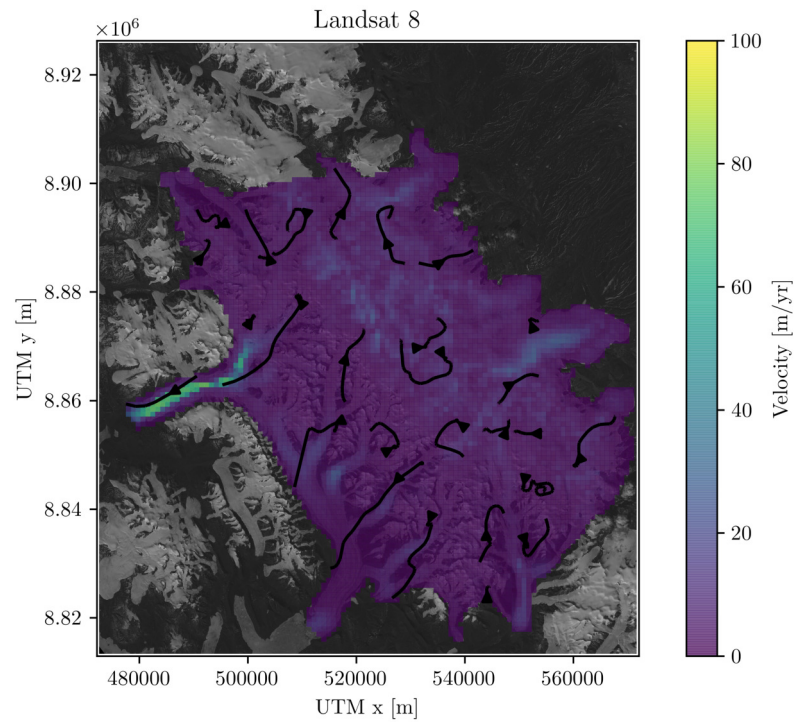


*Figure B.1: Streamplot of the median Landsat 8 velocity map.*

# C   PISM iterations

```python
"""
Created on Tue Dec 10 08:52:21 2019

@author: ann-sofie
"""

import numpy as np
import xarray as xr
import os
import time

### This script makes 10 iterations where the bed is being changed with phi=10 and E
    =1.0

# Polygon of the ice cap
in_poly = np.loadtxt('in_poly.txt')

# Data for the inital run
origdata = xr.open_dataset('iter0.nc', decode_times=False)


B_orig = np.array(origdata['topg']) # Farinotti bedrock
S_orig = np.array(origdata['usurf']) # ArcticDEM



B_old = B_orig

#relaxation parameter
K = np.clip((S_orig-500)/500,0,1)*0.5



E = '1.0'
phi = '10'


for i in range(10):
    cmd = 'srun -v -p bylgja -N 1 -n 32 --constraint=v2 --mpi=pmi2 --kill-on-bad-
        exit pismr -i iter'+str(i)+'.nc -bootstrap -y 2000 -Mx 111 -My 126 -Mz 201 -
        z_spacing equal -Lz 4000 -sia_e '+E+' -ssa_e '+E+' -stress_balance ssa+sia -
        pseudo_plastic -plastic_phi '+phi+' -stress_balance.sia.limit_diffusivity
        true -extra_file extra_iter'+str(i)+'_'+phi+'_'+E+'.nc -extra_vars thk,topg,
        usurf,velsurf,velsurf_mag,tempbase -extra_times 0:100:2000 -ts_file ts_iter'
        +str(i)+'_'+phi+'_'+E+'.nc -ts_times 0:10:2000 -o iter'+str(i)+'_'+phi+'_'+E
        +'.nc &> out.iter'+str(i)+'_'+phi+'_'+E

    os.system(cmd)

    while os.path.isfile('iter'+str(i)+'_'+phi+'_'+E+'.nc') == False:
        time.sleep(60)
```

```python
data = xr.open_dataset('iter'+str(i)+'_'+phi+'_'+E+'.nc', decode_times=False)
S_new = np.array(data['usurf'][0,:,:])


B_new = B_old - K*(S_new-S_orig)
H_new = S_orig - B_new
H_new = H_new * in_poly
H_new[H_new<0] = 0

# Updating the input file to PISM with a new bedrock topography and a new ice
    thickness
origdata['topg'][:,:] = B_new
origdata['thk'][:,:]  = H_new
origdata.to_netcdf('iter'+str(i+1)+'.nc')

# Updating "old" bedrock
B_old = B_new
```

# D   Using a uniform SMB in the SIA inversion

Figure D.1 shows the IceBridge flight line cross section with my modelled bedrock topography using a uniform SMB with ones everywhere on the grid. The modelled bedrock of the entire ice cap using a uniform SMB can be seen in Figure D.2.



*Figure D.1: IceBridge flight line cross section using a uniform SMB with ones everywhere in the grid.*



*Figure D.2: Bedrock topography using a uniform SMB with ones everywhere on the grid.*

# E    Using a uniform SMB in MC without sliding

Figure E.1 shows The IceBridge flight line cross section with my modelled bedrock topography using a uniform SMB with ones everywhere on the grid. The modelled bedrock of the entire ice cap using a uniform SMB can be seen in Figure E.2.
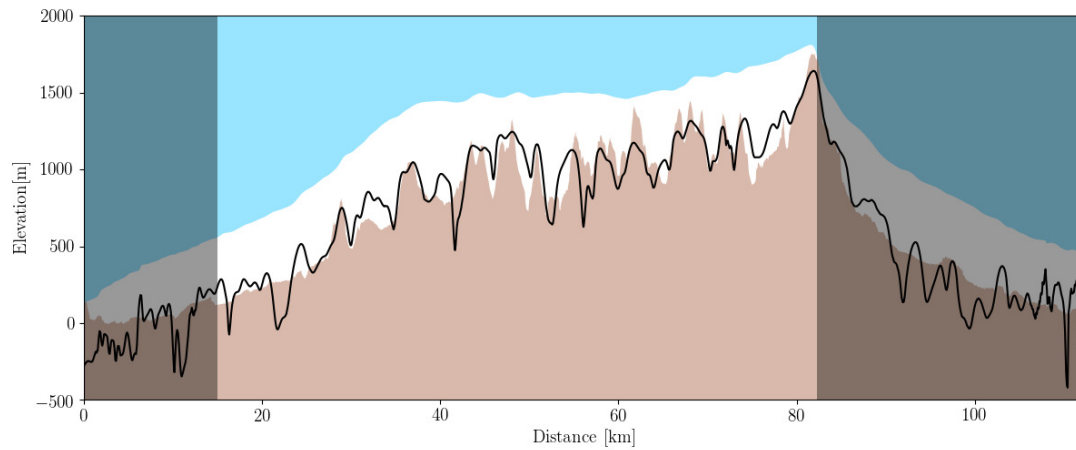


*Figure E.1: IceBridge flight line cross section using a uniform SMB with ones everywhere in the grid.*
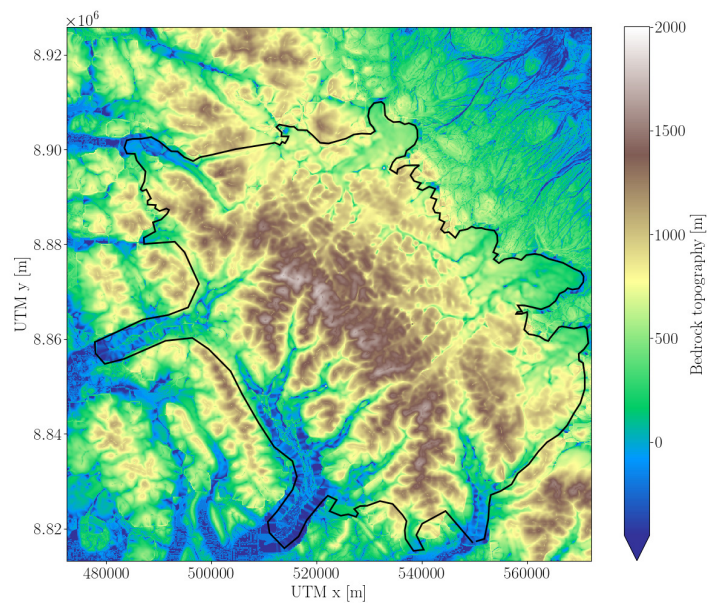


*Figure E.2: Bedrock topography using a uniform SMB with ones everywhere on the grid.*

# F    Using a uniform SMB in MC with sliding

Figure F.1 shows The IceBridge flight line cross section with my modelled bedrock topography using a uniform SMB with ones everywhere on the grid. The modelled bedrock of the entire ice cap using a uniform SMB can be seen in Figure F.2.
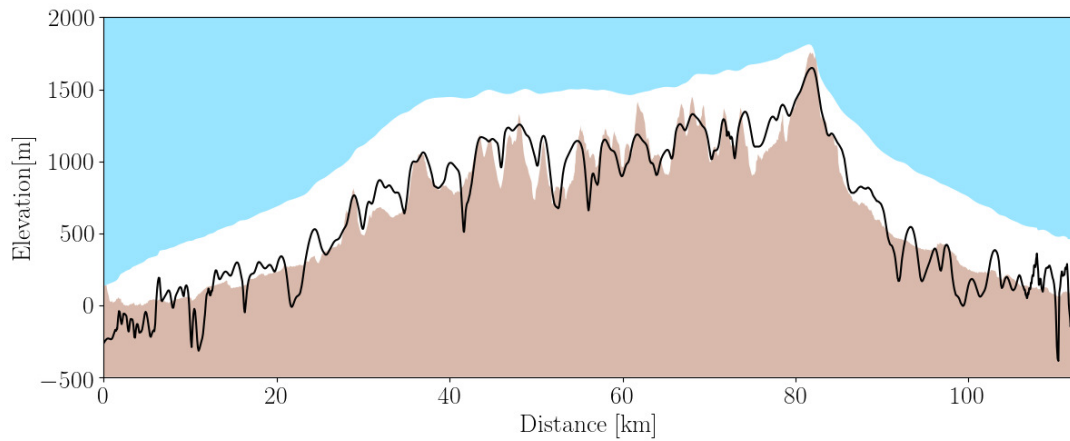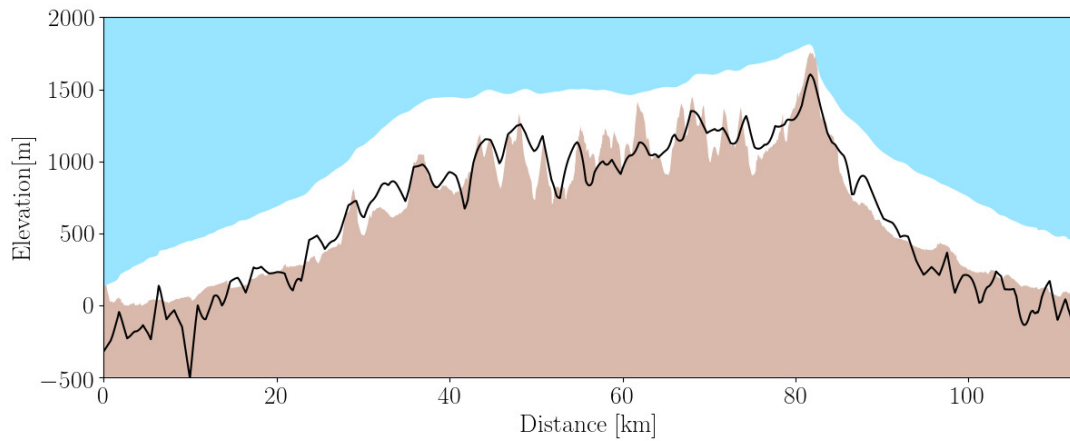


*Figure F.1: IceBridge flight line cross section using a uniform SMB with ones everywhere in the grid.*
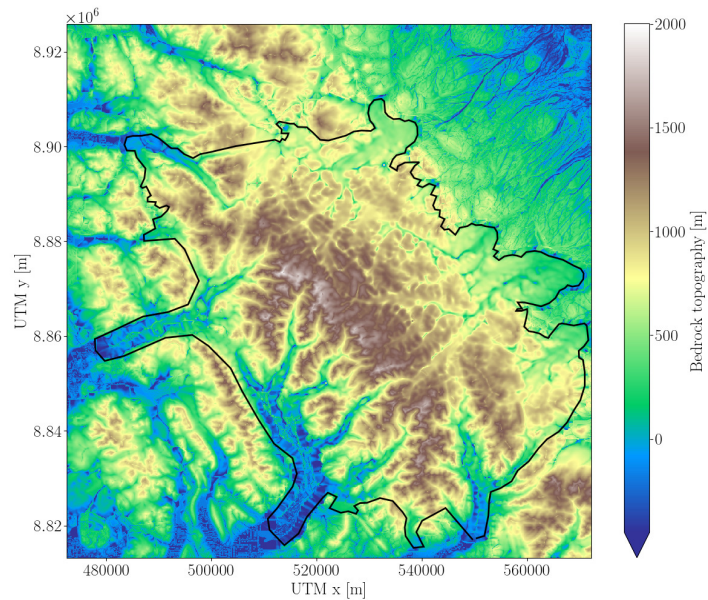


*Figure F.2: Bedrock topography using a uniform SMB with ones everywhere on the grid.*

# G  Drill site suggestions

Table G.1 shows the individual values (i.e. ice thickness, surface elevation etc.) for all of the sites with a score of minimum 7. Be aware that the UTM coordinates are in zone 15 N. "H - XXXX" are the ice thicknesses for the individual models.

*Table G.1: Individual values for all sites with a score of at least 7. "H - XXXX" are the ice thicknesses for the individual models.*

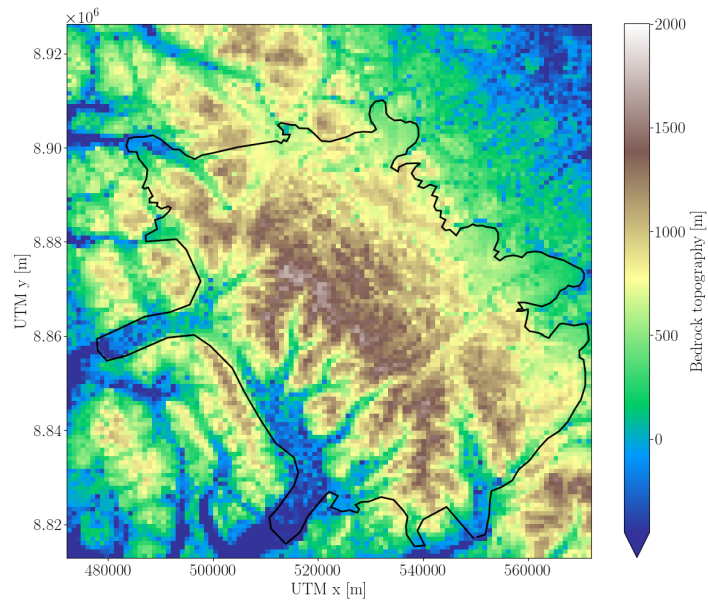| Score | UTMx | UTMy | S [m] | $v_s$ [m yr$^{-1}$] | Melt [d yr$^{-1}$] | H - PISM | H - SIA | H - MC | H - MCsl | H - S+P | Lat. | Lon. |
|---|---|---|---|---|---|---|---|---|---|---|---|---|
| 8 | 515829 | 8882663 | 1602.9 | 1.83 | 24 | 623 | 575 | 557 | 575 | 595 | 80.009 | -92.183 |
| 7 | 514029 | 8881763 | 1629.2 | 3.97 | 25 | 501 | 598 | 578 | 598 | 517 | 80.001 | -92.276 |
| 7 | 518529 | 8881763 | 1606.3 | 4.52 | 24 | 572 | 593 | 575 | 593 | 544 | 80.000 | -92.044 |
| 7 | 521229 | 8881763 | 1614.3 | 4.15 | 17 | 600 | 560 | 542 | 560 | 570 | 80.000 | -91.905 |
| 7 | 518529 | 8880863 | 1624.1 | 4.63 | 22 | 550 | 541 | 525 | 541 | 533 | 79.992 | -92.045 |
| 7 | 523029 | 8879963 | 1611.5 | 3.87 | 22 | 553 | 589 | 570 | 589 | 518 | 79.983 | -91.814 |
| 7 | 517629 | 8878163 | 1713.7 | 7.55 | 16 | 592 | 576 | 558 | 576 | 521 | 79.968 | -92.093 |
| 7 | 522129 | 8875463 | 1730.7 | 9.15 | 16 | 652 | 615 | 596 | 615 | 596 | 79.943 | -91.865 |
| 7 | 519429 | 8874563 | 1758.2 | 4.35 | 14 | 527 | 500 | 484 | 500 | 512 | 79.936 | -92.004 |
| 7 | 523929 | 8874563 | 1745.4 | 4.27 | 16 | 502 | 687 | 665 | 687 | 477 | 79.935 | -91.773 |
| 7 | 530229 | 8873663 | 1640.4 | 2.30 | 17 | 534 | 573 | 555 | 573 | 505 | 79.925 | -91.452 |
| 7 | 522129 | 8872763 | 1785.6 | 3.22 | 15 | 496 | 542 | 524 | 542 | 534 | 79.919 | -91.867 |
| 8 | 523029 | 8872763 | 1782.9 | 1.26 | 13 | 453 | 604 | 585 | 604 | 527 | 79.919 | -91.821 |
| 7 | 524829 | 8870063 | 1839.5 | 3.88 | 13 | 439 | 648 | 627 | 648 | 532 | 79.894 | -91.732 |
| 8 | 524829 | 8869163 | 1839.0 | 0.89 | 13 | 475 | 579 | 560 | 579 | 540 | 79.886 | -91.733 |
| 7 | 524829 | 8868263 | 1837.2 | 2.28 | 14 | 484 | 577 | 559 | 577 | 550 | 79.878 | -91.734 |
| 7 | 525729 | 8868263 | 1824.9 | 3.01 | 13 | 491 | 660 | 639 | 660 | 565 | 79.878 | -91.689 |
| 7 | 522129 | 8867363 | 1895.9 | 1.40 | 13 | 225 | 543 | 525 | 543 | 285 | 79.871 | -91.873 |
| 8 | 525729 | 8867363 | 1814.3 | 3.02 | 14 | 535 | 539 | 522 | 539 | 589 | 79.870 | -91.690 |
| 8 | 526629 | 8867363 | 1795.1 | 3.97 | 13 | 537 | 692 | 670 | 692 | 542 | 79.870 | -91.644 |
| 7 | 532029 | 8867363 | 1666.8 | 1.95 | 19 | 509 | 594 | 576 | 594 | 492 | 79.869 | -91.369 |
| 7 | 532929 | 8867363 | 1648.5 | 3.60 | 19 | 603 | 716 | 695 | 716 | 597 | 79.868 | -91.323 |
| 7 | 523929 | 8866463 | 1850.2 | 1.00 | 14 | 323 | 526 | 509 | 526 | 451 | 79.862 | -91.782 |
| 8 | 524829 | 8866463 | 1835.1 | 1.63 | 12 | 480 | 640 | 620 | 640 | 563 | 79.862 | -91.736 |
| 9 | 526629 | 8866463 | 1804.1 | 1.21 | 14 | 535 | 579 | 560 | 579 | 562 | 79.862 | -91.645 |
| 7 | 525729 | 8865563 | 1816.1 | 3.21 | 14 | 490 | 616 | 596 | 616 | 544 | 79.854 | -91.692 |
| 7 | 526629 | 8865563 | 1817.9 | 3.84 | 14 | 479 | 566 | 547 | 566 | 546 | 79.854 | -91.646 |
| 8 | 532029 | 8864663 | 1711.4 | 0.91 | 15 | 529 | 623 | 604 | 623 | 460 | 79.844 | -91.373 |
| 7 | 528429 | 8863763 | 1791.0 | 1.88 | 14 | 307 | 550 | 532 | 550 | 388 | 79.837 | -91.557 |
| 7 | 531129 | 8861963 | 1792.1 | 0.60 | 14 | 386 | 568 | 551 | 568 | 393 | 79.820 | -91.422 |
| 7 | 536529 | 8859263 | 1664.9 | 3.72 | 18 | 568 | 568 | 550 | 568 | 513 | 79.795 | -91.153 |
| 8 | 537429 | 8856563 | 1683.4 | 0.39 | 19 | 507 | 678 | 657 | 678 | 509 | 79.770 | -91.112 |
| 7 | 540129 | 8851163 | 1509.8 | 1.25 | 34 | 590 | 552 | 534 | 552 | 595 | 79.721 | -90.985 |